AD-A179 476 COHERENT MULTIPLE APERTURE OPTICAL IMAGING SYSTEMS: 1/2
ANALYSIS AND DESIGN(U) AIR FORCE INST OF TECH
WRIGHT-PATTERSON AFB OH SCHOOL OF ENGINEERING
UNCLASSIFIED D J BERGEY MAR 87 AFIT/GE/ENG/87M-1 F/G 20/6 NL

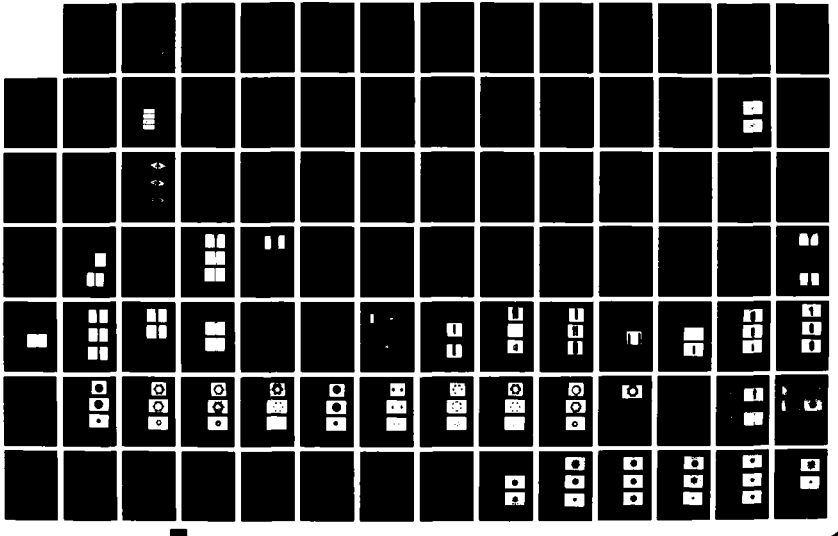

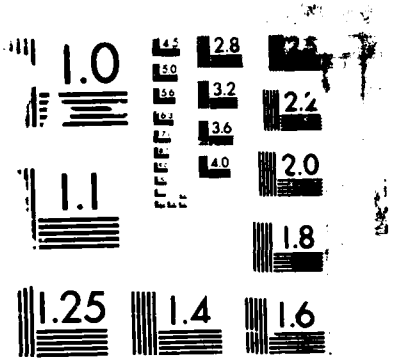
1.0
1.1
1.25
1.4
1.6
1.8
2.0
2.2
2.8
3.2
3.6
4.0

COHERENT MULTIPLE APERTURE OPTICAL IMAGING SYSTEMS: ANALYSIS AND DESIGN

THESIS

Dana J. Bergey
Second Lieutenant, USAF

AFIT/GE/ENG/87M-1

DEPARTMENT OF THE AIR FORCE
AIR UNIVERSITY
AIR FORCE INSTITUTE OF TECHNOLOGY

Wright-Patterson Air Force Base, Ohio

AFIT/GE/ENG/87

COHERENT MULTIPLE APERTURE OPTICAL IMAGING SYSTEMS: ANALYSIS AND DESIGN

THESIS

Dana J. Bergey
Second Lieutenant, USAF

AFIT/GE/ENG/87M-1

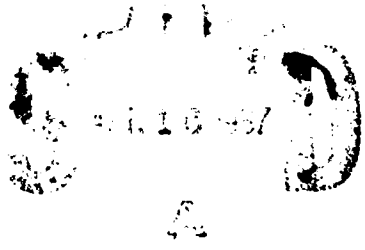

Approved for public release; distribution unlimited

AFIT/GE/ENG/87M-1

COHERENT MULTIPLE APERTURE OPTICAL IMAGING SYSTEMS: ANALYSIS AND DESIGN

THESIS

Presented to the Faculty of the School of Engineering
of the Air Force Institute of Technology
Air University
In Partial Fulfillment of the
Requirements for the Degree of
Master of Science in Electrical Engineering

Dana J. Bergey, B.S.
Second Lieutenant, USAF

March 1987

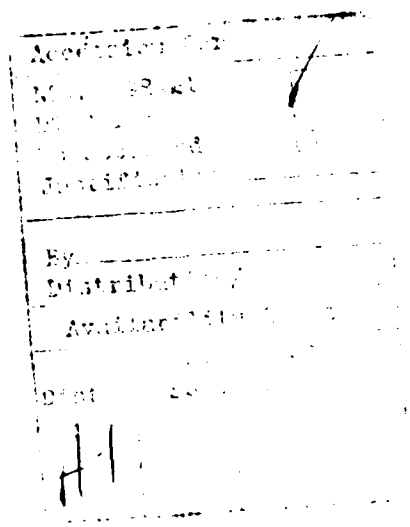

Preface

The purpose of this study was to investigate the important aspects of coherent multiaperture optical imaging. This work represents some of the initial research in this area. It is my hope that this document will serve as a stepping-stone for other researchers into the area of coherent multiple aperture optical imaging.

Since coherent multiaperture imaging is a relatively new area of interest, this thesis does not limit itself to one particular method of analysis. Rather, it includes a theoretical development, a computer prediction, and an experimental analysis of the properties exhibited by various multiple aperture telescope configurations when imaging simple objects. After the idea of multiaperture imaging is developed, predictions are derived concerning how different aperture geometries will affect imaging. The experimental results cataloged in this thesis confirm the validity of the theoretical developments and computer programs.

The analysis of the various multiple apertures brought out a number of important characteristics unique to multiaperture imaging. These characteristics point to various design criteria that should be considered when designing a multiple aperture imaging system. The topics identified would be crucial to the design of any multiple aperture system that supports the Strategic Defense Initiative.

I would like to thank my advisor, Maj. Jim Mills, who took me under his wing as soon as I arrived at AFIT and extended friendly guidance and continued support throughout this entire thesis effort. I also wish to thank Jack Tiffany and Tim Hancock of the AFIT Model Shop, who produced the apertures and aperture spinner used in my experiments. Of course, these experiments would have been impossible without the aid of Ron Gabriel, who put up with my daily questions and requests and assisted me in every way possible. Most importantly, I want to thank my fiancée, Bella, who single-handedly arranged a wedding, endured many weeks without letters, listened compfortingly to months of complaining, and is still going to marry me in June.

Dana Joel Bergey

Table of Contents

List of Figures

List of Tables

ABSTRACT

The imaging of simple objects through coherent multiple aperture optical imaging systems was investigated. Multiple aperture telescopes are a candidate technology for the Strategic Defense Initiative missions of surveillance, tracking, and kill assessment. In this thesis, the multiaperture images of edges, slits, rectangles, and circles were theoretically predicted and experimentally produced. The images of the one-dimensional objects were predicted analytically, while a computer program was developed to predict the images of the two-dimensional objects. Photographs of the actual images produced in the lab were compared to the theoretical images, and the analytical and computer prediction techniques were found to be accurate.

All of the results were analyzed to determine how different multiaperture geometries affected the images. It was found that multiaperture imaging produces edge enhancement. The position of a single edge could be found exactly, while multiple edges sometimes produced slight edge shifts. A computer program was developed that predicts the edge shifts that will be observed when imaging through a given multiple aperture. Larger sub-aperture spacings were found to exhibit better resolution but produced more ringing about the edges. The possibility of rotating the multiple aperture system to gather more information was discussed, as well as designs that include a central sub-aperture. All of the important results were discussed as they apply to the design of systems that support the Strategic Defense Initiative.

COHERENT MULTIPLE APERTURE OPTICAL IMAGING SYSTEMS: ANALYSIS AND DESIGN

I. INTRODUCTION

I.1. Problem Statement

In this thesis, coherent imaging of simple objects through various multiple aperture telescope configurations was investigated. Coherent multiaperture images of edges, slits, rectangles, and circles were theoretically predicted and experimentally produced. These images were analyzed to determine the effects that different aperture configurations have on imaging. From this analysis, some conclusions were drawn to aid in the design of coherent multiaperture optical imaging systems.

I.2. Importance to the Air Force

The Strategic Defense Initiative is an attempt to develop a system that could defend the United States and its allies from nuclear attack. An important characteristic of such a system is its ability to detect ICBM warheads throughout their trajectory. The system must be able to resolve each warhead, and since resolving power is directly related to the diameter of the aperture, engineers are trying to produce very large mirrors for space telescopes. These large diameter optics are very expensive and difficult to produce. "Their sheer size and weight make them awk-

ward to use. Thus, there is a practical limit of about eight meters on how big a single aperture system can be made " (8:3). There are even more practical constraints on the size of large apertures. Since SDI plans call for the use of space based laser satellites, another size limitation becomes evident. "This limit is smaller for space based scenerios since the space shuttle can only lift optics of less than 2 meters in diameter" (8:4). One solution to this problem is the use of multiple aperture systems. These multiple aperture systems sometimes exhibit better resolution than their corresponding single apertures (2). Since each component is smaller, the system is less expensive, easier to produce, and easier to lift into space. These benefits make multiple aperture imaging systems important to the Air Force.

I.3. Multiple Apertures

In the field of optics, the term 'aperture' is used to mean an 'opening' through which a scene or an object is viewed. This opening could be a lens, a mirror, or even just a hole through which an optical system images an object. A multiple (or synthetic) aperture is formed when separate optical systems are combined to function as a single larger aperture (3:2). The synthesized aperture exhibits many of the same properties as a single aperture. An example of a multiple aperture system is shown in Figure 1. The actual multiple apertures analyzed in this thesis effort are described in section I.5.

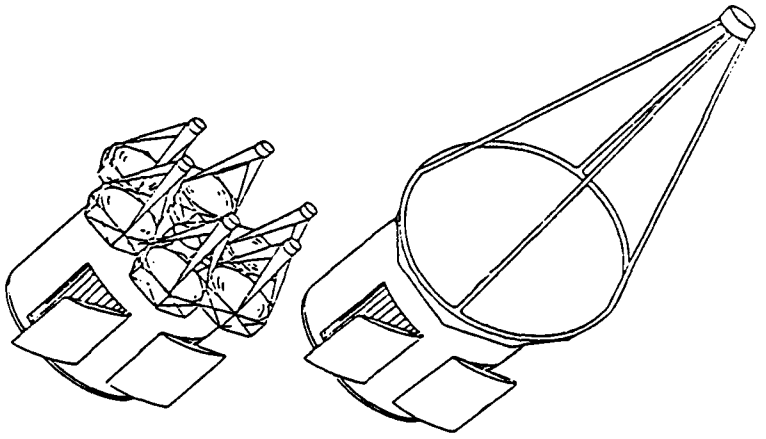

Figure 1. Multiple Aperture System and 'equivalent' Single Aperture System (3:3)

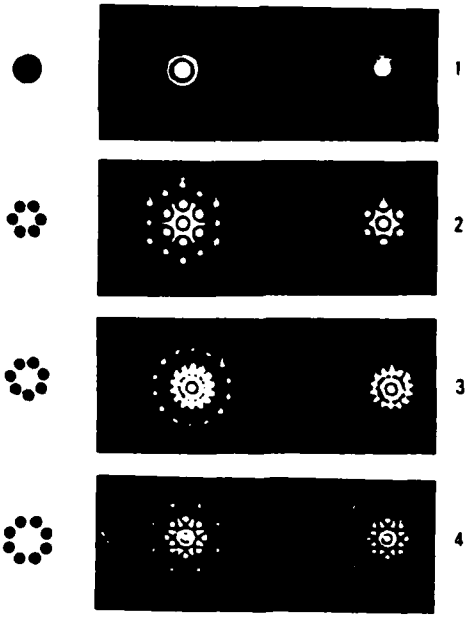

Figure 2. Point Source imaged through different Apertures (12:158)

(1) single aperture (2) six-aperture array

(3) seven-aperture array (4) eight-aperture array

Images viewed through a multiple aperture system using coherent illumination are significantly distorted. Figure 2 shows the image of a distant point source as seen through several apertures. Although some characteristics of the image, such as the circular ringing, are discernible through all of the apertures, the fine structure is drastically altered. Even though the images have been significantly changed, much information can be recovered from them.

I.4 Background

Some historians credit the first recorded use of aperture synthesis to Archimedes, the Greek mathematician, physicist, and inventor (6:xxi). In approximately 214 B.C., Archimedes' native city of Syracuse was besieged by the Roman general Marcus Claudius Marcellus. Legend holds that Archimedes constructed a ring of mirrors around the city's harbor. These mirrors synthesized part of a large concave mirror that set the Roman ships aflame by focusing the sun's rays on them.

In this thesis we are interested only in multiple aperture systems as they apply to imaging, so our story begins some two thousand years later. If we define the field of synthetic aperture optics to include any method for achieving, with one or more small apertures, the resolution normally associated with a single large aperture, then "the first historical example of an aperture synthesis instrument is the Michelson stellar interferometer, which was successfully used by Michelson and Pease in the early 1900's " (11:4). Michelson used a two-aperture optical system

to determine the width of stars. " In 1966-67 there occurred a significant advance in the field of synthetic aperture optics. This was the system that Perkin-Elmer developed, which they called the active optics system" (11:5). This system was a segmented mirror in which each segment was separately controlled and phased. The system acted as a multiple aperture. Now," it is well established that multiaperture systems show promise of providing greater angular resolution capabilities over that of single aperture systems. The Multiple Mirror Telescope (MMT) of the University of Arizona and several other MMT-type projects which are in the works now, point to the potential of the approach" (8:2).

Most of the multiaperture work currently being pursued concerns incoherent imaging (7) and point source imaging (12:149-201). This thesis explores the area of coherent imaging of simple objects.

I.5. Scope

For SDI purposes, a satellite or some other complex shape can be modeled as a collection of simple objects; edges, slits, rectangles, and circles. In this thesis, the objects listed above will be imaged through a series of different multiple apertures. The apertures will be studied to determine how the spacing, the size, and the number of sub-apertures affect the images. Finally, the observed characteristics of the multiple apertures will be used to ascertain the important areas that must be considered in the design of multiaperture optical imaging systems.

The actual multiple apertures that were designed and built for this project are shown in Figure 3. These apertures are simply masks that are placed in front of a single imaging lens. In this way, phasing problems can be ignored. In a real system each of the sub-apertures would be a separate lens or mirror, and the array would have to be carefully aligned. This thesis ignores all alignment or phasing problems, so the apertures are aluminum disks with holes drilled in them.

This thesis will deal only with coherent imaging. In Chapter 2, coherent imaging itself is discussed. Theoretical considerations are developed and the experimental configuration is explained. Chapter 2 closes with a discussion of criteria for 'good' imaging. The multiaperture images of 1-dimensional simple objects (edges and slits) are analyzed in Chapter 3. Theoretical predictions are compared with experimental results, and conclusions are drawn. Chapter 4 then extends this analysis to 2-dimensional simple objects (rectangles and circles). Chapter 5 summarizes the conclusions of this thesis, as they relate to design, and discusses recommendations for future research.

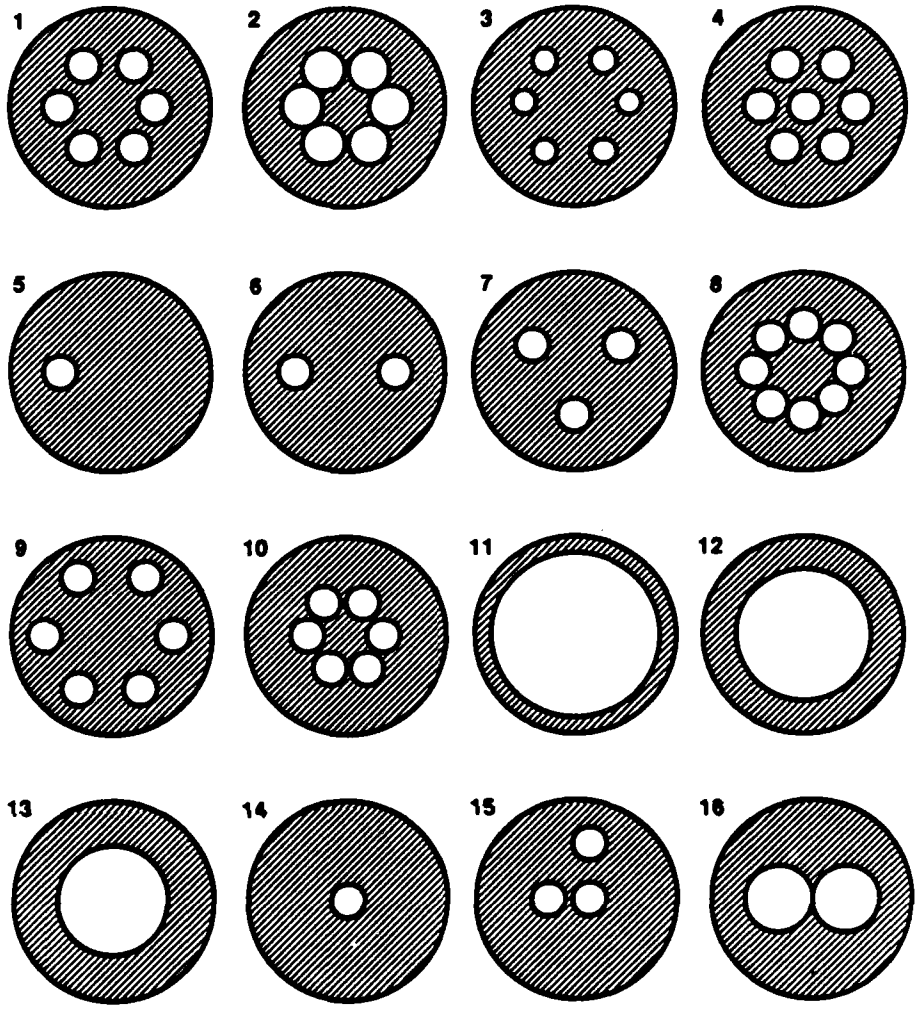

Figure 3. The Multiple Apertures used in this Thesis
(The actual dimensions of each aperture
can be found in Appendix A.)

II. IMAGING

This chapter develops the concept of imaging. A general imaging equation is derived from the geometry of a multiple aperture system. Then, a theoretical configuration and an experimental setup are devised that will realize the imaging equation. The impulse response of an arbitrary multiple aperture is analyzed to determine the effects of aperture parameters. Finally, the concept of 'good' imaging is addressed.

II.1. The General Imaging Equation

Figure 4 shows the geometry of a general multiaperture optical imaging system. The system is made up of several small optics, each aligned to share a common focal point. The detector

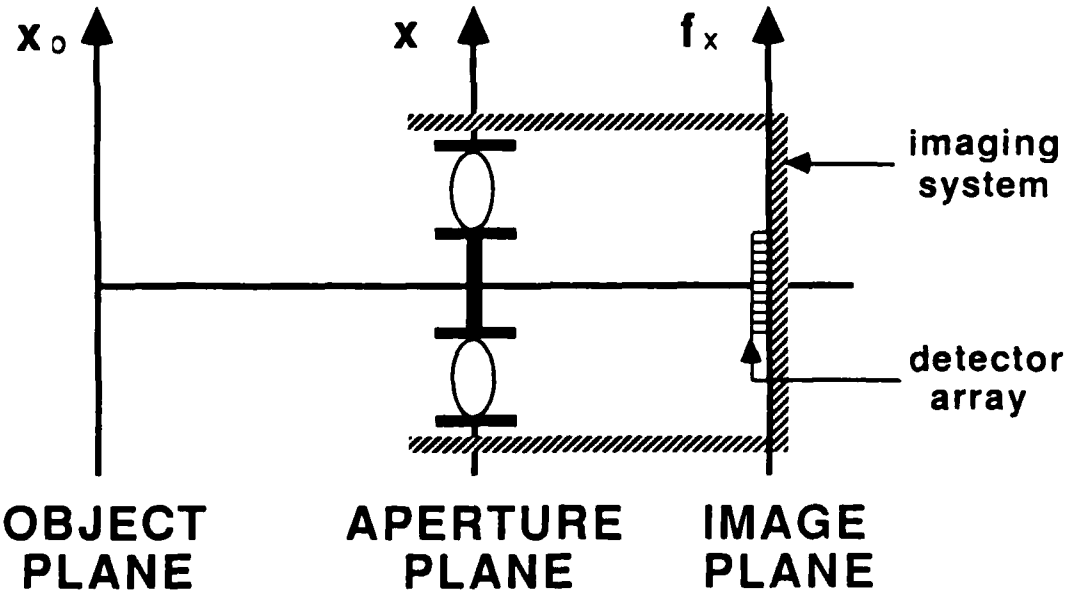

Figure 4. Imaging Geometry of a Multiple Aperture System

array is centered on the image plane, denoted by the axis f_x. The distance between the image plane and the plane of the optics is variable so that objects at various ranges can be imaged. The common result (5:96)

$$U_i(f_x) = h(f_x) * U_o(-f_x) \tag{1}$$

can be applied in this case, where * implies convolution, and the minus sign accounts for the inversion of the image. Many books drop the minus sign and invert the f_x axis, but this analysis will keep track of all minus signs.

$U_i(f_x)$ = the field in the image plane

$h(f_x)$ = the scaled impulse response of the system

and $U_o(-f_x)$ = the scaled and inverted field in the object plane

The impulse response is defined by

$$h(x) = F\{p(x)\}, \tag{2}$$

where the symbol $F\{\ \}$ signifies the Fourier transform of the function inside the brackets. The function $p(x)$ describes the pupil transmittance.

Using the convolution theorem (5:10), the imaging equation, Eq (1), can be written

$$F\{U_i(f_x)\} = F\{h(f_x)\} \cdot F\{U_o(-f_x)\}, \tag{3}$$

which is equivalent to

$$U_i(f_x) = F^{-1}\{F\{U_o(-f_x)\} \cdot p(-f_x)\}, \tag{4}$$

where $F^{-1}\{\ \}$ denotes the inverse Fourier transform.

This expression is equivalent to

$$U_i(f_x) = F\{F\{U_o(f_x)\}\cdot p(f_x)\} \qquad (5)$$

This equation states that the field in the image plane is equal to the Fourier transform of the product of the pupil function and the Fourier transform of the field in the object plane. This result can also be arrived at by utilizing the optical setup shown in Figure 5.

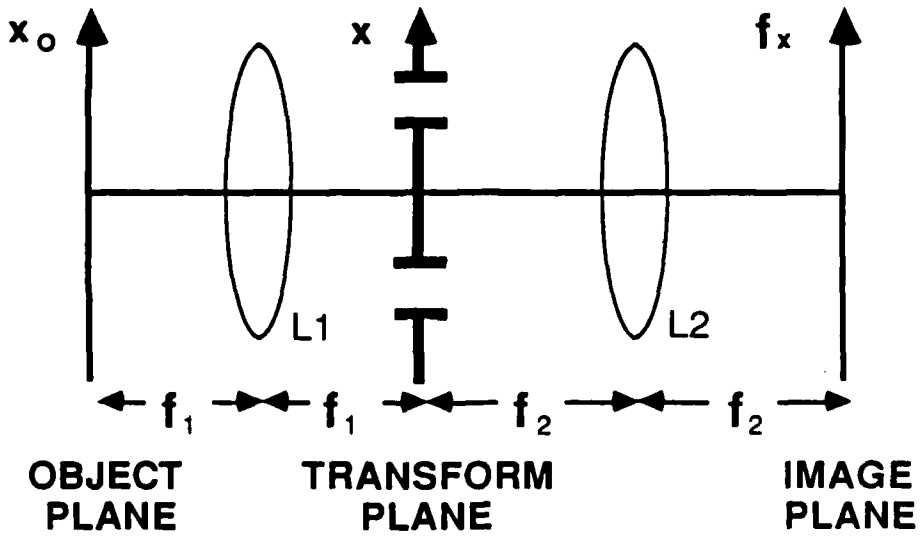

Figure 5. Imaging Configuration used in this Thesis

The object to be imaged is placed in the object plane where it is illuminated by a coherent plane wave. The transforming lens, L1, is a focal length away from the object plane. Therefore the field in the transform plane is proportional to the Fourier transform of the field leaving the object plane. The multiple

aperture is placed in the transform plane, and the imaging lens, L2, produces an image a focal length away at the image plane. This image is actually the Fourier transform of the field just behind the aperture. In other words,

$$U_i(f_x) = F\{F\{U_o(f_x)\} \cdot p(f_x)\} \qquad (6)$$

Equation (6), which was developed from Figure 5, is exactly the same as equation (5), which had been derived from the geometry of an actual multiple aperture imaging system. Since the geometry of Figure 5 is easier to simulate in the laboratory, the imaging conventions implied in that figure will be used throughout this thesis in all theoretical developments.

II.2. Experimental Setup

The experimental setup outlined in Figure 6 is used to produce the images analyzed in this thesis.

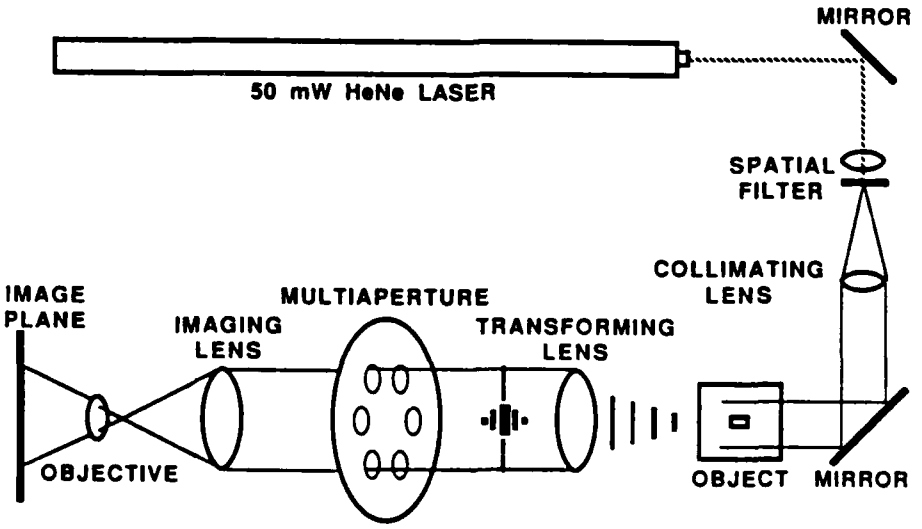

Figure 6. Experimental Setup

In the laboratory, a pinhole was illuminated using a 50mW HeNe laser. The pinhole acted as a spatial filter to clean up the beam. A collimating lens, placed one focal length away, produced a plane wave which illuminated the object to be imaged. The light from the object propagated to the transforming lens which was located one focal length from the object. A focal length past the transforming lens was the transform plane where the multiple aperture was placed. An imaging lens, also one focal length's distance from the transform plane, produced an image that was magnified with a microscope objective. The resulting intensity pattern in the image plane was photographed with a 35mm camera.

II.3. The Impulse Response

Equation (1) implied that the field in the image plane was equal to the field in the object plane, inverted, scaled, and convolved with the impulse response of the aperture. The impulse response of a single circular aperture is the classical Airy pattern (1). The imaging properties of this impulse response have been studied and are well understood (9). However, the impulse response of a multiple aperture system is significantly different from that of a single aperture. Figure 7 shows the impulse responses of a simple circular aperture and a 6-subaperture multiple aperture. One can easily see how a convolution with the multiaperture impulse response will produce a much more complicated result. Each differently configured multiple aperture will possess a slightly different impulse response. (Photographs of the impulse responses of each multiaperture analyzed in this the-

sis can be found in Appendix B.) It is not the objective of this thesis to derive each impulse response, but one possible geometry will be analyzed. This analysis will illustrate how the different geometrical parameters influence the shape of the impulse response.

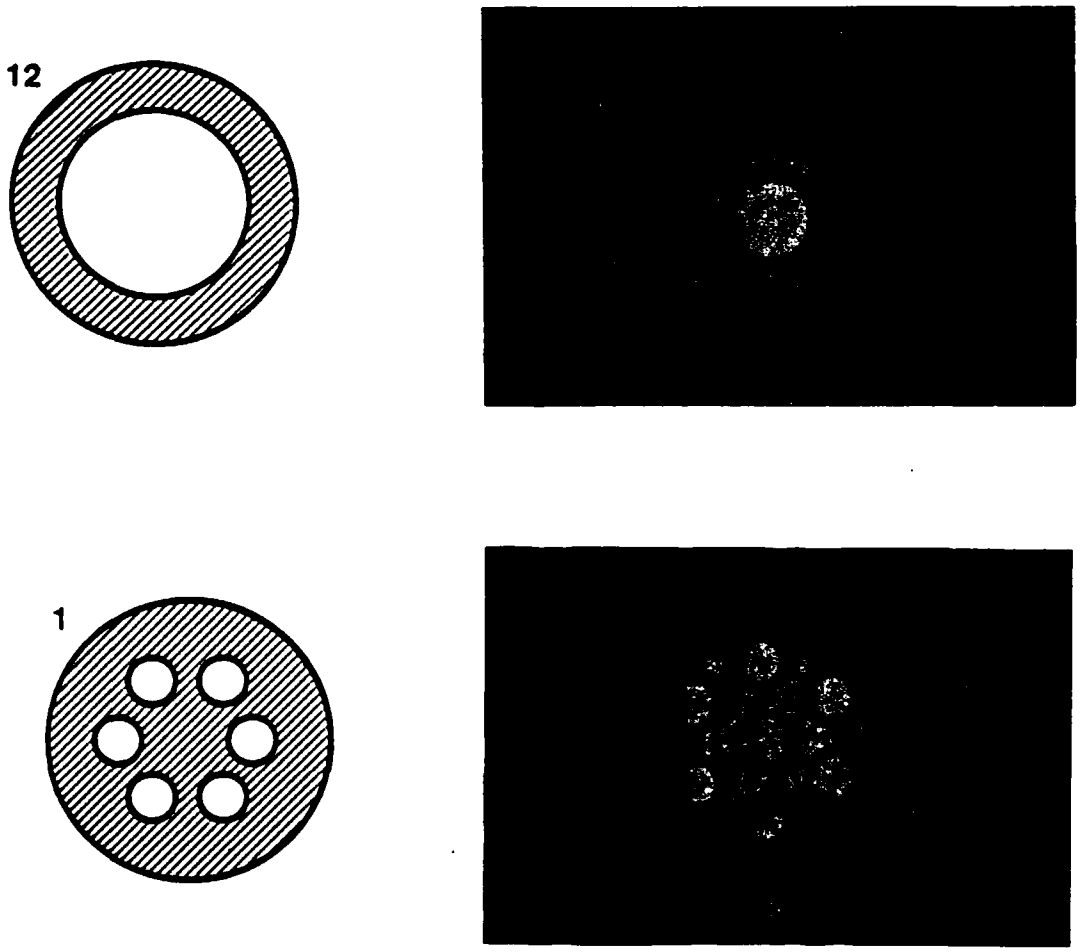

Figure 7. Single Aperture and Multiple Aperture with Corresponding Impulse Responses

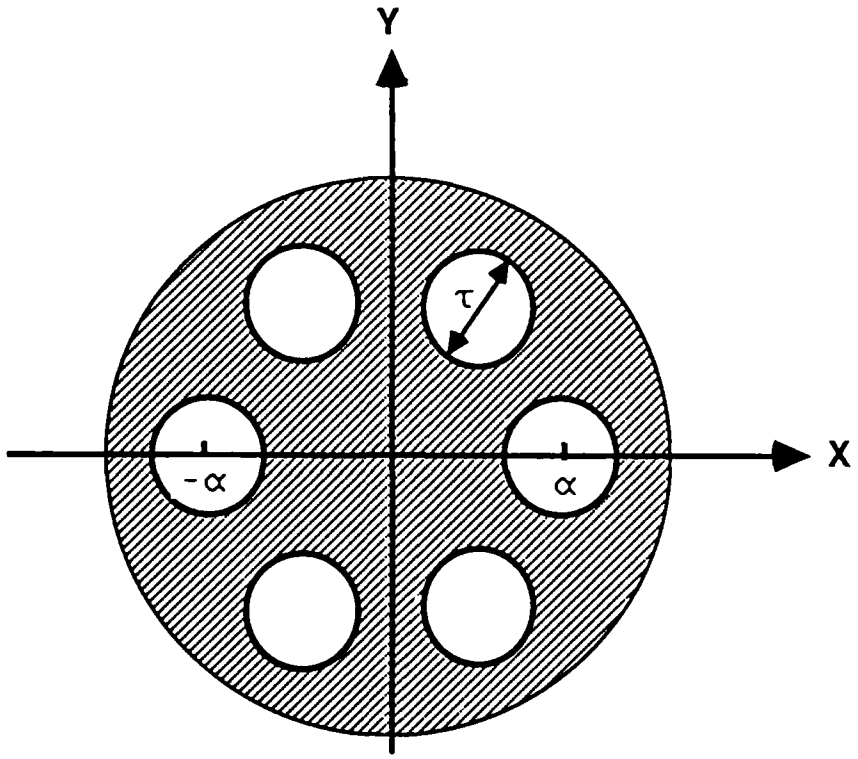

Figure 8. Multiple Aperture Geometry

Mills (10) describes the multiple aperture shown in Figure 8. The pupil function is composed of six identical circular apertures of diameter τ. The centers of each circle are a distance α from the origin and are equidistant from the centers of the nearest neighboring circular apertures. The factor α controls the separation of the sub-apertures but should not be confused with the 'dilution' of the multiaperture. Dilution is normally defined as the diameter of the circle that the sub-apertures are centered on divided by the diameter of a sub-aperture (which in this case equals $2\alpha/\tau$). Mills presents a mathematical representation of the aperture's pupil function as

$$p(x,y) = [g(x,y)\cdot\delta(r-\alpha)] * \mathrm{cyl}(r/\tau), \qquad r^2=x^2+y^2 \qquad (7)$$

where the function $g(x,y)$ represents a skewed two-dimensional comb function described by

$$g(x,y) = \frac{\sqrt{3}(\alpha)2}{2} \sum_{n=-\infty}^{\infty} \sum_{m=-\infty}^{\infty} \delta\left(x + \frac{\alpha n}{2} - \frac{\alpha m}{2}\right) \delta\left(y + \frac{\sqrt{3}\,\alpha n}{2} + \frac{\sqrt{3}\,\alpha m}{2}\right) \quad (8)$$

The circular delta function, $\delta(r-\alpha)$, selects the six delta functions from $g(x,y)$ corresponding to the centers of the six subapertures in Figure 8. Convolving with the cylinder function, $cyl(r/\tau)$, describes circles of diameter τ centered on each of the delta functions. This construction is shown in Figure 9a.

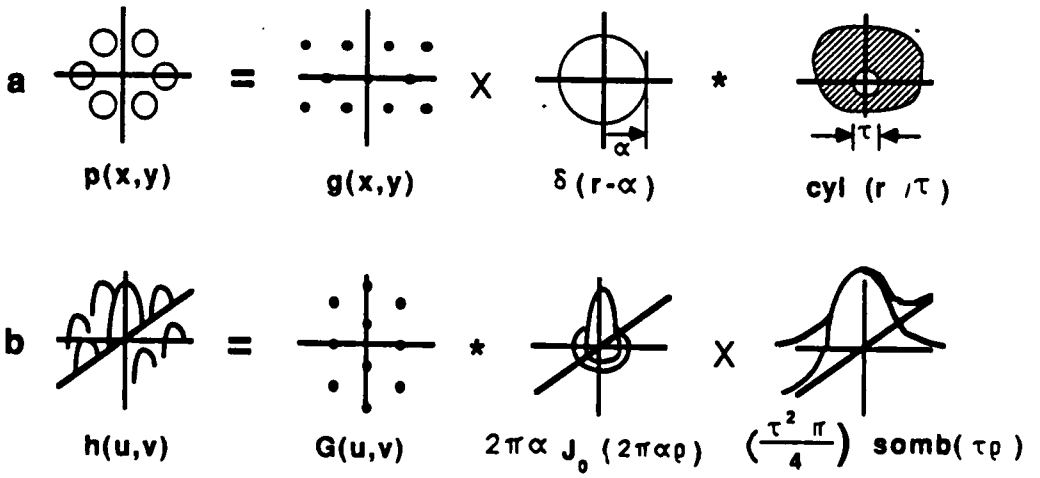

Figure 9. Sketch of Equations (7) and (9)

(a) construction of the pupil function

(b) construction of the impulse response

Taking the Fourier transform of the pupil function gives us the aperture's impulse response.

$$h(u,v) = [G(u,v)*[2\pi\alpha J_0(2\pi\alpha\rho)]].[\frac{\tau^2\pi}{4}somb(\tau\rho)] \qquad (9)$$

where $\rho^2=u^2+v^2$

$G(\ )$, another skewed comb function, is the transform of $g(\ )$

$J_0(\ )$ is the zeroth order Bessel function

and $somb(\ )$ is the Sombrero function.

All of the functions used in equations (7) and (9) are described in the Gaskill text (4) and are sketched in Figure 9.

Although equation (9) is a complicated function, the effects of altering parameters such as the sub-aperture diameter, τ, or the aperture spacing, α, can be directly noted. Keeping the spacing the same and enlarging the sub-aperture radius would cause the somb function envelope to shrink toward the origin. This would result in a lowering of the sidelobes relative to the central peak. Keeping the sub-aperture radius the same but spacing them further apart would cause the zeroes of the Bessel functions to shrink towards their peaks. This would cause more ringing to occur inside of the main somb function peak. This effect is illustrated in Figure 10 where the impulse responses of three of the apertures are shown.

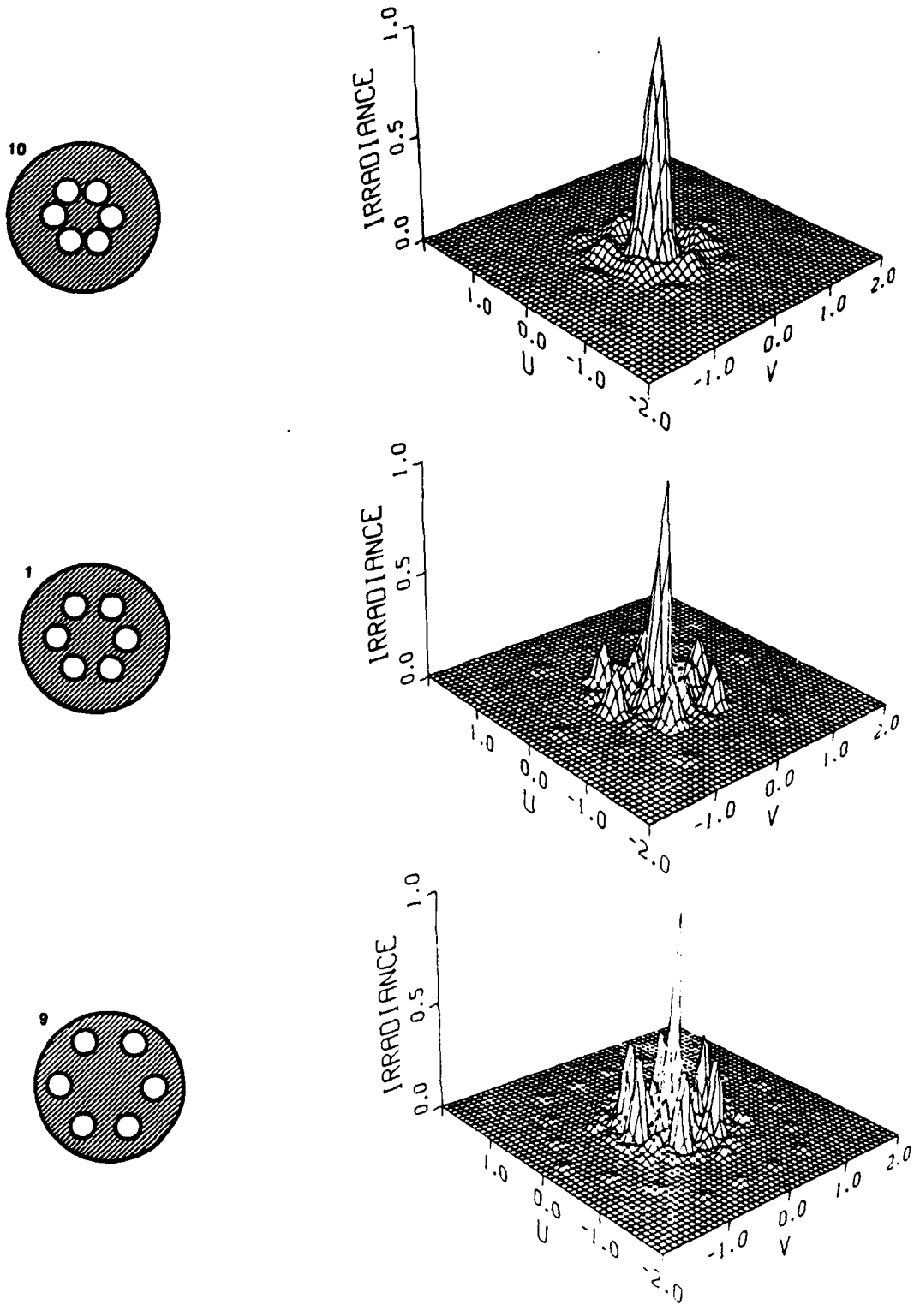

Figure 10. Different Sub-aperture Spacings and their resulting Impulse Responses

These characteristics can be more easily seen if we restrict our attention to the one-dimensional case. Chapter 3 deals with the imaging of 1-D objects, and since the Fourier transform of a 1-dimensional object collapses to being contained along a single axis, this simplification of the impulse response is warranted.

If we assume that the transform of our 1-dimensional object is oriented along the x-axis of Figure 8, then we can define the simpler pupil function, shown in Figure 11, as

$$p(x) = \text{rect}\left[\frac{(x-\alpha)}{\tau}\right] + \text{rect}\left[\frac{(x+\alpha)}{\tau}\right] \qquad (10)$$

The 1-D impulse response, shown in Figure 12, is the Fourier transform of the 1-D pupil function and can be written

$$h(f_x) = 2\tau\ \text{sinc}(\tau f_x)\cdot\cos(2\pi f_x \alpha) \qquad (11)$$

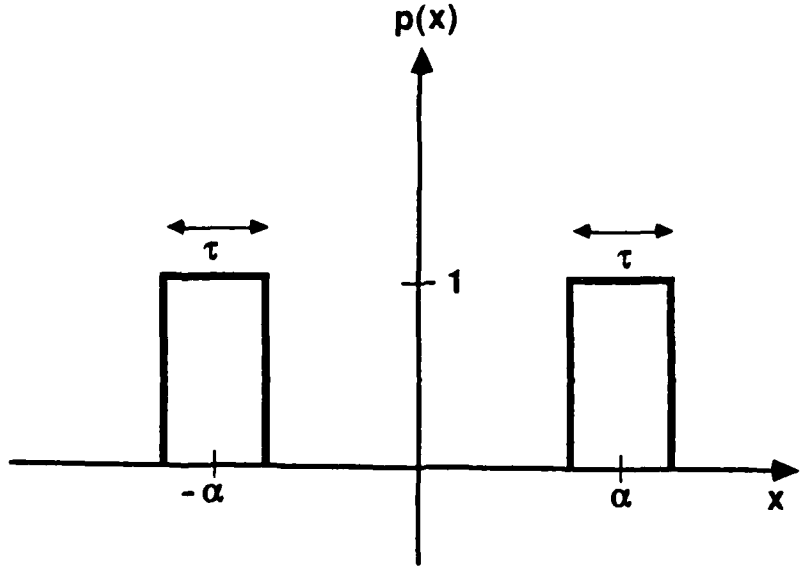

Figure 11. Pupil Function of the 1-D Aperture

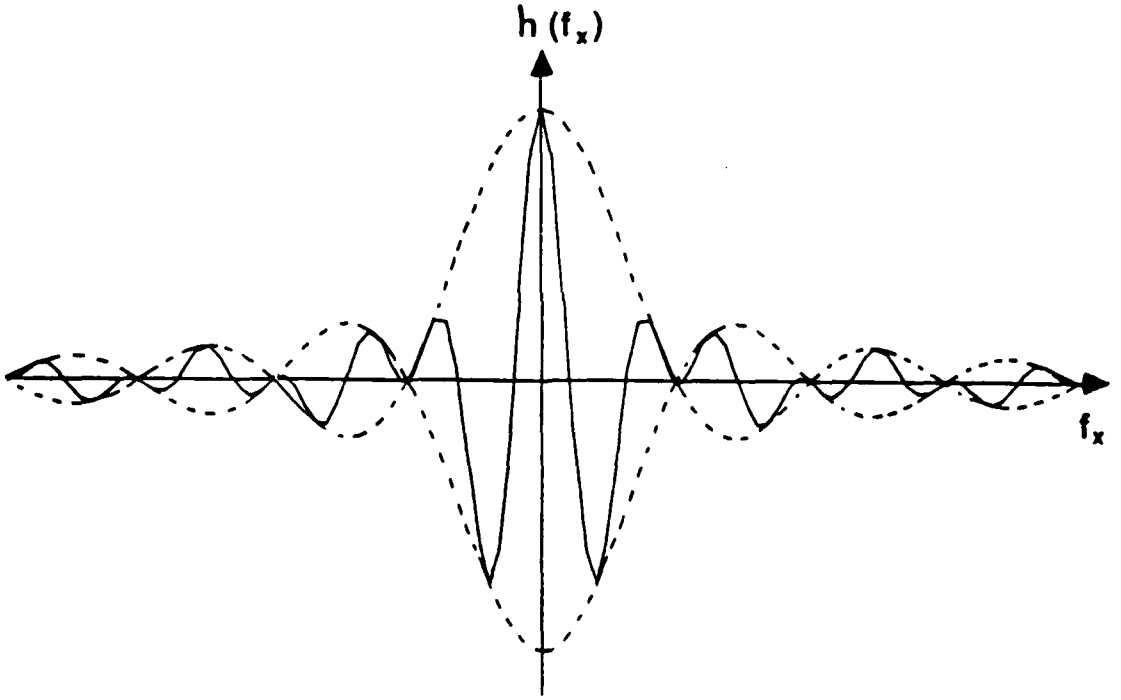

Figure 12. Impulse Response of the 1-D Aperture shown in Fig.11.

From Equation (11), one can easily observe how the sub-aperture diameter and spacing, τ and α, affect the impulse response. If τ is increased, the zeroes of the sinc function envelope shrink towards the origin. This allows fewer cosine fringes to be within the main lobe of the sinc function, and most of the fringes are severely attenuated. If τ is decreased, the sinc envelope spreads out and more of the cosine fringes are inside of the main lobe where they are not as severely attenuated. On the other hand, if α is increased, the cosine fringes squeeze in toward the origin, and more of them move into the main lobe of the sinc envelope. And if α is decreased, the cosine fringes spread out causing fewer to remain inside of the main lobe. In other words, the impulse response will have higher sidelobes if

the sub-apertures' diameters are decreased or their spacing is increased. The sidelobes will be lower if the sub-apertures' diameters are increased or their spacing is decreased. We will see how this affects imaging in the next two chapters.

II.4. Criteria for 'Good' Imaging

If we are to discuss imaging and compare the images produced by different apertures, then we need to define what makes one image 'better' than another image. Since we are imaging simple objects, we will have simple criteria for comparing the images. Obviously we would like to be able to identify the object, so the basic shape must be discernible. We will say that one imaging system is better than another if its images are closer in shape to the corresponding objects. Since our objects contain only edges and no other distinguishing features, we would like to know exactly where those edges are. We will say that one imaging system is better than another if the edges in its images correspond more closely to the actual positions of the object's edges. Finally, we would like to be able to image small objects which would correspond to targets far away. We will say that one imaging system is better than another if it can resolve smaller objects.

II.5. Summary

This chapter outlined our approach to imaging. Section 1 described the general imaging equation and the schematic and conventions that will be used in the theoretical developments of this thesis. Section 2 presented the experimental setup used to create and record the images analyzed in this thesis. Section 3 analyzed the impulse responses of multiaperture imaging systems. Finally, section 4 set criteria for the comparison of imaging systems. With this foundation in imaging, we are prepared to analyze the multiaperture images of specific objects.

III. EDGES AND SLITS

This chapter describes our analysis of the images of one-dimensional objects. The analysis leads to a set of predictions that are tested in the laboratory. Experimental results of edge and slit imaging are then presented and compared to the their predictions.

III.1. Theoretical Analysis (The Image of an Edge)

Figure 13 shows the setup for imaging an edge. In this case, the field in the object plane can be written as

$$u(x_0) = \text{step}(-x_0) \qquad (12)$$

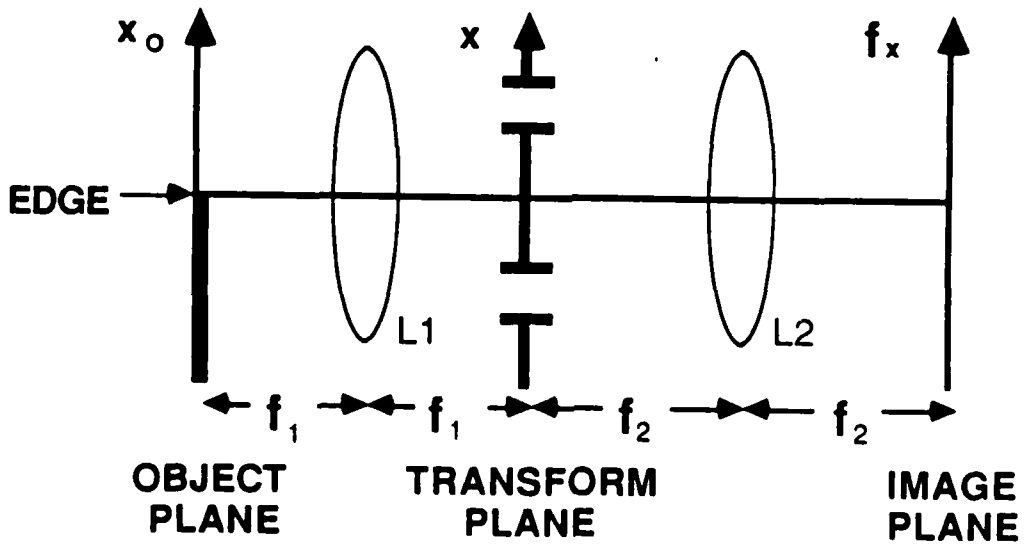

Figure 13. Edge Imaging

The field just before the aperture would then be the Fourier transform of $u(x_0)$.

$$U(f_{x_0}) = F\{u(x_0)\}$$

$$= \tfrac{1}{2}\left[\delta(f_{x_0}) - \frac{1}{j\pi f_{x_0}}\right]\Big|_{f_{x_0}=\frac{x}{\lambda f_1}} \qquad (13)$$

Since the Fourier transform of edges and slits collapse to being contained along a single axis, this chapter will use the 1-dimensional aperture function and impulse response in its analyses. Substituting in for f_{x_0} and multiplying by the aperture's pupil function gives us the field just behind the aperture.

$$U'(x) = \tfrac{1}{2}\left[\delta\left(\frac{x}{\lambda f_1}\right) - \frac{\lambda f_1}{j\pi x}\right]\left[\text{rect}\left(\frac{x-\alpha}{\tau}\right) + \text{rect}\left(\frac{x+\alpha}{\tau}\right)\right] \qquad (14)$$

Since the aperture blocks the very center of the field, the δ-function term drops out, leaving

$$U'(x) = \frac{-\lambda f_1}{2j\pi x}\left[\text{rect}\left(\frac{x-\alpha}{\tau}\right) + \text{rect}\left(\frac{x+\alpha}{\tau}\right)\right] \qquad (15)$$

Now, the field in the image plane will be the Fourier transform of $U'(x)$.

$$v(f_x) = F\{U'(x)\} \qquad (16)$$

$$= \frac{-\lambda f_1}{2}\left[-\text{sgn}(f_x)\right] * \left[2\tau\,\text{sinc}(\tau f_x)\cos(2\pi\alpha f_x)\right]$$

$$= \frac{\lambda f_1}{2}\left[\text{sgn}(f_x)\right] * \left[2\tau\,\text{sinc}(\tau f_x)\cos(2\pi\alpha f_x)\right]$$

The function $sgn(f_x)$ is called a signum function and $2\tau sinc(\tau f_x)cos(2\pi\alpha f_x)$ is the 1-dimensional impulse response derived in the previous chapter. Both of these functions are illustrated in Figure 14.

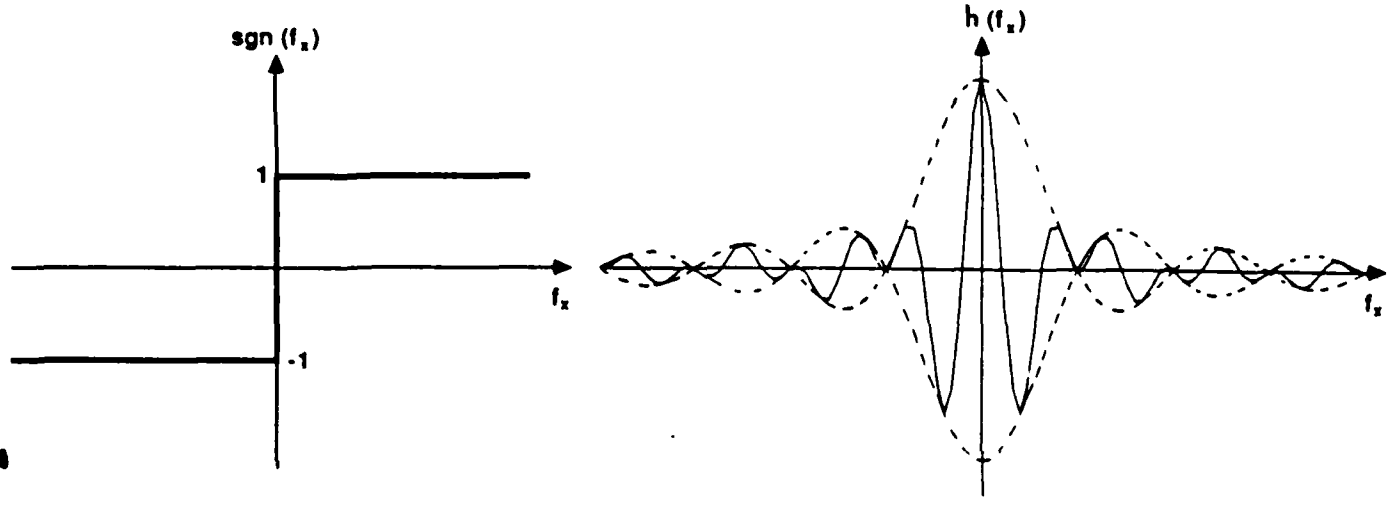

Figure 14. The Signum Function and 1-D Impulse Response

Figure 15a is a sketch of the convolution of the two functions pictured above. The sketch is an example of a possible field distribution in the image plane. Figure 15b is the intensity pattern that would be observed when detecting such a field.

This analysis leads us to expect that when we image an edge through a multiple aperture system with a central block, the result is not a single edge with light on one side and darkness on the other, but rather a series of stripes running parallel to the position of the geometric edge. The stripes on either side of the

actual edge are the brightest (highest intensity), and those further away diminish in a manner similar to the sidelobes of the impulse response. Observing Equation (16), we would also expect the widths and relative intensities of the stripes to depend on the geometrical parameters of the aperture in the same way that the sidelobes of the impulse response do. In other words, the larger the sub-aperture radius, the fewer the number of relatively high intensity stripes. Also, a larger spacing between sub-apertures would cause the stripes to be narrower and cause more of them to have a high relative intensity.

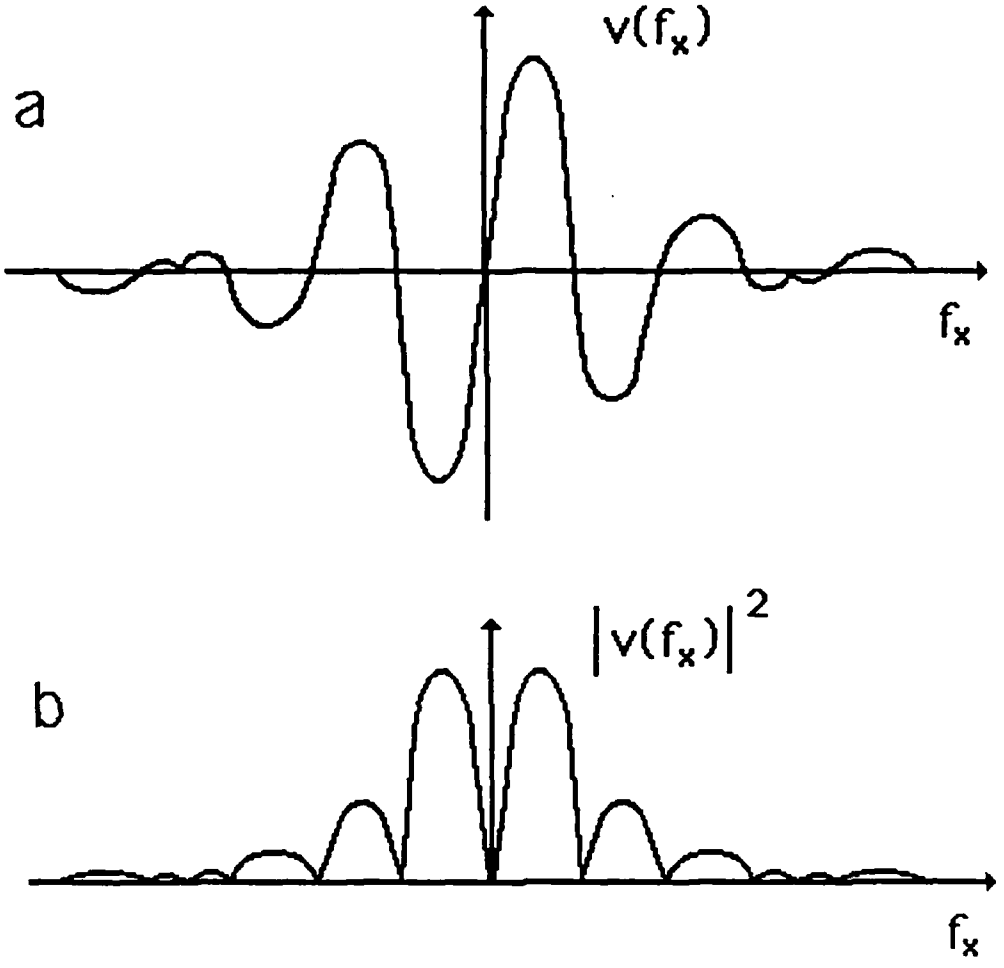

Figure 15. Multiple Aperture Image of an Edge

(a) field distribution in the image plane

(b) intensity pattern in the image plane

III.2. Summary of Predictions for Edge Imaging

1) The intensity pattern will be a series of stripes.

The analysis in the previous section concluded that the multiaperture image of an edge will not be a single line dividing light from darkness, but rather a series of stripes. This is quite different from the coherent and incoherent images of an edge as seen through a single aperture. (see Figure 16.)

2) The stripe pattern will be centered on the actual edge.

Figure 15 revealed that the intensity pattern will have a zero at the origin, which is the position of the actual edge being imaged. Since the stripe pattern is centered on the origin, the exact position of an edge can be easily determined from a multiple aperture image of that edge. It is exactly at the center of the stripe pattern. One should note that this is not the case for an edge imaged through a single aperture, as evidenced by Figure 16.

3) The stripe pattern will be brightest near the actual edge.

The previous section concluded that the relative intensity of the stripes will drop off and approach zero as we move away from the actual position of the edge. In this way, multiple aperture imaging acts as an edge enhancement procedure. This makes sense since the multiaperture effectively blocks the low spatial frequency components of the object's Fourier transform. This feature becomes more evident in Chapter 4 when 2-dimensional objects are analyzed.

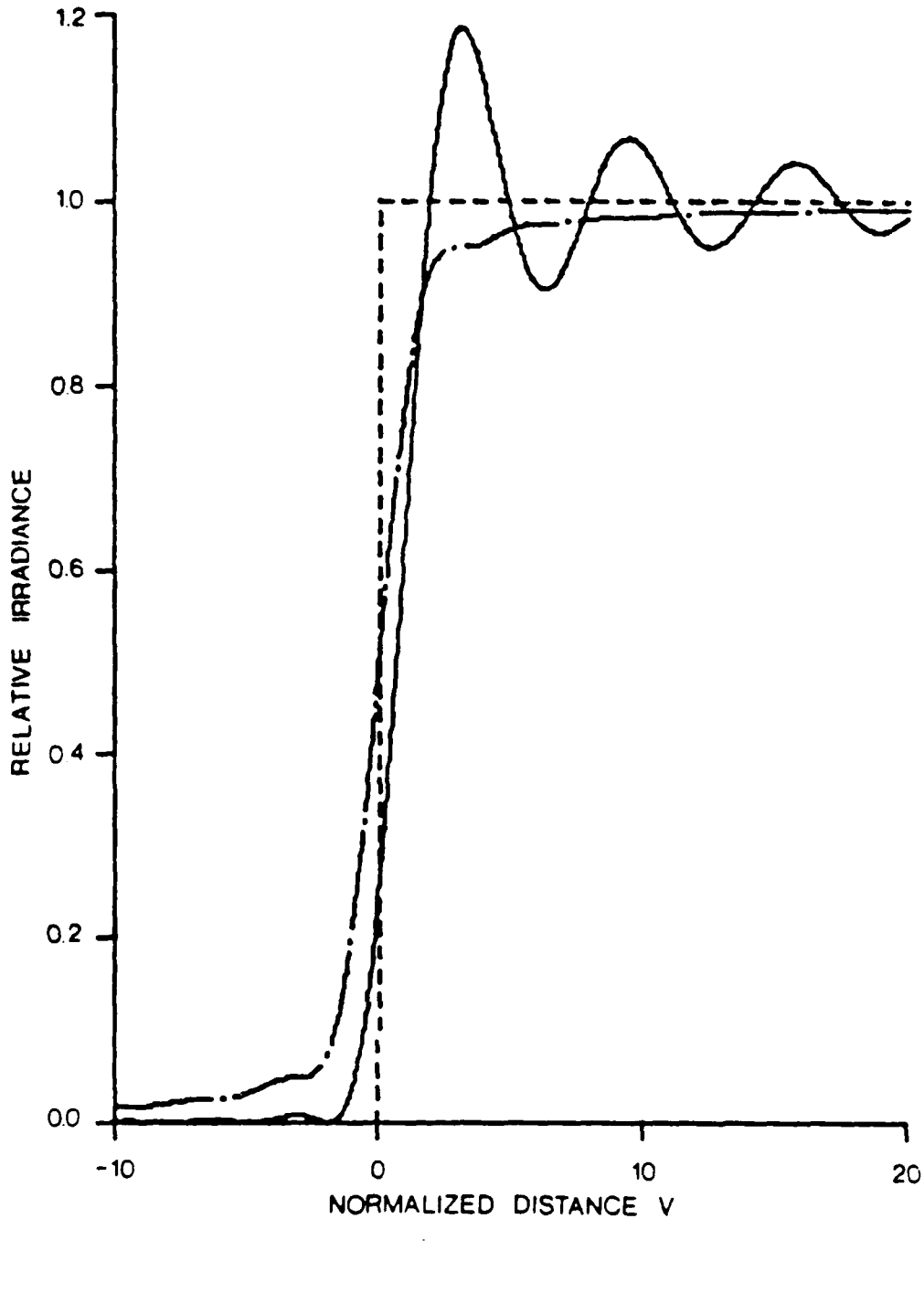

Figure 16. Edge imaged through a Single Aperture

(————coherent, —·—·—incoherent, -------actual position of edge)

4) The spacing of the stripes and their relative intensities will depend upon the geometrical parameters of the multiple aperture.

As Equation (16) implies, the shape of the stripe pattern depends on the diameter of the sub-apertures and their spacing, in the same way the aperture's impulse response does. Smaller sub-apertures or larger spacings will cause the stripes to be closer together and more of them to have a relatively high intensity. Larger sub-apertures or smaller spacings will produce fewer bright stripes, and the stripes will be spaced further apart.

III.3. Experimental Results of Edge Imaging

The first object that was imaged in the laboratory was an edge. Figure 17 is a picture of the edge as imaged through a single aperture (Aperture-12). The characteristic ringing associated with coherent imaging is evident. This same edge, when imaged through a multiple aperture, appears quite different. Figure 18 shows the results of imaging the edge through Aperture-1.

Figure 17. Edge Imaged through Aperture-12

Figure 18. Edge Imaged through Aperture-1

This image is consistent with predictions 1-3 discussed in section III.2. The intensity pattern is indeed a series of stripes. The actual edge is located at the center of the pattern, with three bright stripes on either side of it. The position is a zero and can be easily located. As was predicted, the stripe pattern is brightest near the edge. The relative intensities of the stripes fall off to zero then rise slightly and fall off again in a pattern expected from the convolution with the impulse response of the aperture. Images of the edge as viewed through some other multiple apertures are shown in Figure 19.

Analyzing the images in Figure 19 prove that prediction 4 was also correct. Aperture-10 has the same size sub-apertures as Aperture-1, but they are spaced closer together. As expected, the stripes are therefore wider, and less of them fall within the mainlobe of the sinc envelope. The images of Aperture-3 and Aperture-9 also confirm our predictions. Aperture-9 has larger sub-apertures than Aperture-3, and therefore its impulse response produced an image with a narrower bright area. This is because larger sub-apertures produce a narrower sinc envelope. The sub-apertures of Aperture-9 are also spaced further apart than those of Aperture-3. According to our predictions, this should cause the stripes to be narrower and closer together. Both of these characteristics can be noted in Figure 19.

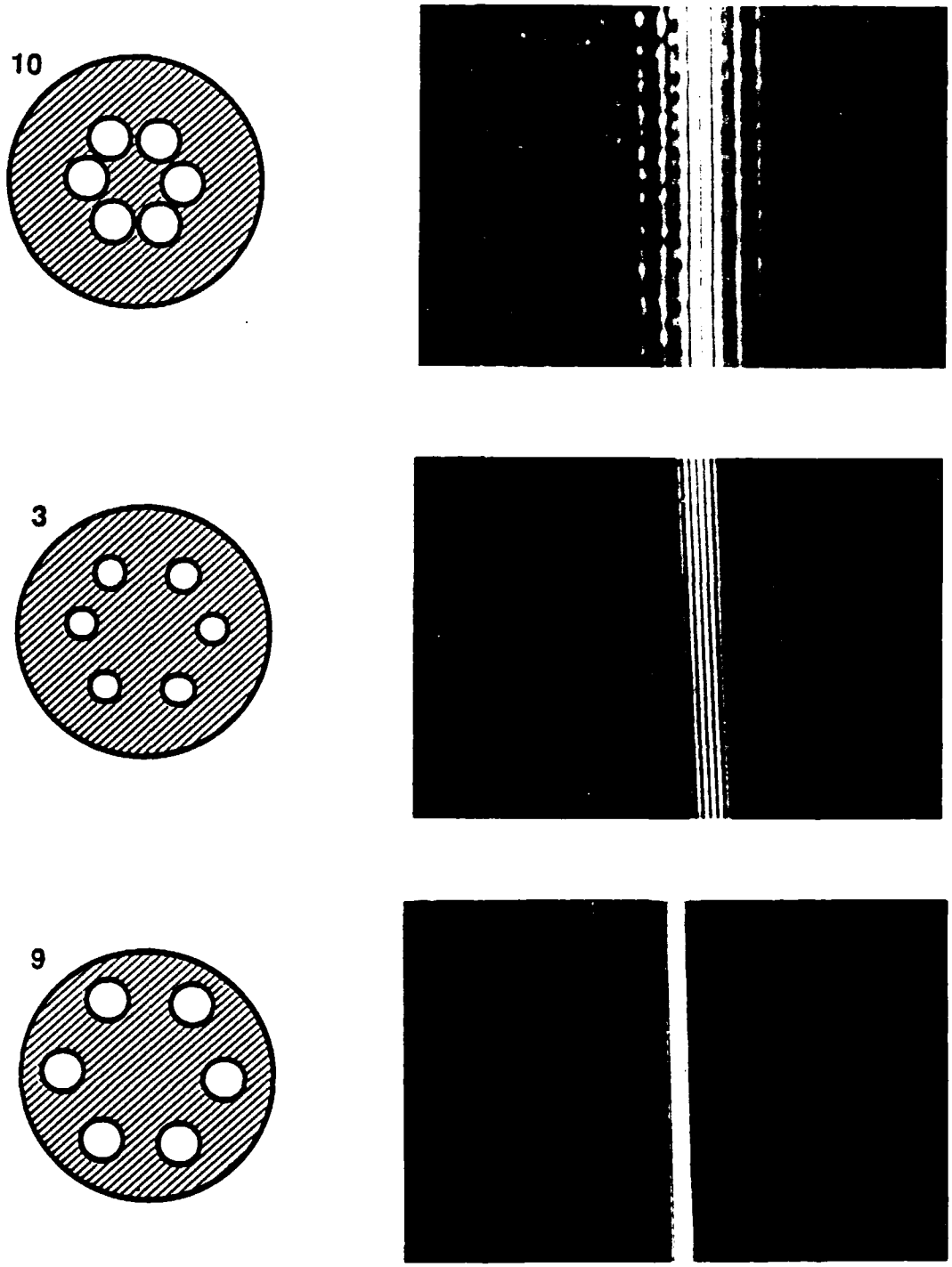

Figure 19. Edge Imaged through Apertures 10, 3, and 9

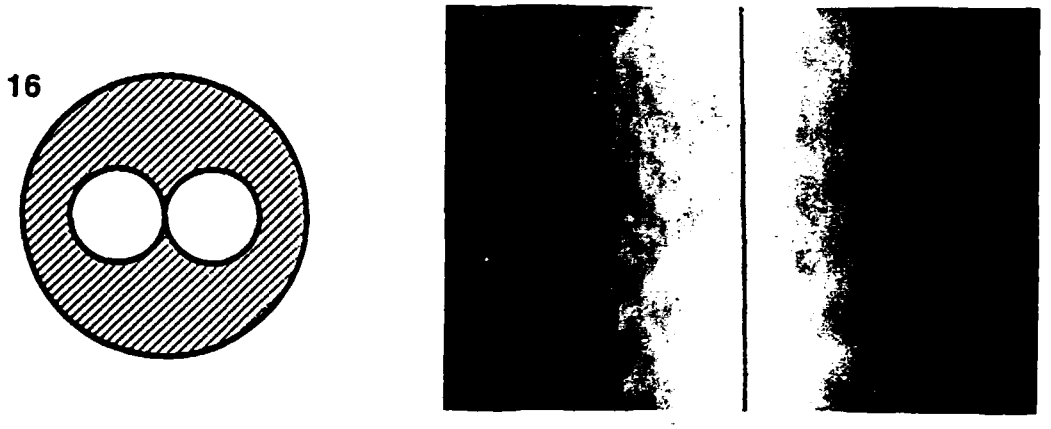

Figure 20. Edge Imaged through Aperture-16

Figure 20 illustrates just how easily the edge can be located in a multiaperture image. The configuration of Aperture-16 yields a mass of stripes of the same relative intensity. But they are perfectly centered on one dark line. This line is the actual position of the edge.

One must remember that these images were produced with the aperture oriented such that the transform of the edge fell along the x-axis of Figure 8. Had the aperture been rotated slightly, it would have blocked out the entire transform, and no images would have been observed.

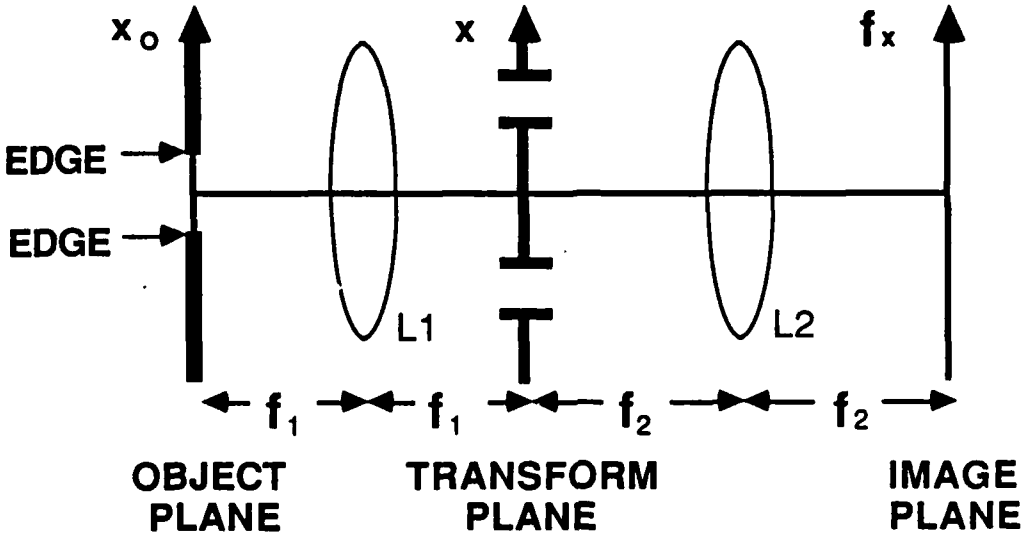

Figure 21. Slit Imaging

III.4. Theoretical Analysis (The Image of a Slit)

After imaging an edge, the next logical step is to add a second edge and image the resulting slit. Figure 21 shows the setup for imaging a slit. The field in the object plane can be written as

$$u(x_o) = \text{rect}\left(\frac{x_o}{\beta}\right) \qquad (17)$$

This function is illustrated in Figure 22.

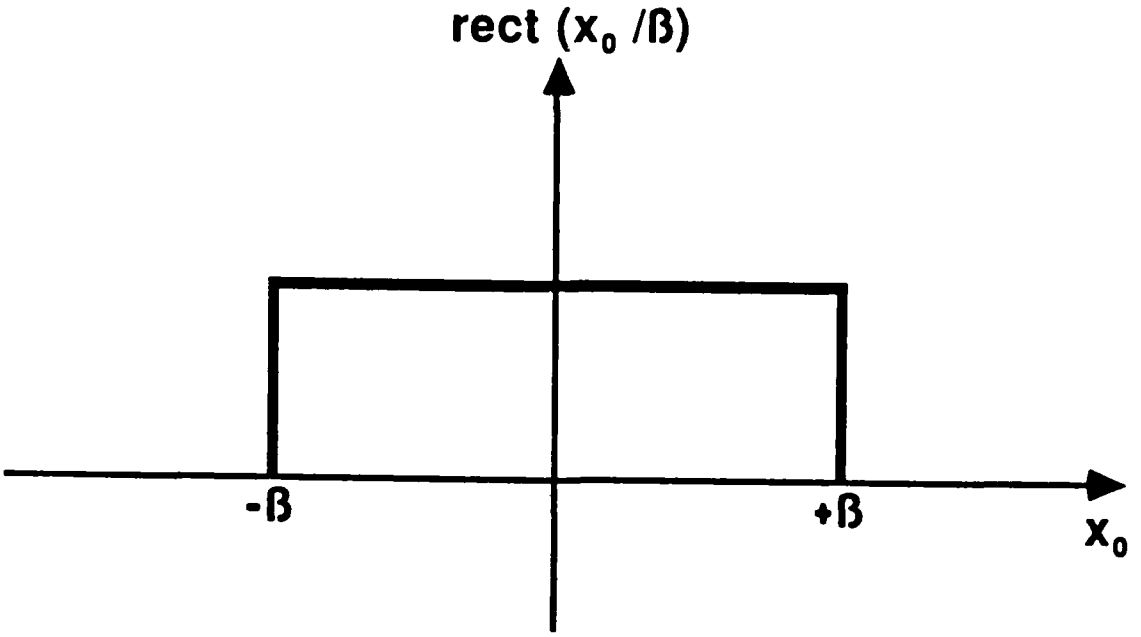

Figure 22. Field in Object Plane for Slit Imaging

$u(x_0)$ can also be expressed as follows

$$u(x_0) = \text{step}(x_0+\beta) - \text{step}(x_0-\beta) \tag{18}$$

We will use Equation (18) so that the analysis will be very similar to that of a single edge. In this case, the field just before the aperture is

$$U(f_{x_0}) = F\{u(x_0)\}$$

$$= \tfrac{1}{2}\left[\delta(f_{x_0}) + \frac{1}{j\pi f_{x_0}}\right]\exp(j2\pi f_{x_0}\beta)$$

$$- \tfrac{1}{2}\left[\delta(f_{x_0}) + \frac{1}{j\pi f_{x_0}}\right]\exp(-j2\pi f_{x_0}\beta)$$

$$= \left[\delta(f_{x_0}) + \frac{1}{j\pi f_{x_0}}\right]\left[j\sin(2\pi\beta f_{x_0})\right] \tag{19}$$

where $f_{x_0} = \dfrac{x}{\lambda f_1}$.

Multiplying by the aperture's pupil function gives the field just behind the aperture.

$$U'(x) = \frac{\lambda f_1}{j\pi x}\left[j\sin\left(\frac{2\pi\beta x}{\lambda f_1}\right)\right]\left[\text{rect}\left(\frac{x-\alpha}{\tau}\right) + \text{rect}\left(\frac{x+\alpha}{\tau}\right)\right] \qquad (20)$$

Once again the aperture blocks out the very center of the field, so the delta-function was dropped. The field in the image plane is the Fourier Transform of the field just after the aperture.

$$v(f_x) = F\{U'(x)\} \qquad (21)$$

$$= -\lambda f_1 \text{sgn}(f_x) * \left[-\tfrac{1}{2}\left[\delta\left(f_x + \frac{\beta}{\lambda f_1}\right) - \delta\left(f_x - \frac{\beta}{\lambda f_1}\right)\right]\right] * \left[2\tau\,\text{sinc}(\tau f_x)\cos(2\pi\alpha f_x)\right]$$

$$= \lambda f_1 \tau\left[\text{sgn}\left(f_x + \frac{\beta}{\lambda f_1}\right) - \text{sgn}\left(f_x - \frac{\beta}{\lambda f_1}\right)\right] * \text{sinc}(\tau f_x)\cos(2\pi\alpha f_x)$$

where $f_x = \frac{x_i}{\lambda f_2}$.

Equation (21) says that the field in the image plane is the difference of two signum functions convolved with the impulse response. The difference of the two signum functions produces the rect function shown in Figure 23. It is more straightforward, however, to analyze the function as the combination of two signum functions. In that case, the result of the convolution will be the sum of two edge fields, one flipped about its edge with respect to the other. Figure 24 shows a sketch of a possible field distribution and intensity pattern.

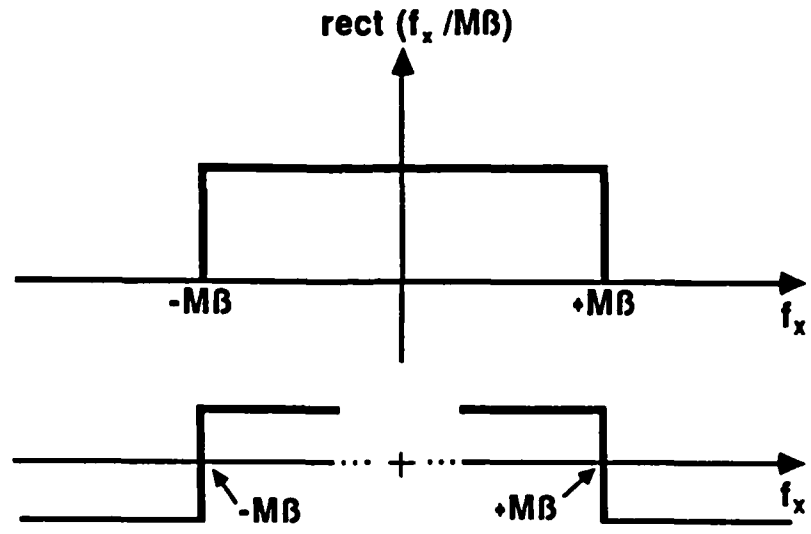

Figure 23. Rect Function and Sum of Signum Functions

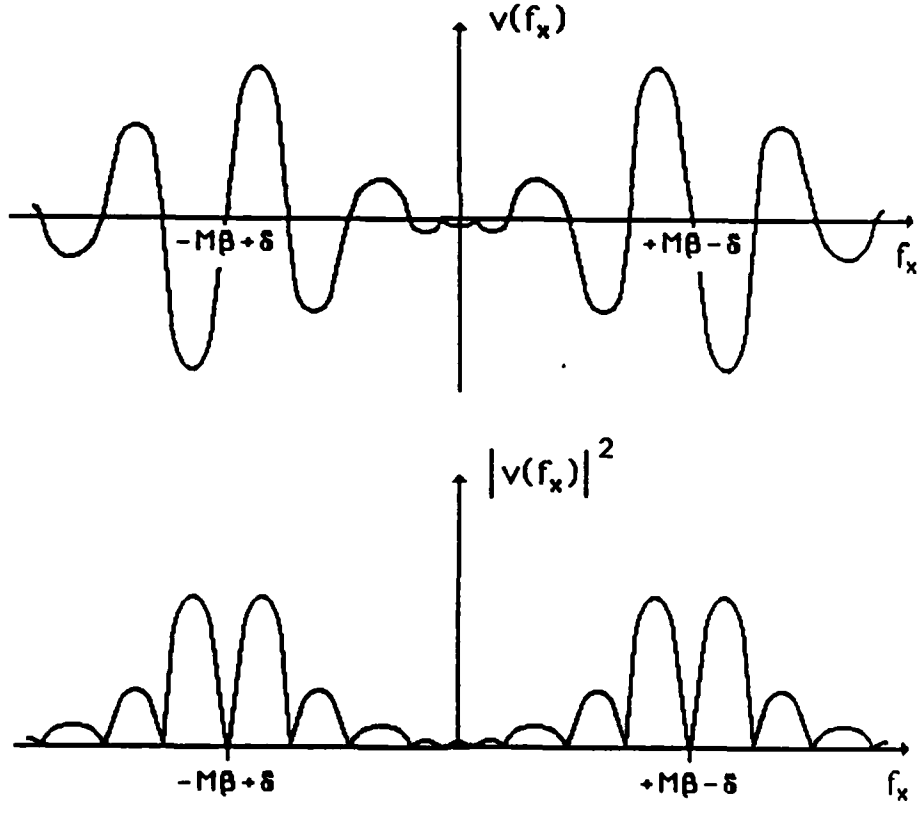

Figure 24. Multiple Aperture Image of a Slit

(a) field distribution in the image plane

(b) intensity pattern in the image plane

III.5. Summary of Predictions for Slit Imaging

1) The intensity pattern will be the summation of two 'single edge' intensity patterns.

In the previous section the image of a slit was shown to be the sum of the fields produced by each of the slit's edges. The intensity pattern will be a series of stripes, with the most intense stripes being located near the two edges. The width, spacing, and relative intensity of the stripes will depend on the geometrical parameters of the aperture in the same way they did for single edge imaging.

2) The edges in the slit image may be shifted from their actual positions.

Figure 24 implied that the slit is magnified (by the factor M) when imaged, and the edges have shifted (by the factor δ). This 'edge shift' is attributed to the fact that two fields are being added. The zero corresponding to the position of one edge will remain unshifted only if the field produced by the other edge also has a zero at that location. Otherwise, when the two fields are added, the resulting field will have a zero that is slightly displaced from the original position. This phenomenon is illustrated in Figure 25. Figure 25.1a shows the case in which both fields have zeros at the actual position of the edge. The sum of these two fields is shown in Figure 25.1b. In this case, the edge does not shift. In Figure 25.2a the slit is slightly narrower, and the field produced by the left edge does not have a

zero where the right edge is located. Therefore, the resulting field, shown in Figure 25.2b, has a shifted edge. By symmetry, the left edge will be shifted by the same amount but in the opposite direction.

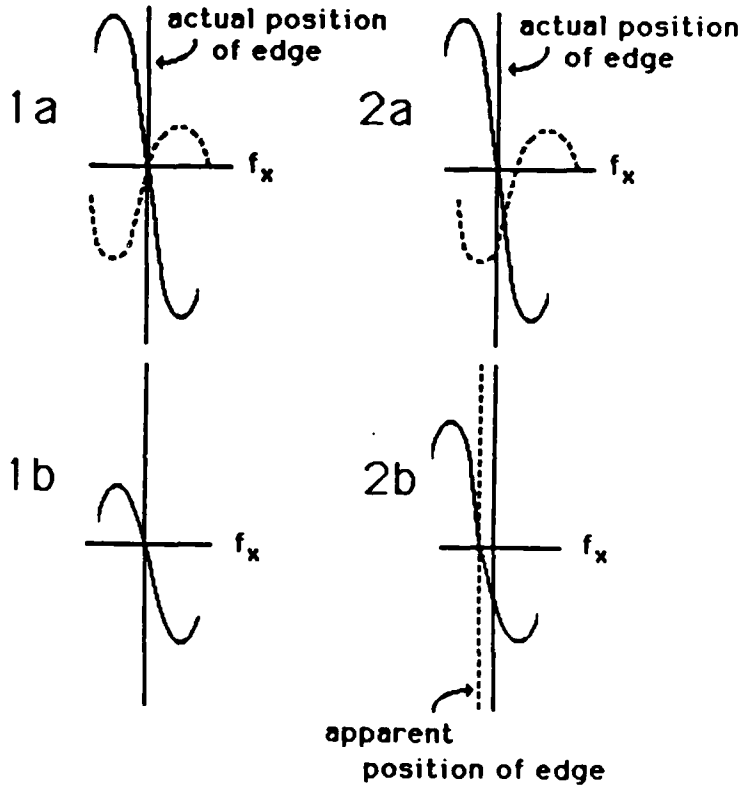

Figure 25. Edge Shift

(------- field from left edge, ——— field from right edge)

1a) Case 1: Both fields have zeros at the location of the edge

1b) Sum of fields corresponding to Case 1. NO EDGE SHIFT

2a) Case 2: Field from left edge doesn't have zero at right edge

2b) Sum of fields corresponding to Case 2. EDGE SHIFT

This edge shift will only be significant when imaging very small objects. Since the field from each edge falls off to zero, an edge shift will only be noticeable when the edges are very close together. It is possible to predict, for a given aperture, what the edge shift will be for a specific slit width. The computer program Delta, described in Appendix C, makes such a prediction. Figure 26 is an example of the output from this program. All parameters are determined with respect to the left edge. The Half-Width of Slit is the distance (in number of pixels) from the center of the slit to the left edge, assuming no edge shift. A positive edge shift indicates the edge will appear shifted to the right of its actual position. A negative edge shift indicates a shift to the left. Edge shift units are also pixels.

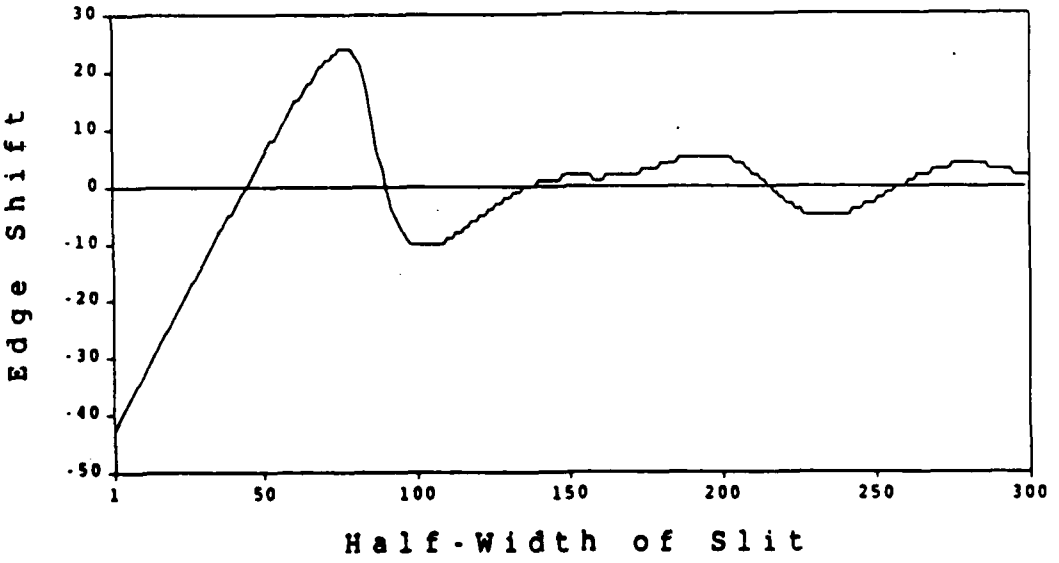

Figure 26. Computer Prediction of Edge Shift

For the particular aperture being analyzed, the computer program predicts significant edge shifting for slits of widths

less than about 200 pixels. (This cutoff was arbitrarily chosen as the maximum slit width for which an edge shift of 10 pixels occurs. In Figure 26, this cutoff occurs at a half-width of approximately 100.) For a different aperture, one with its sub-apertures spaced further apart, the computer program outputs the prediction shown in Figure 27. In this case, the maximum edge shift is less, and the cutoff for significant edge shift has decreased. In other words, this aperture can image smaller objects with less edge shift.

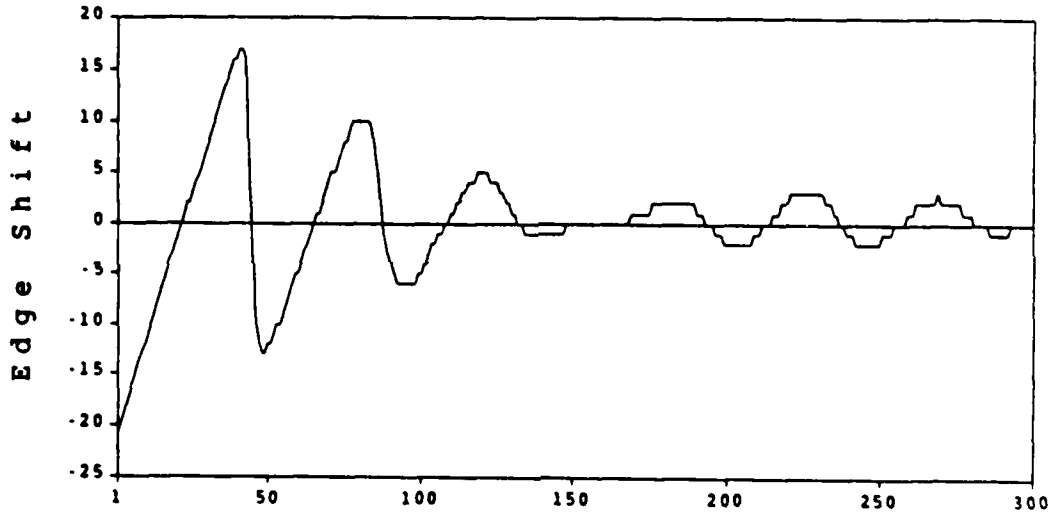

Figure 27. Edge Shift for Aperture with Sub-apertures spaced further apart than those used to produce Fig. 26

This result seems intuitively pleasing. Since a multiple aperture with its sub-apertures spaced further apart is synthesizing a larger aperture, one should expect it to exhibit better resolution. An extended analysis of the resolution of multiaperture systems can be found in the thesis by Watson (13).

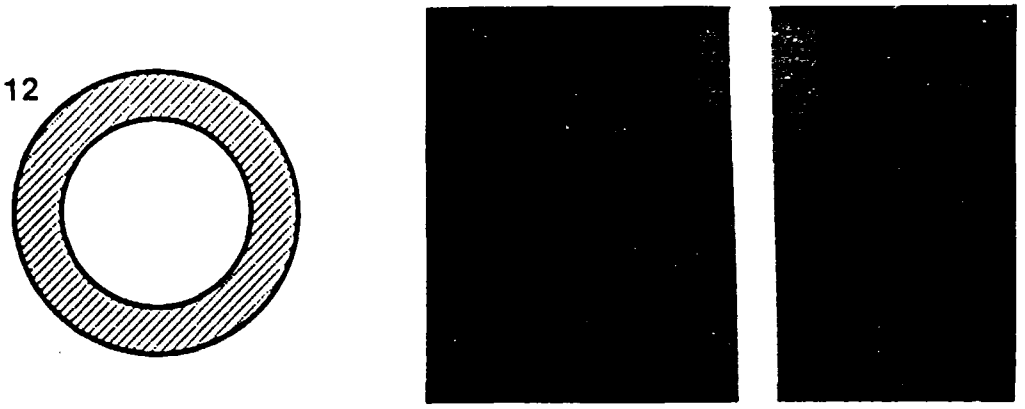

Figure 28. Slit Imaged through Aperture-12

III.6. Experimental Results of Slit Imaging

Figure 28 is a picture of a slit as imaged through a single aperture. The edges in the image are sufficiently 'sharp' as to lead one to say that this aperture was large enough to resolve the slit. On the other hand, when imaged through a smaller aperture, the edges of the slit become blurred, as shown in Figure 29.

Figure 29. Slit Imaged through Aperture-14

(One should note that the location of the actual edges of the slit are not easily discernible even in Figure 28. As implied by Figure 16, the actual position of the edge in the image is one quarter of the way up the intensity profile.) It would seem that Aperture-14 is just too small to resolve the slit. But if six apertures, the same size as Aperture-14, are arranged into the configuration of Aperture-1, then the image of Figure 30 can be produced. We have effectively 'synthesized' a larger aperture with a greater resolving power. In fact, the actual edges of the slit can be located exactly (using a plot like that of Fig. 27) when imaging through this multiple aperture.

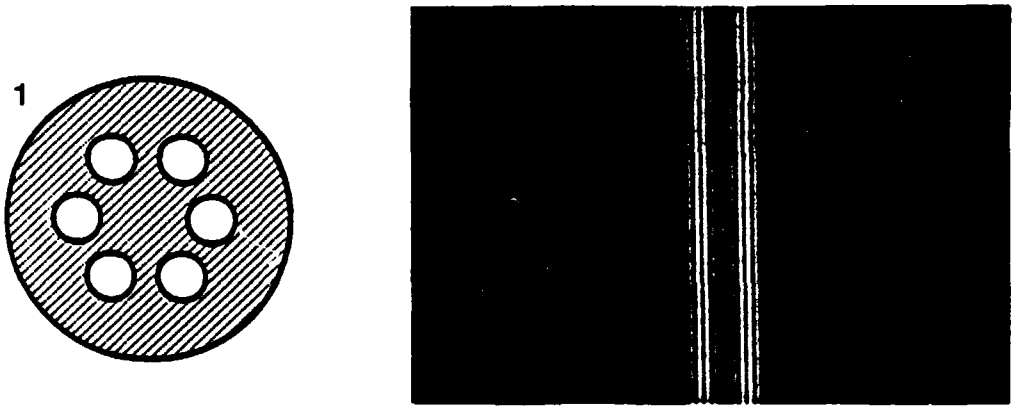

Figure 30. Slit Imaged through Aperture-1

The same slit was imaged through various other multiaperture configurations. These images are shown in Figures 31 and 32.

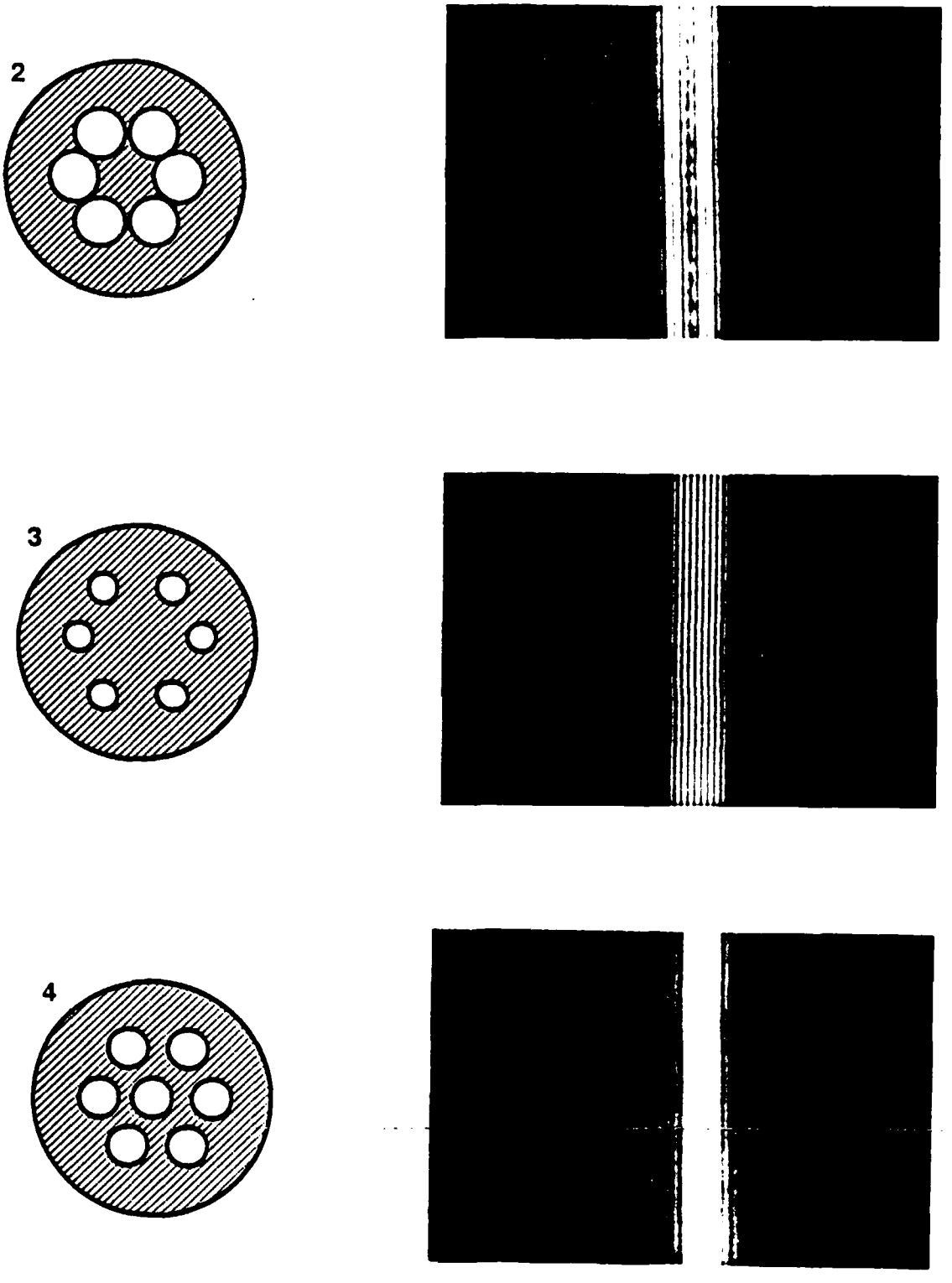

Figure 31. Slit Imaged through Apertures 2, 3, and 4

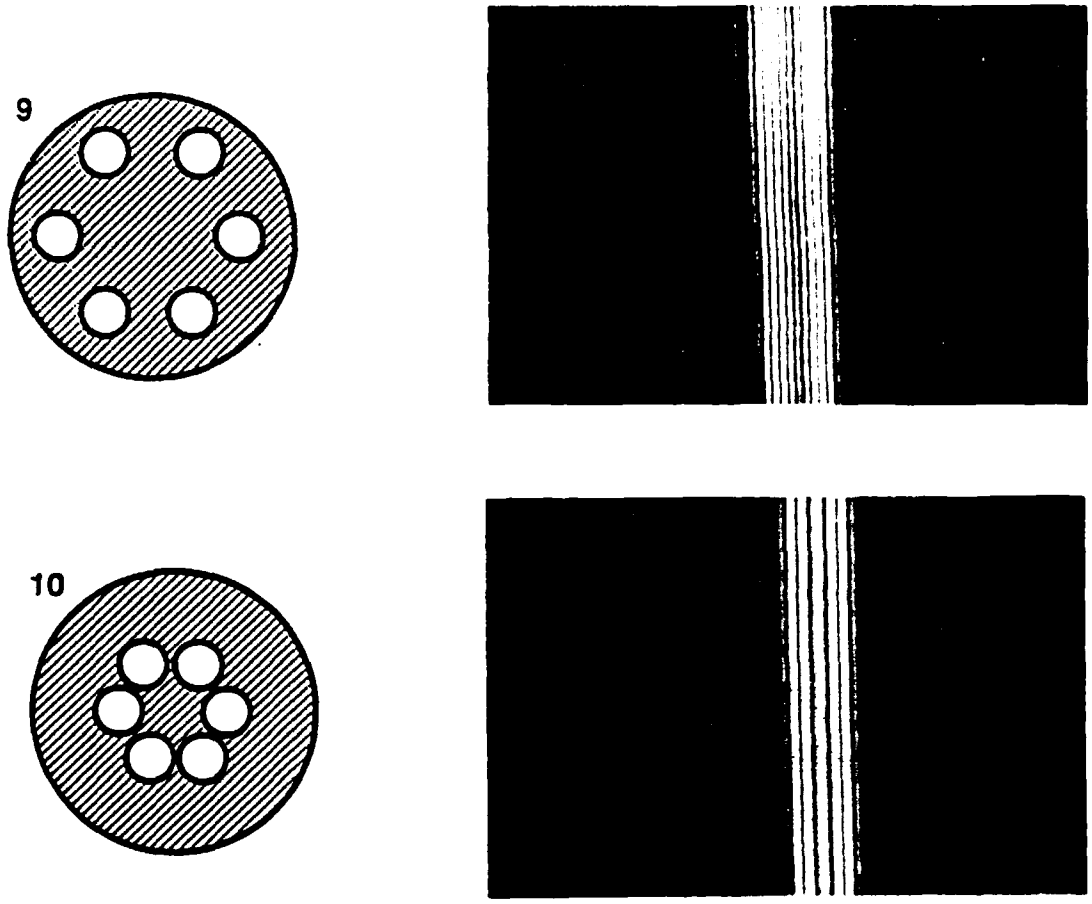

Figure 32. Slit Imaged through Apertures 9 and 10

These experimental observations once again confirm the predictions of the preceding section. Apertures 1-3 have different size sub-apertures. This affects the number of relatively high intensity stripes bordering each edge by shrinking or enlarging the sinc envelope in their impulse responses. Aperture-4 is the same as Aperture-1 except that it also contains a central sub-aperture. This central sub-aperture allows the dc component of the field through and produces an image with a shape closer to that of the object, but the locations of the edges have been lost.

Apertures 9 and 10 have the same size sub-apertures as Aperture-1, but they are at different spacings. This affects the widths and spacings of the individual stripes. Aperture-10, which had the smallest sub-aperture spacing, produced the widest stripes. Conversely, Aperture-9 produced the narrowest stripes.

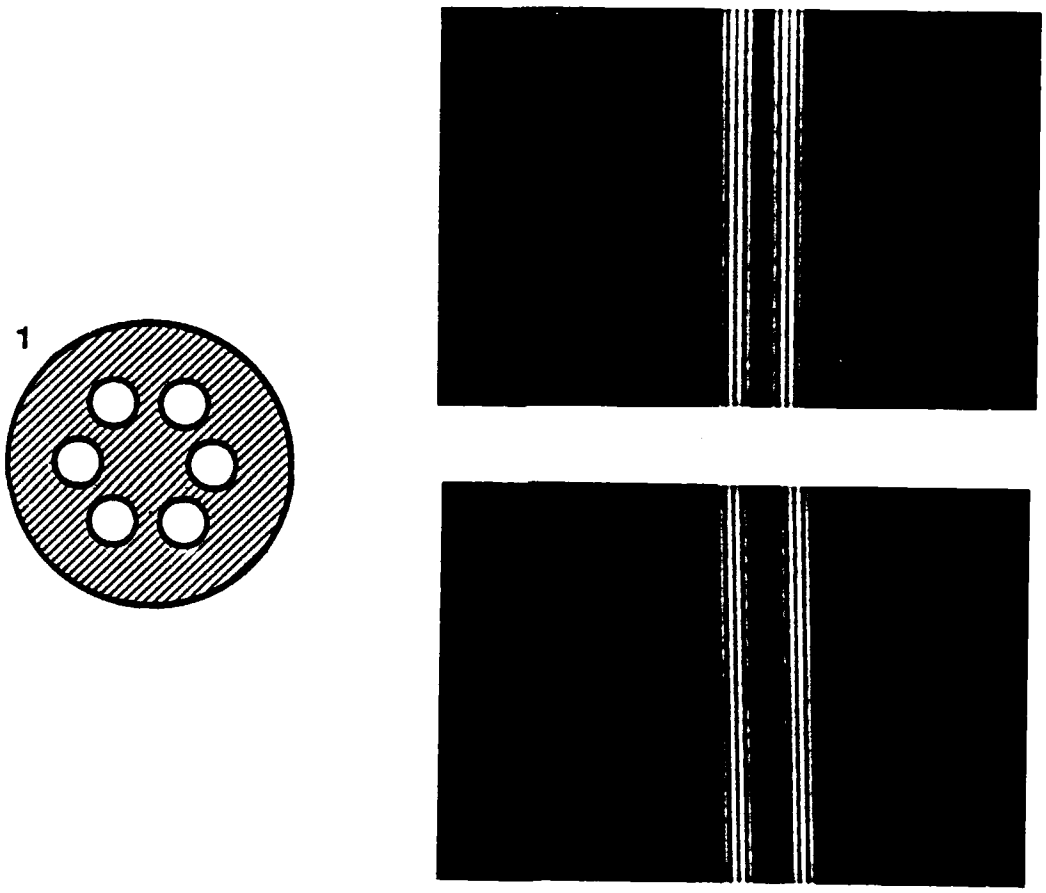

Figure 33. Images of Slits with Different Widths

Figure 33 shows the images of two slits as seen through Aperture-1. Although the slits have different widths, the stripe patterns about each edge are exactly the same for both images. This confirms the fact that a slit image is the sum of two edge

fields. Since a given aperture has a unique edge field, slits imaged through the aperture will exhibit the sum of two such edge fields, spaced accordingly.

Limitations in the slit positioner precluded the verification of the edge-shift phenomenon. The author believes that detailed measurements, wherein one edge can be accurately positioned with respect to the other, will confirm the predicted edge-shifts.

III.7. Summary

This chapter described the theoretical predictions and experimental results of imaging one-dimensional objects through multiple aperture systems. Section 1 developed the theoretical analysis of edge imaging. Then, section 2 summarized what one would expect to observe in the laboratory. Section 3 presented the actual experimental results of edge imaging and compared the results to the predictions of section 2. Section 4 outlined the theoretical analysis of slit imaging, while section 5 summarized the predicted observations of slit imaging. Finally, section 6 presented the laboratory results of slit imaging and compared the results to the predictions of section 5. After gaining this understanding of multiaperture imaging of one-dimensional objects, one can now turn to the more complicated case of two-dimensional objects.

IV. RECTANGLES AND CIRCLES

This chapter deals with the imaging of 2-dimensional objects. A logical progression from 1-D to 2-D objects would be to add two more edges to the previously analyzed slit, making it into a rectangle. In the case of 2-dimensional objects, the Fourier transform does not collapse to being contained along a single axis as in the 1-D case. In fact, spatial frequency information can be distributed anywhere in the two-dimensional transform plane (aperture plane). Therefore, the simplified 1-D impulse response derived in section II.3 cannot be used. Since the 2-D impulse response described by Equation (9) does not lend itself to a manageable analytical analysis, the prediction of 2-dimensional multiaperture images was left to a computer. The imaging programs, described in Appendix D, were run on a VAX 11-780. The intensity pattern arrays were displayed as images on an Evans and Sutherland PS-300 terminal. These images were then photographed and were used to predict what the 2-D images would look like in the laboratory.

IV.1. Theoretical Analysis (The Image of a Rectangle)

The Fourier transform of a rectangle is sketched in Figure 34. The image of the rectangle will depend on the orientation of the aperture. In this section, we will assume that all apertures are oriented as shown in Figure 35.

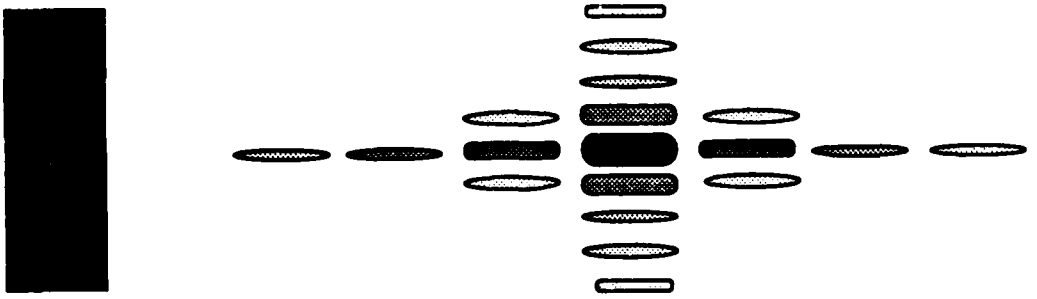

Rectangle **Transform of a Rectangle**

Figure 34. Sketch of Rectangle and its Fourier Transform

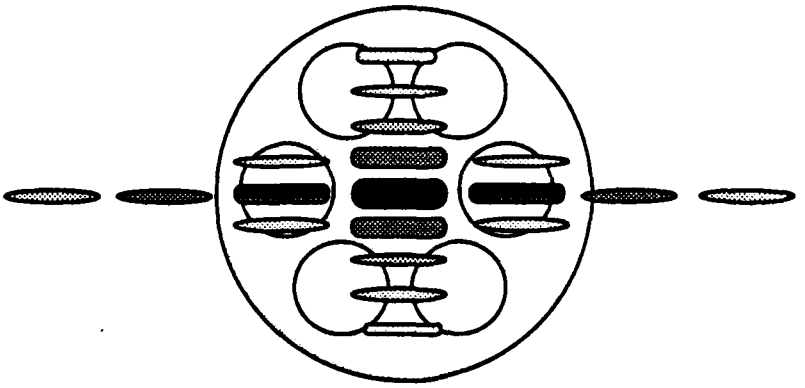

Orientation of Aperture in Transform Plane

Figure 35. Orientation of Apertures in this Section

Figure 36 shows the computer prediction of a rectangle as imaged through Aperture-11. Once again, Aperture-14 is too small to effectively resolve a rectangle of this size. This is indicated by Figure 37. As before, this problem can be solved by synthesizing a larger aperture. The computer predicted images of the rectangle as viewed through various multiple apertures are displayed in Figures 38 and 39.

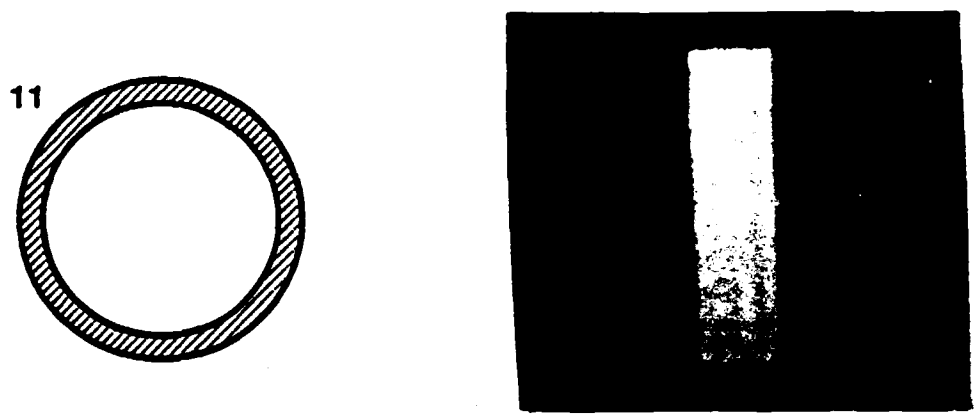

Figure 36. COMPUTER PREDICTION Rectangle Imaged through Aperture-11

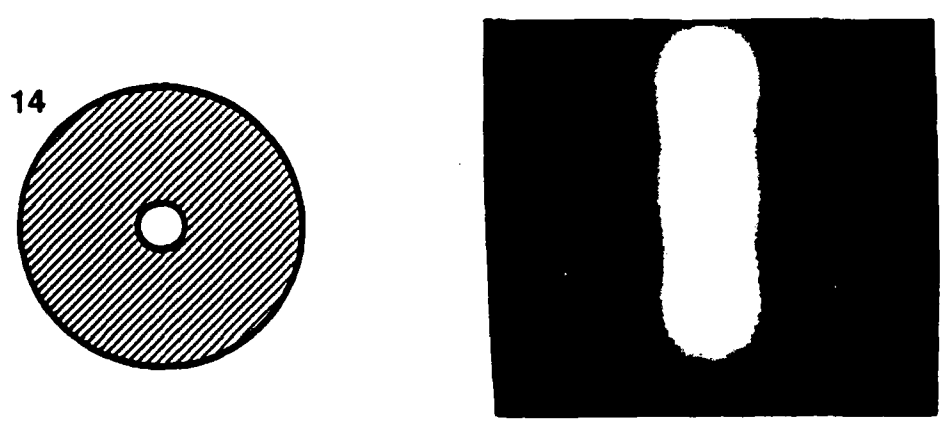

Figure 37. COMPUTER PREDICTION Rectangle Imaged through Aperture-14

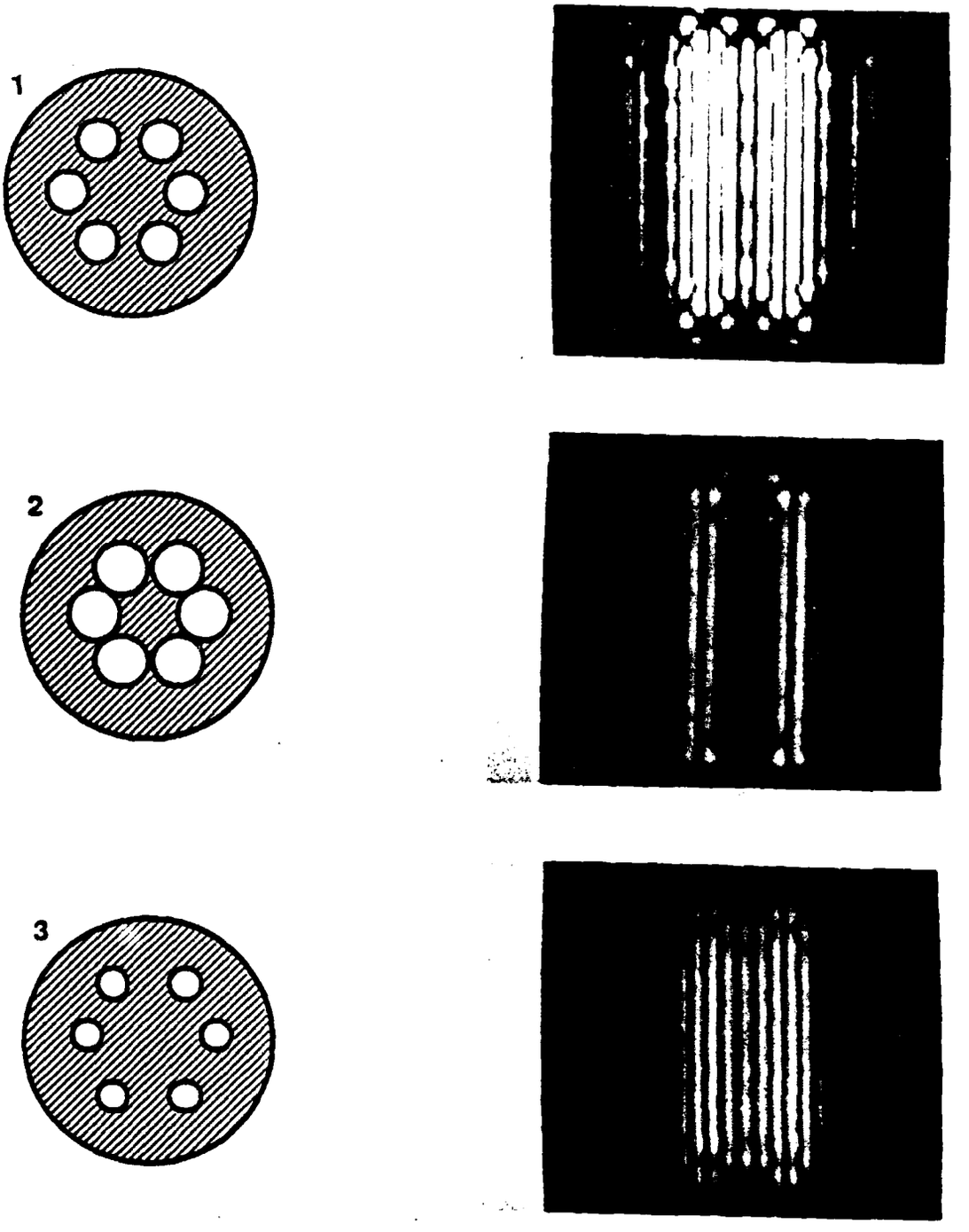

Figure 38. COMPUTER PREDICTION Rectangle Imaged through Apertures 1, 2, and 3

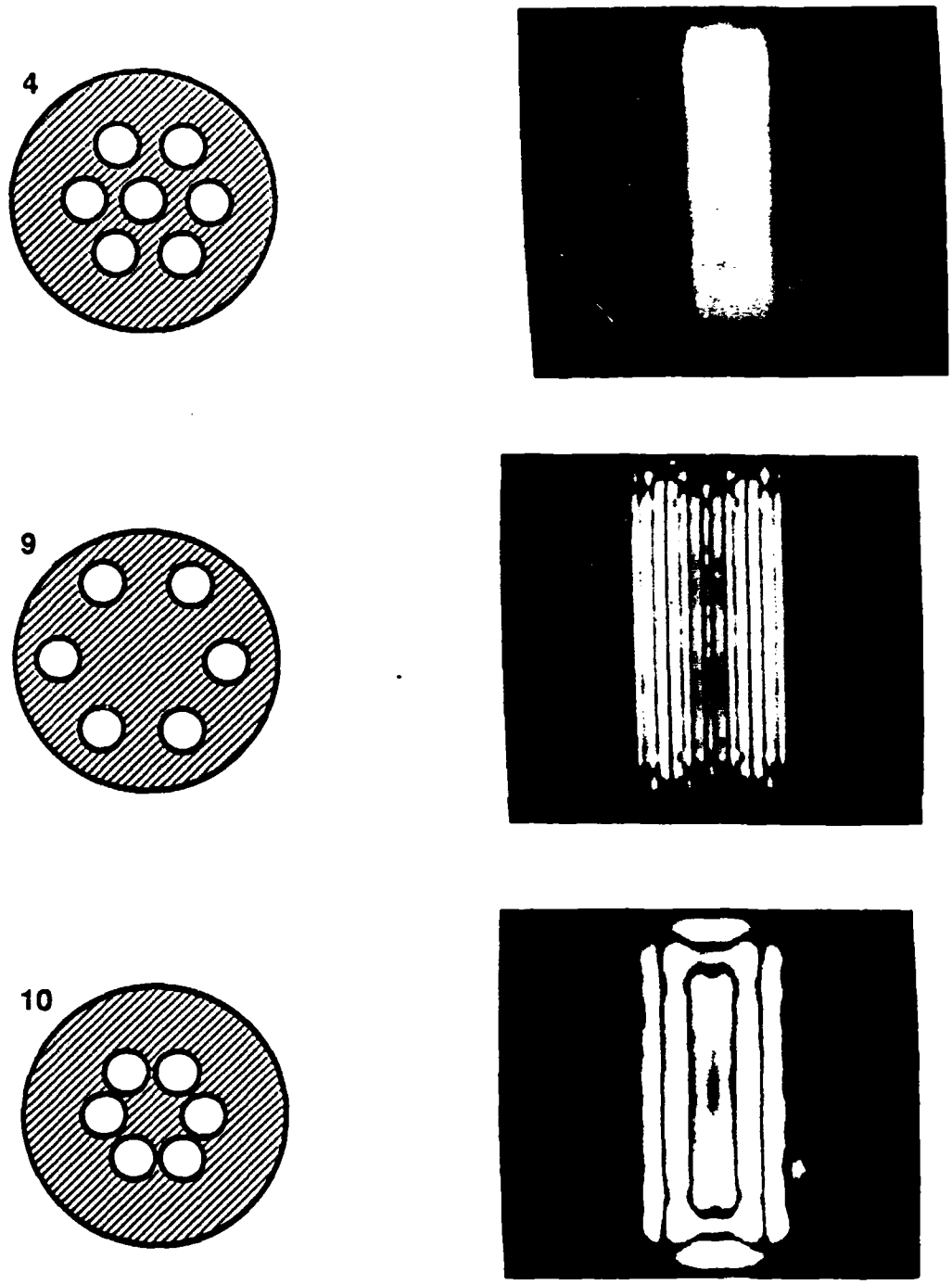

Figure 39. COMPUTER PREDICTION Rectangle Imaged through Apertures 4, 9, and 10

The computer predictions above imply that the multiple aperture images of a rectangle should have the same basic characteristics as the multiaperture images of a slit of the same width. Because of the specified orientation of the aperture, only two sides of the rectangle can be effectively located (These edges may exhibit edge-shift.). The aperture parameters should have the same effect on imaging as was previously observed. Figure 40 shows the predicted multiaperture image of a wide rectangle. In this case, one can note that two sides of the rectangle each produce equivalent edge fields as described in section III.1.

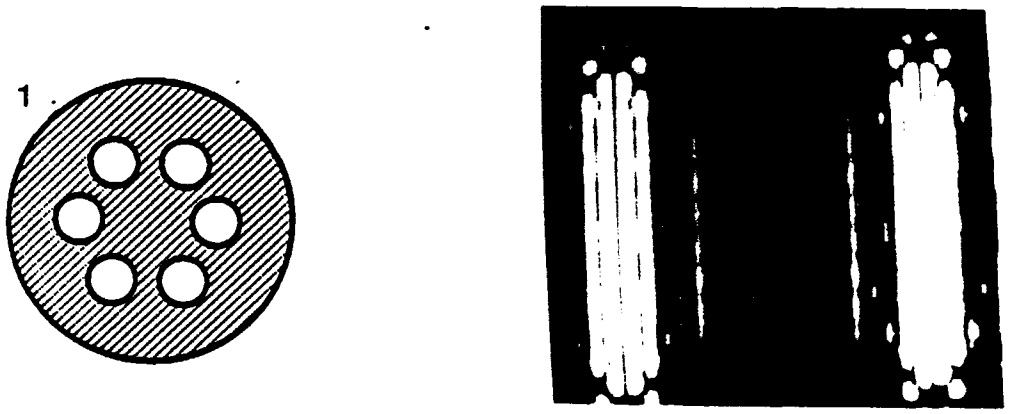

Figure 40. COMPUTER PREDICTION Wide Rectangle Imaged through Aperture-1

IV.2. Experimental Results of Rectangle Imaging

Once again, the laboratory observations confirm our previous analyses and predictions. The close similarity of the laser images and the earlier computer predictions also confirm the validity of the computer program. The images of Figures 41-43 should be compared with the predictions of Figures 36-39. Note that there is a small change of size due to the way the computer scales its transforms.

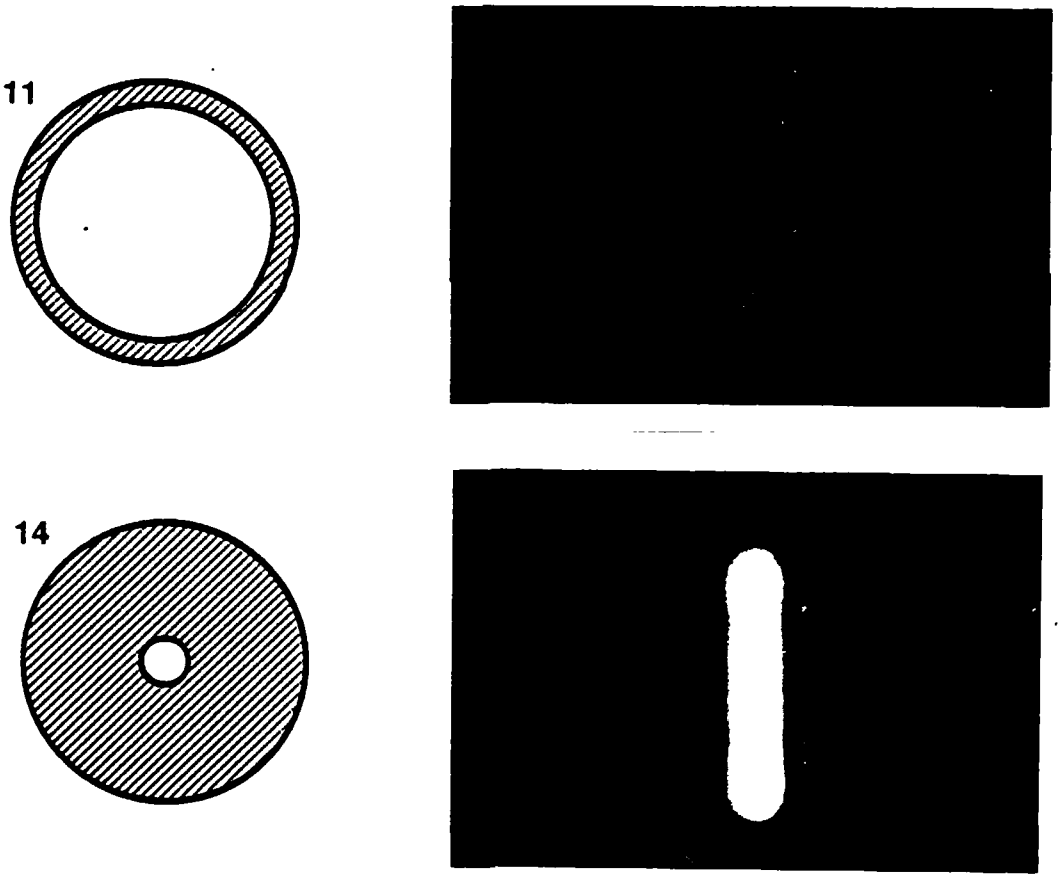

Figure 41. Rectangle Imaged through Apertures 11 and 14

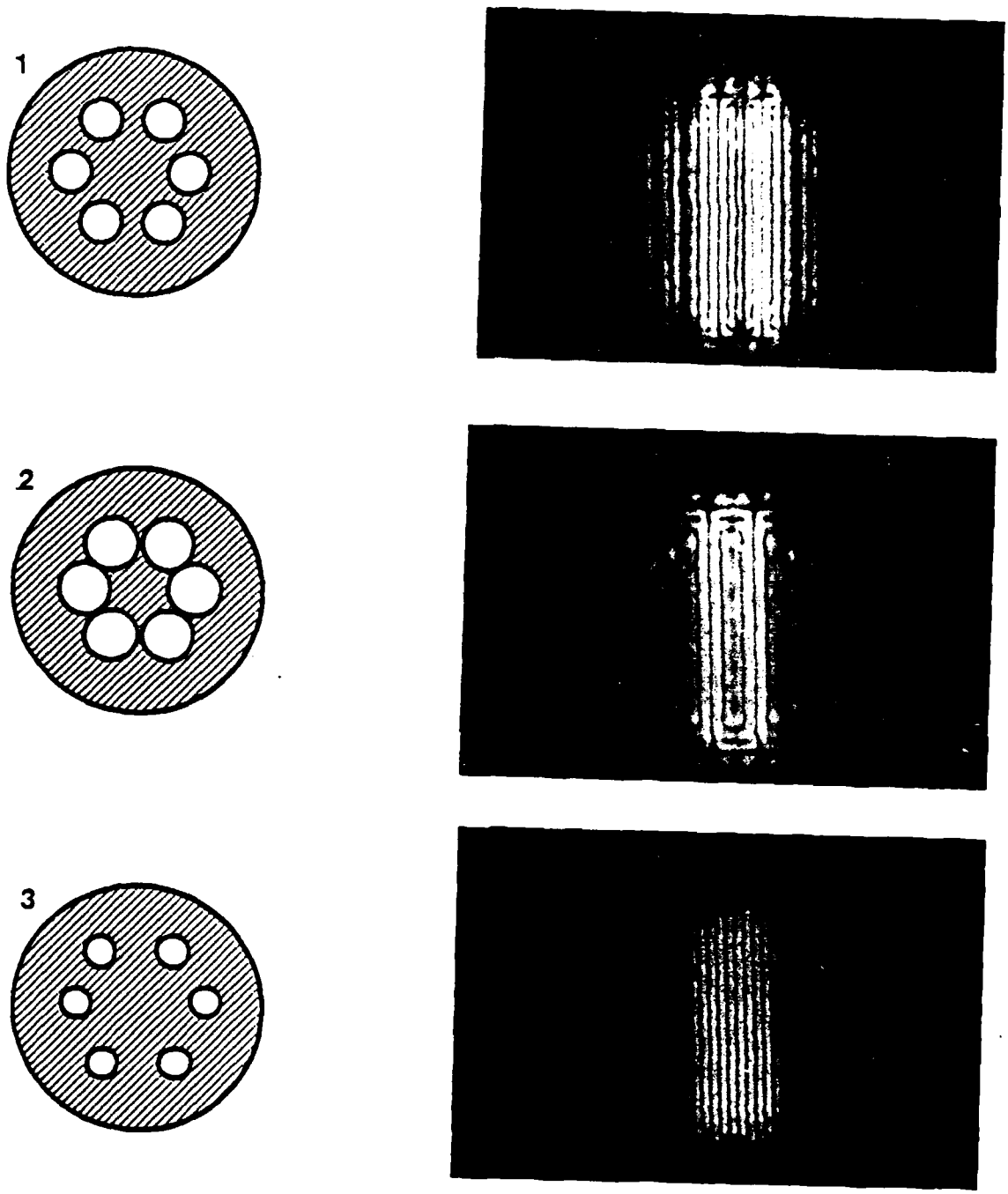

Figure 42. Rectangle Imaged through Apertures 1, 2, and 3

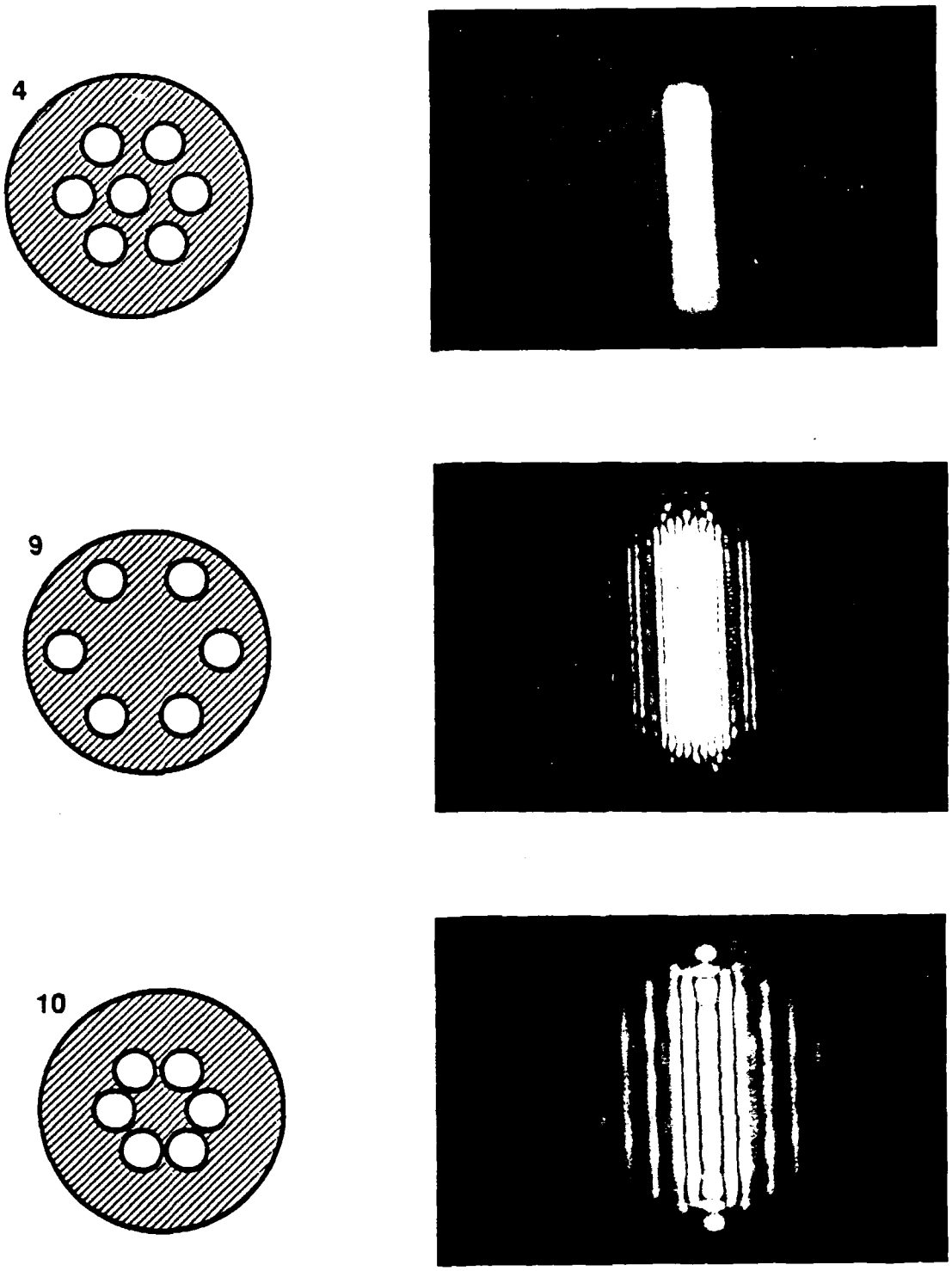

Figure 43. Rectangle Imaged through Apertures 4, 9, and 10

IV.3. Summary of Predictions and Results for Circle Imaging

In this section, another 2-dimensional object, the circle, is analyzed. This time, the data is presented in a different manner which allows for easier comparison of the experimental and predicted results. Also, two circles of different sizes were experimentally imaged. Each aperture is shown with the images that it produced (theoretically and experimentally). The image on top is the computer prediction, the one in the center is the large circle, and the image on the bottom is the small circle.

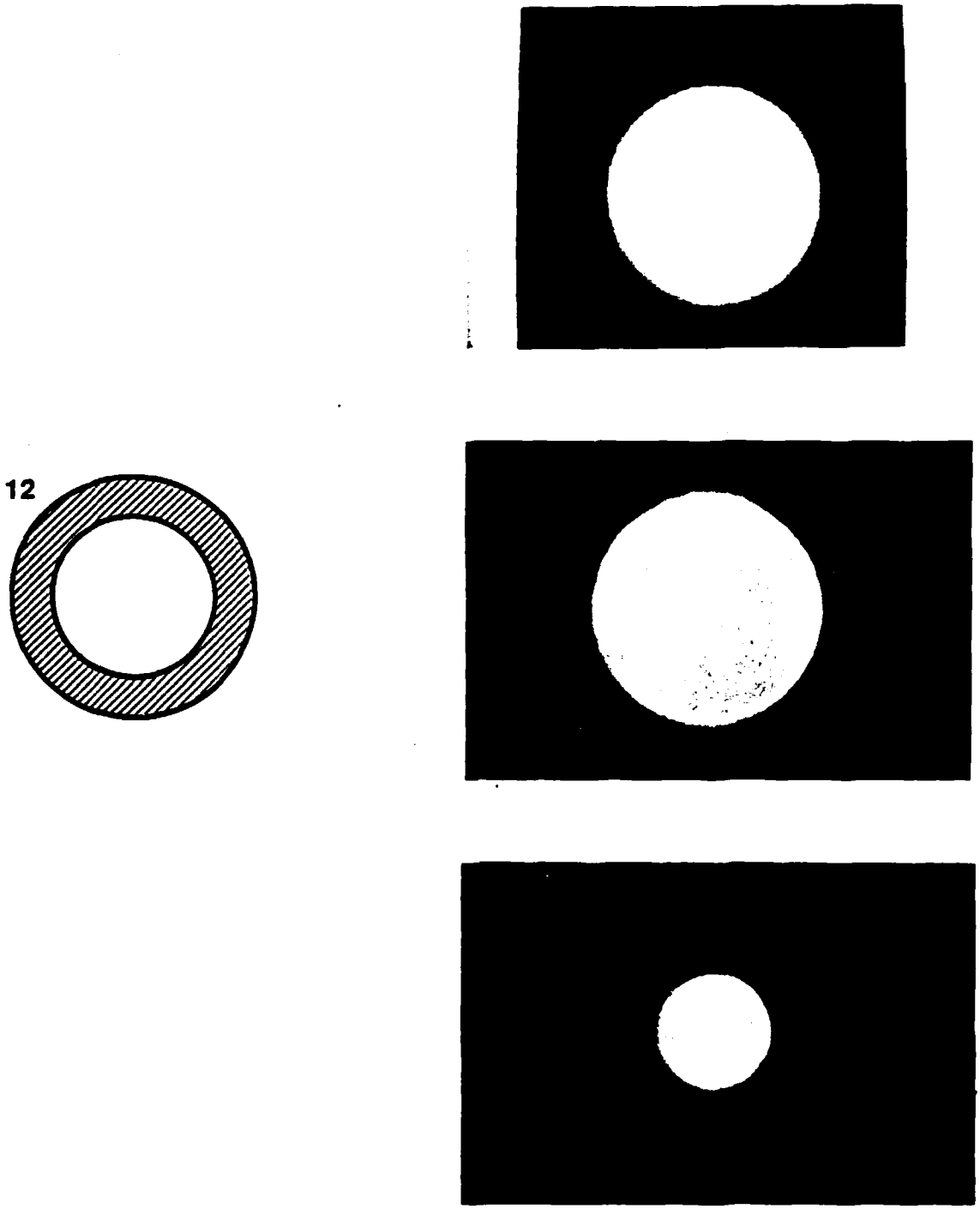

Figure 44. Computer Prediction and Images of Two Circles through Aperture-12

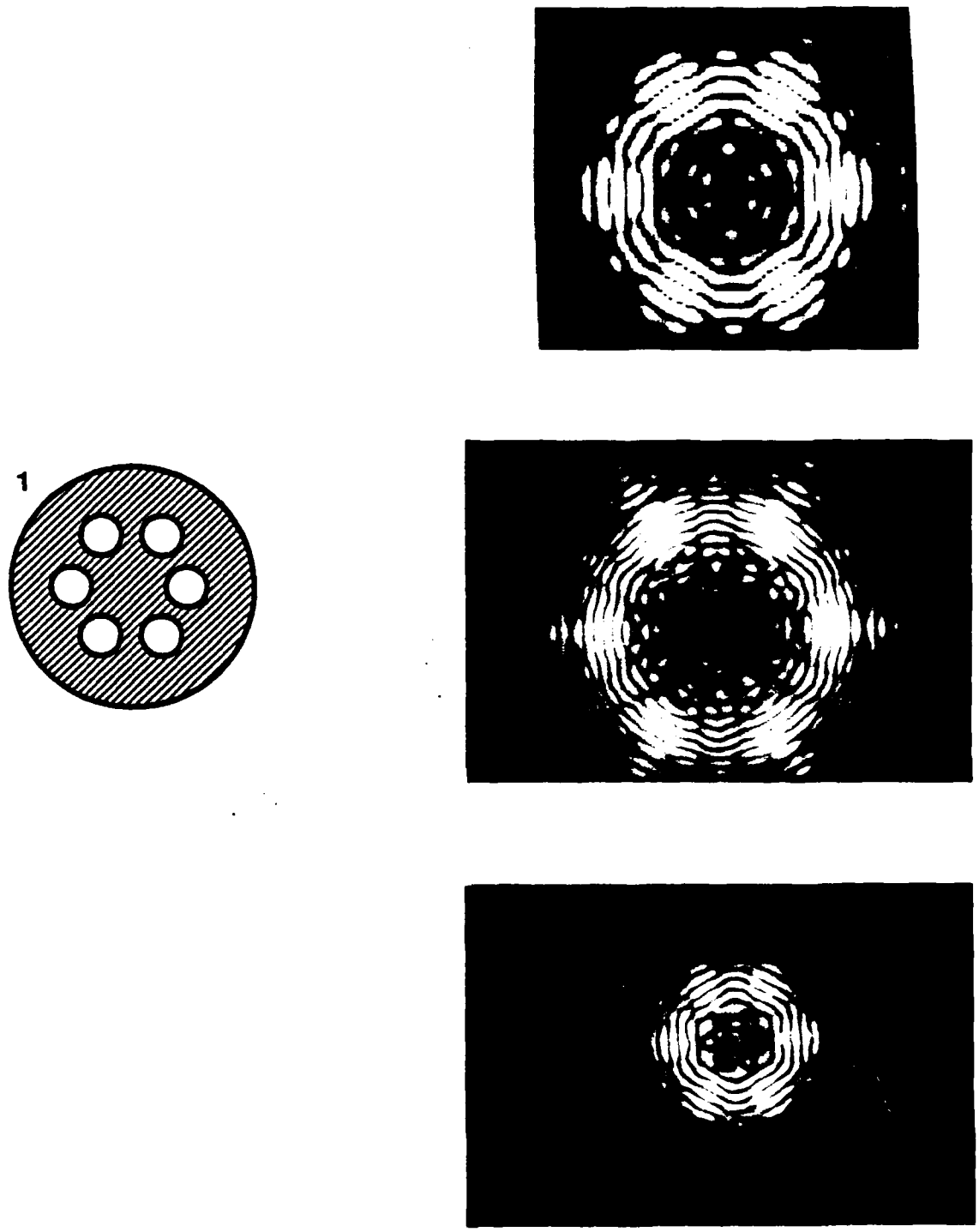

Figure 45. Computer Prediction and Images of Two Circles through Aperture-1

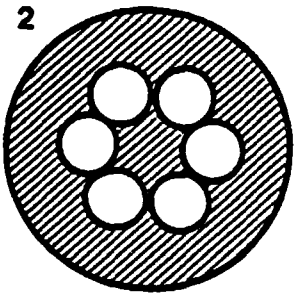

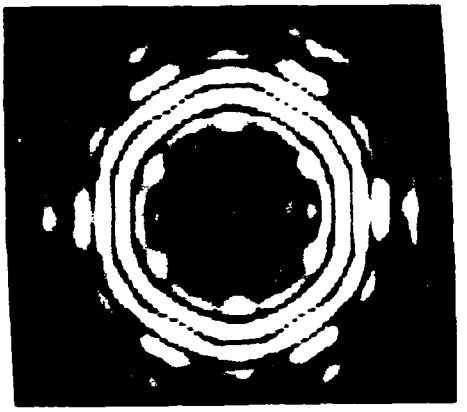

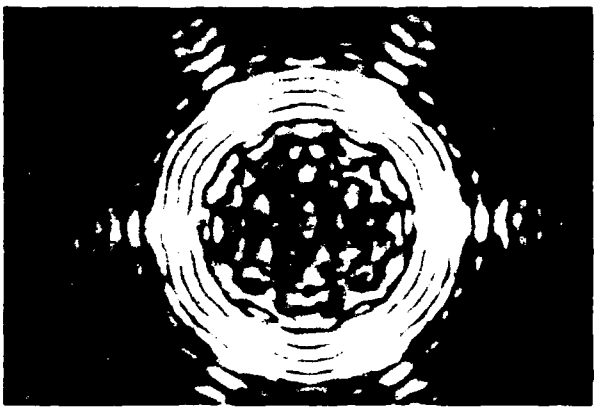

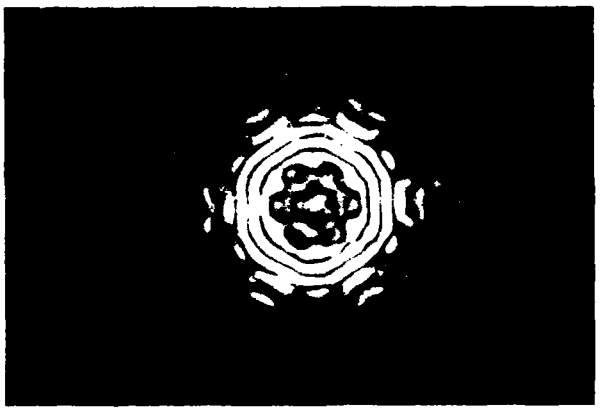

Figure 46. Computer Prediction and Images of Two Circles through Aperture-2

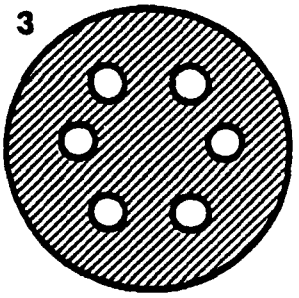

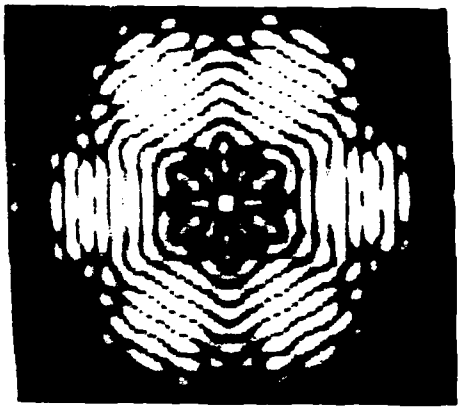

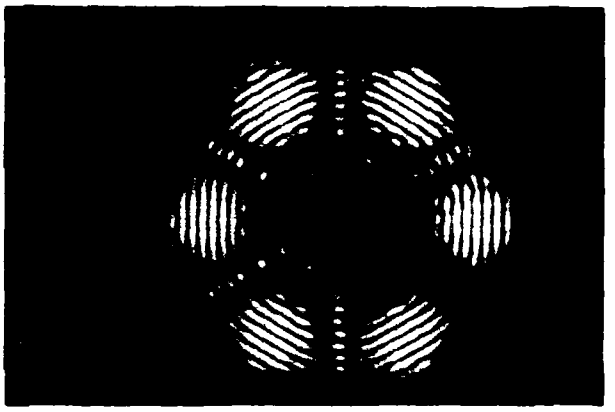

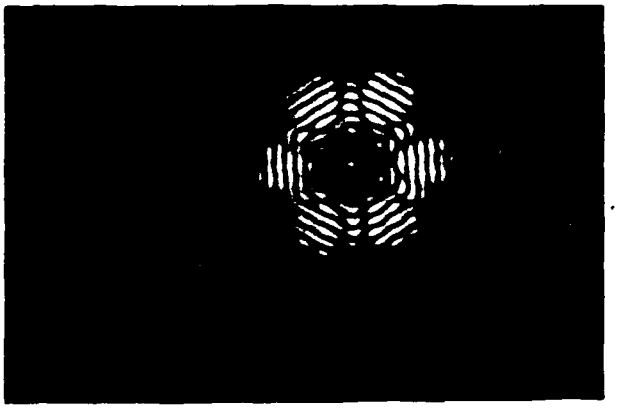

Figure 47. Computer Prediction and Images of Two Circles through Aperture-3

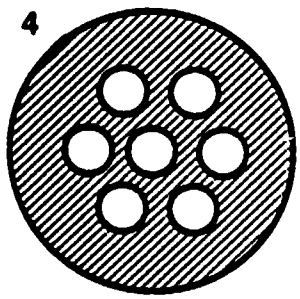

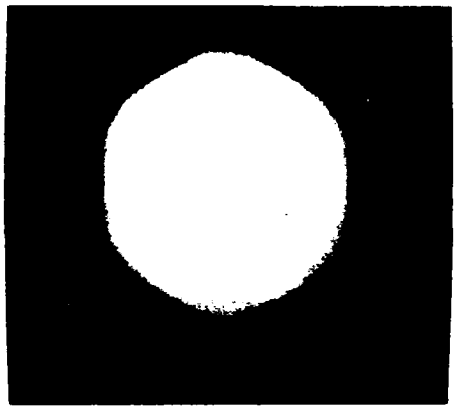

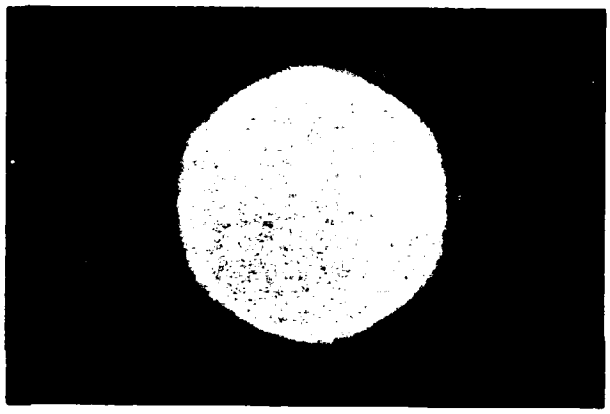

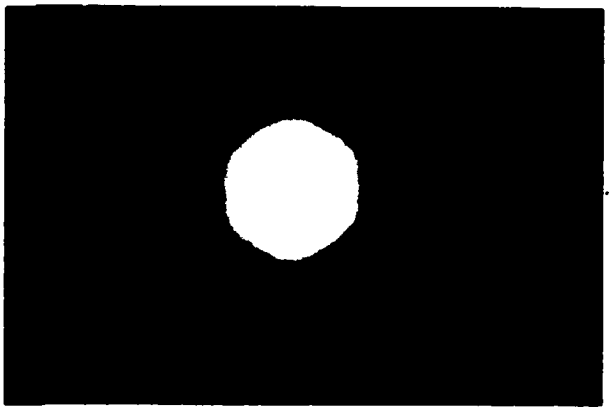

Figure 48. Computer Prediction and Images of Two Circles through Aperture-4

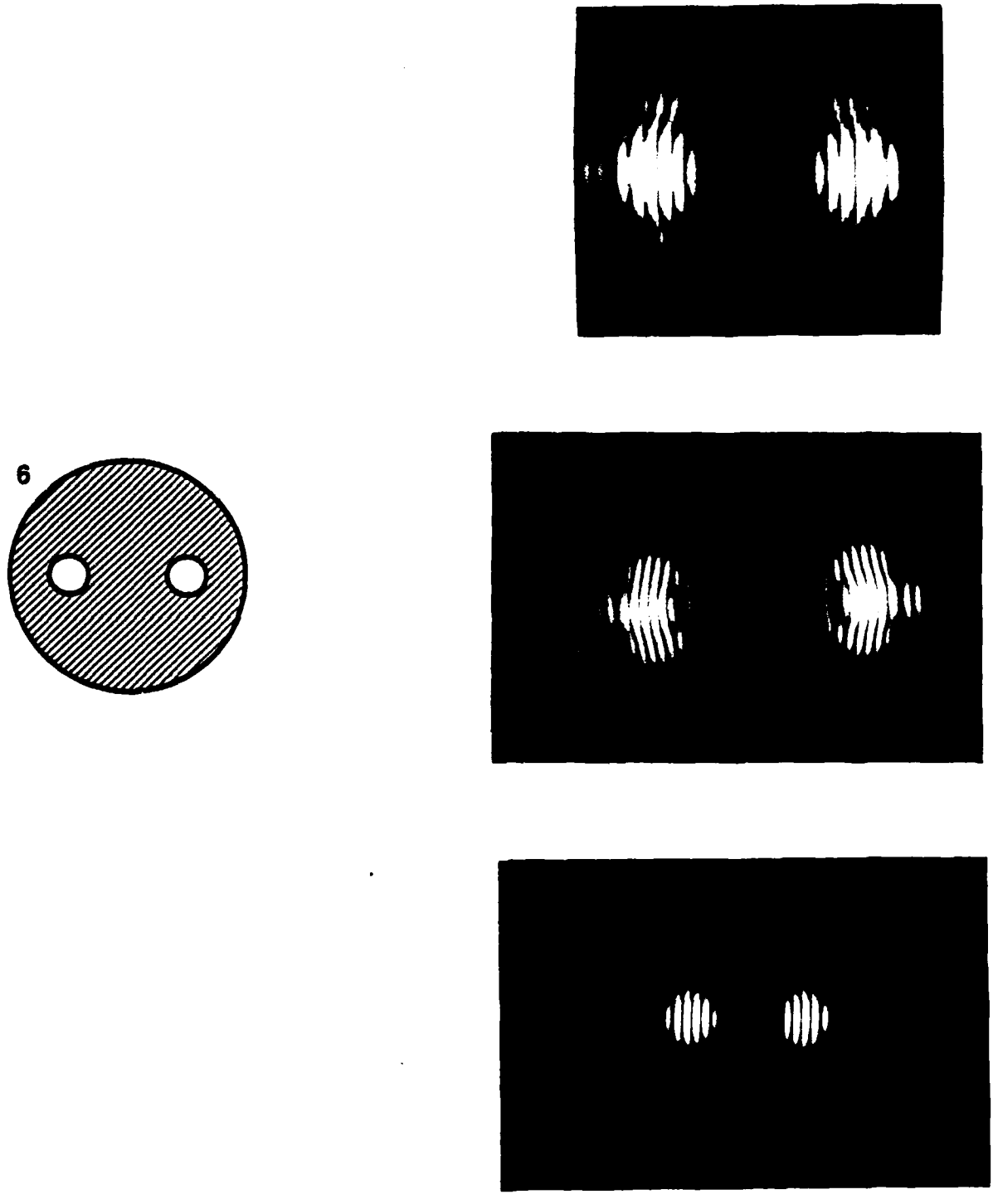

Figure 49. Computer Prediction and Images of Two Circles through Aperture-6

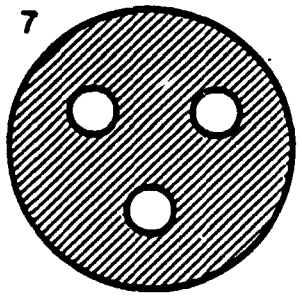

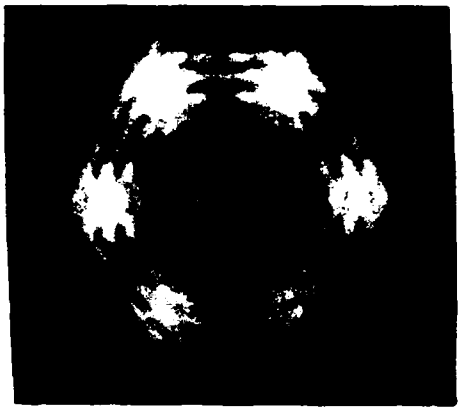

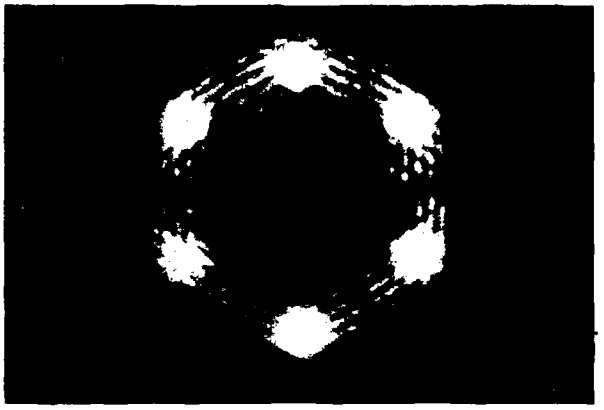

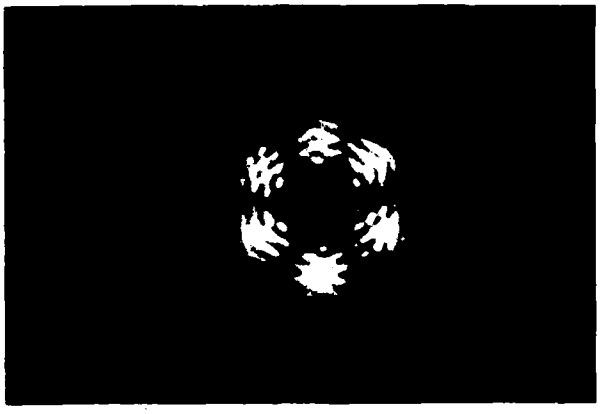

Figure 50. Computer Prediction and Images of Two Circles through Aperture-7

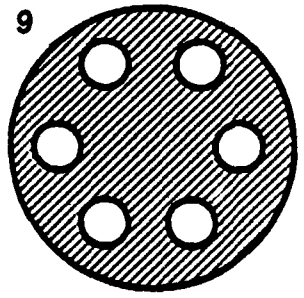

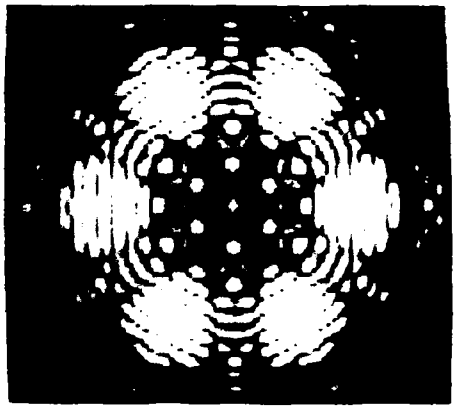

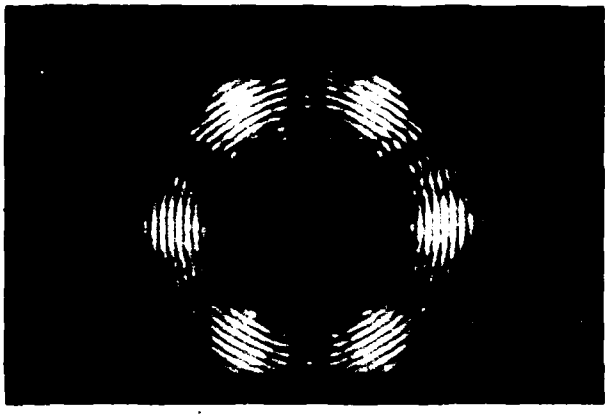

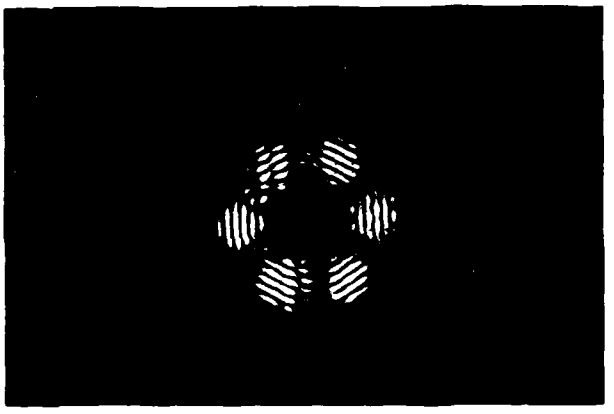

Figure 51. Computer Prediction and Images of Two Circles through Aperture-9

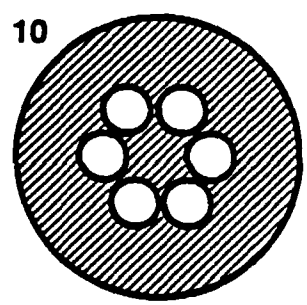

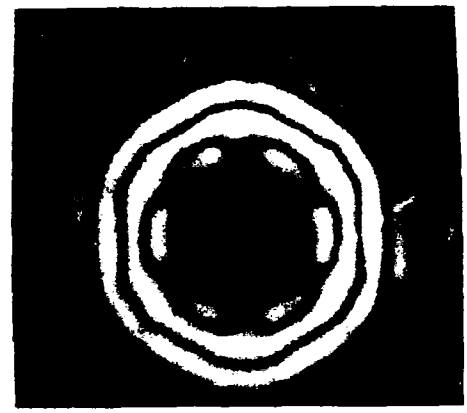

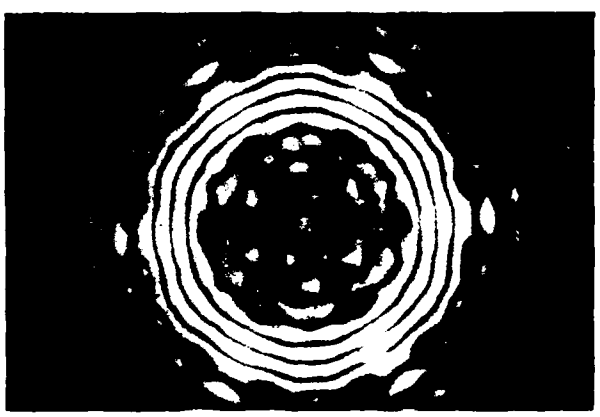

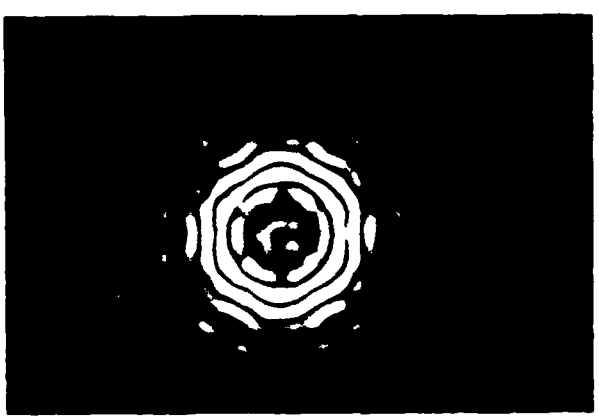

Figure 52. Computer Prediction and Images of Two Circles through Aperture-10

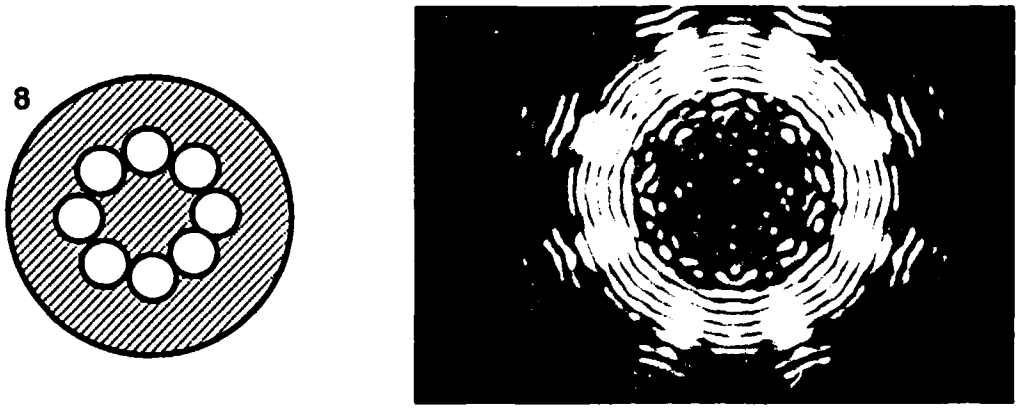

Figure 53. Circle Imaged through Aperture-8

The results of circle imaging reiterated the fact that once an aperture's edge field is determined, images of various sized objects can be predicted. Comparing the multiaperture images of the two different size circles, one notes that a given aperture produces a given intensity distribution. This distribution is just centered on a larger or smaller circle, depending on the size of the object being imaged.

Since the Fourier transform of a circle is angularly symmetric, there were no linear components to line the aperture up on, as in the case of a rectangle. Therefore, the orientation of the aperture was arbitrary. An aperture that was rotated by a given amount produced an image that was rotated by the same amount. Since the aperture did not have to be oriented such that a particular part of the transform passed through two sub-apertures, as in the previous analyses, multiple apertures with different numbers of sub-apertures could be analyzed. Figure 53

shows the image of a circle as viewed through a multiple aperture with eight sub-apertures.

An important result was illustrated in Figure 50. That was an example of an aperture with an odd number of sub-apertures. There was no pair of sub-apertures to produce the ringing we have observed in the other images. This had the undesirable effect of obscuring the location of the circle's edge.

IV.4. Rotating the Aperture

Until the analysis of circle imaging, the orientation of the multiple aperture had been very important. The orientation that was picked produced an image with information about the left and right edges of the rectangle but little information about the top and bottom edges. Had the aperture been rotated 90°, then the opposite would have been true. The resulting image would have contained information about the top and bottom edges but not the left or right edges. Figure 54 illustrates these two extremes.

Ideally, one would like to obtain information about all four sides. One solution to this problem is to rotate the multiple aperture system. This should be feasible for a space-based system. As the system rotates, it would simply sum the field as it changed in the image plane. Some images produced by rotating apertures are shown in Figure 55.

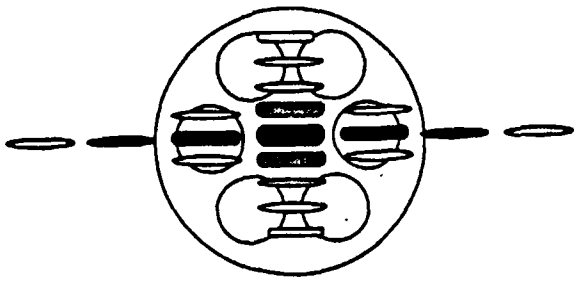

Previous Orientation of Aperture

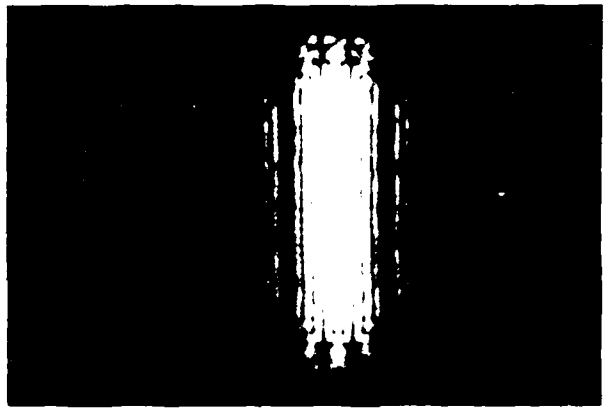

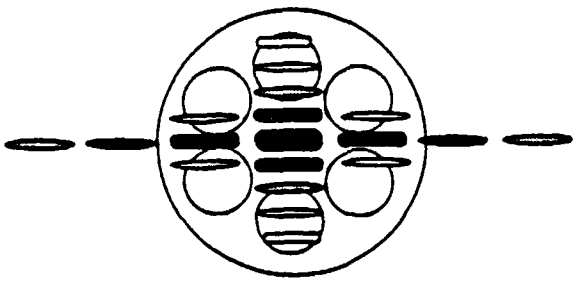

90 degree Rotation of Aperture

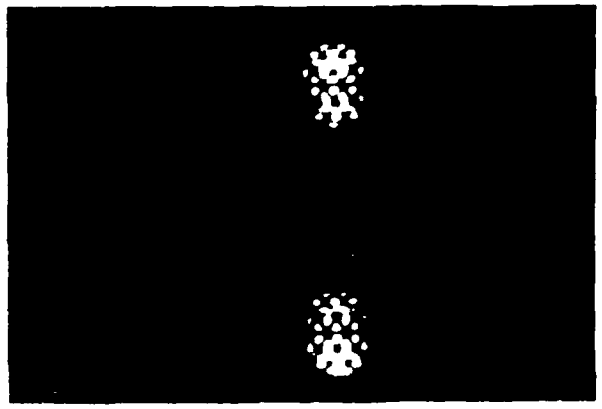

Figure 54. Different Aperture Orientations and Their Resulting Images

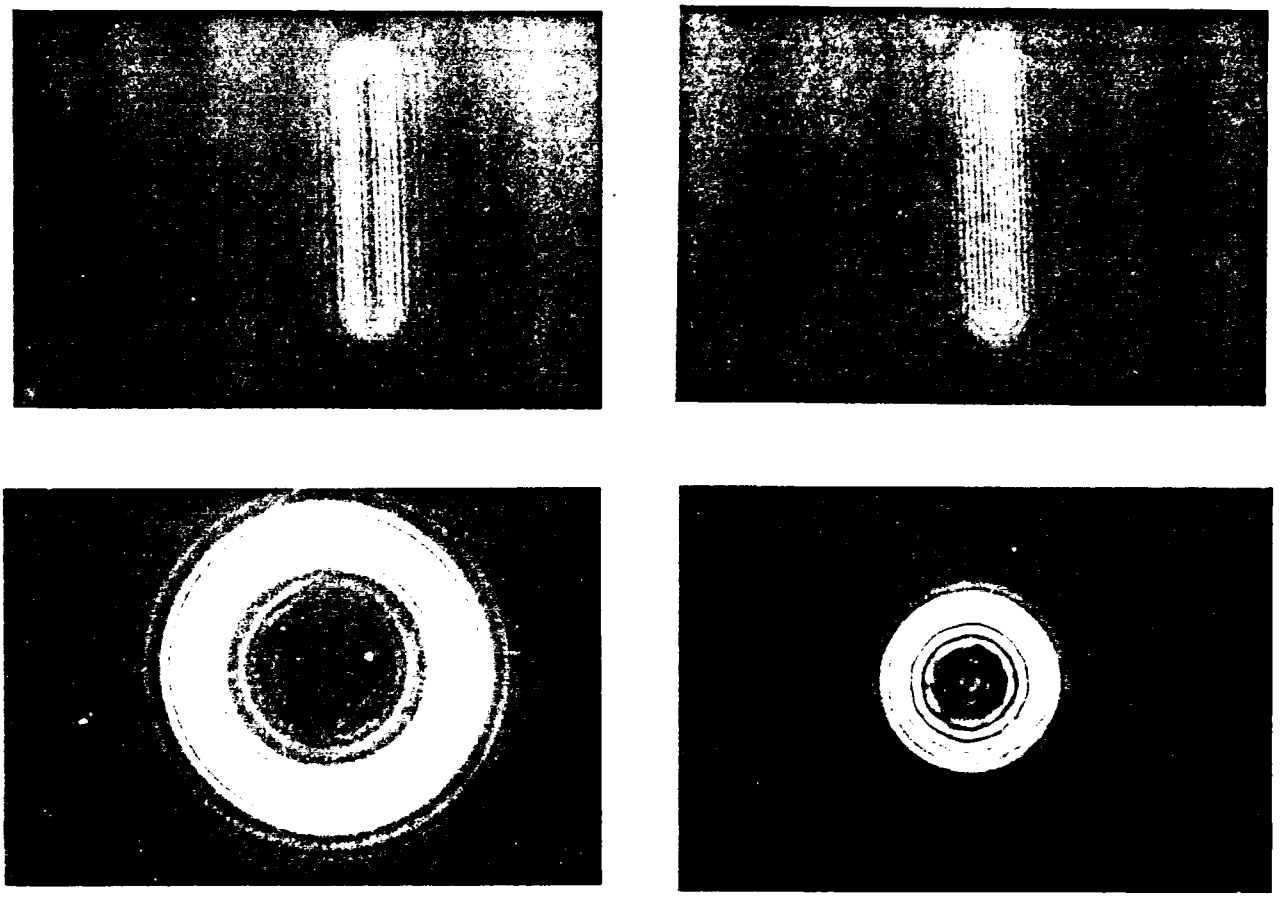

Figure 55. Images Produced by a Rotating Aperture

Upper left: rectangle imaged through Aperture-1

Upper right: rectangle imaged through Aperture-9

Lower left: large circle imaged through Aperture-1

Lower right: small circle imaged through Aperture-1

It is evident that more information is available from images produced by rotating apertures than from images produced by stationary apertures. In particular, all four edges can be located in the rectangle images. Also, it is apparent that the small circle has some defects. These imperfections were not visible in

the stationary aperture images of the circle.

IV.5. Summary

This chapter described the theoretical predictions and experimental results of imaging two-dimensional objects through multiple aperture systems. Section 1 described the added complexities of analyzing the imaging of 2-dimensional objects and then predicted multiaperture rectangle images. Section 2 then discussed the experimental results and compared them to the predictions of section 1. Section 3 summarized the predictions and experimental results of circle imaging. Finally, section 4 introduced the possibility of rotating the aperture to access more information about the object. The conclusion of our analysis leads to the possibility of identifying the areas of multiaperture imaging that require consideration when designing multiple aperture imaging systems.

V. CONCLUSIONS APPLICABLE TO DESIGN

V.1. The Design of Coherent Multiaperture Optical Imaging Systems

This thesis embodies a number of significant breakthroughs in the area of coherent multiple aperture optical imaging. The results of this work are directly applicable to the design of systems which support the Strategic Defense Initiative. This chapter summarizes the important topics that must be considered when designing a coherent multiple aperture optical imaging system. These topics and conclusions were drawn from the previous analysis of multiaperture imaging. They include a study of how the number of sub-apertures affects imaging, a look at the possibility of rotating the aperture, a discussion of the benefits and drawbacks of including a central sub-aperture, and an analysis of how sub-aperture size and spacing affect resolving power and edge location.

V.2. Number of Sub-apertures

One of the important results of this thesis which must be addressed when designing a coherent multiple aperture optical imaging system is an answer to the question, 'How many sub-apertures are neccessary ?' Obviously, the greater the number of sub-apertures, the greater the cost of the system. This thesis determined that an even number of sub-apertures is required to produce the ringing from which the actual position of an edge can

be located. Only two sub-apertures are needed to satisfy this condition. However, other requirements might warrant the use of six or eight sub-apertures. If the system must image very faint objects, then a greater light-gathering capability might be called for, and more sub-apertures should be used. Also, if SDI plans call for a rotating-aperture system, the number of sub-apertures becomes important in another way. For a given spin-rate, an eight sub-aperture system can complete a scan in one-fourth of the time it takes for a two sub-aperture system to do so. All of these factors must be taken into account when designing a multiaperture system. Some factors will become more important than others, depending on the system requirements.

V.3. Rotating the Aperture

Another question that must be answered during the design process is whether or not to make a rotating-aperture system. This thesis proposed the idea of rotating the aperture in order to pass more spatial frequency information. It was shown that more information was indeed contained in a rotating-aperture image. Of course, a rotating system will require more structural support, engines, and a control system to produce and monitor the rotation. Once again the added cost and complexity must be weighed against the requirements and objectives of the system. It is this author's belief that the imaging performance required in any SDI application would warrant the use of a rotating system.

V.4. Central Sub-apertures

A third area of consideration identified by this thesis is the question of including a central sub-aperture. A central sub-aperture will produce images that include the dc component. The overall shape will be closer to the shape of the object being imaged, but the ringing effect will disappear and the actual locations of the edges will be more difficult to determine. However, one can visualize the possibility of using a central sub-aperture that can be turned on and off. Whether by using some kind of aperture block or phasing the central sub-aperture differently, the effects of the sub-aperture could be called upon when required. This feature could give any SDI system more flexibility. Turning on the central sub-aperture would also dramatically increase the light-gathering ability of the system.

V.5. Ringing vs. Resolution

The major area investigated in this thesis, was the question of ringing versus resolution. These two features are regulated by the size and spacing of the sub-apertures. In section III.5, it was shown that systems with larger sub-aperture spacings produced better resolution than systems with smaller spacings, in that smaller objects could be imaged with less edge shift problems. But throughout this thesis, the results have shown that greater sub-aperture spacings cause more ringing, making it more difficult to determine the location of edges. Therefore, the choice of sub-aperture size and spacing will depend on the sensitivity of the

imaging system's detector. The more sensitive the detector, the easier it can pick out an edge location from an intensity pattern with severe ringing. Noise considerations must also be taken into account. So, the resolution of the imaging system is indirectly dependent on the sensitivity of the detector.

V.6. One Last Feature

One final feature of multiple aperture imaging must be noted. It is the fact that coherent multiaperture imaging is inherently an edge enhancement process. In fact, most of the images displayed in this thesis show only ringing around the edges. This feature can be very important to a pattern recognition system. These systems most often use digital means to extract the edges from an image. Multiple aperture imaging systems extract the edges optically.

V.7. Recommendations for Future Research

This thesis effort was a thorough investigation of coherent multiple aperture optical imaging. This work, which contains many significant results, also points to many possible extensions. Future research efforts might include the analysis of non-redundant aperture configurations such as Aperture-15, shown in Figure 56. Also, the area of incoherent multiaperture imaging requires the same indepth analysis afforded coherent imaging by this thesis.

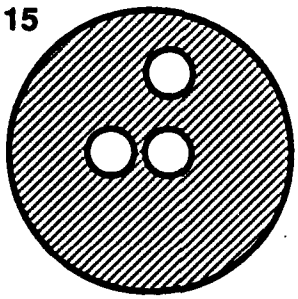

Figure 56. Aperture-15 (non-redundant array)

APPENDIX A

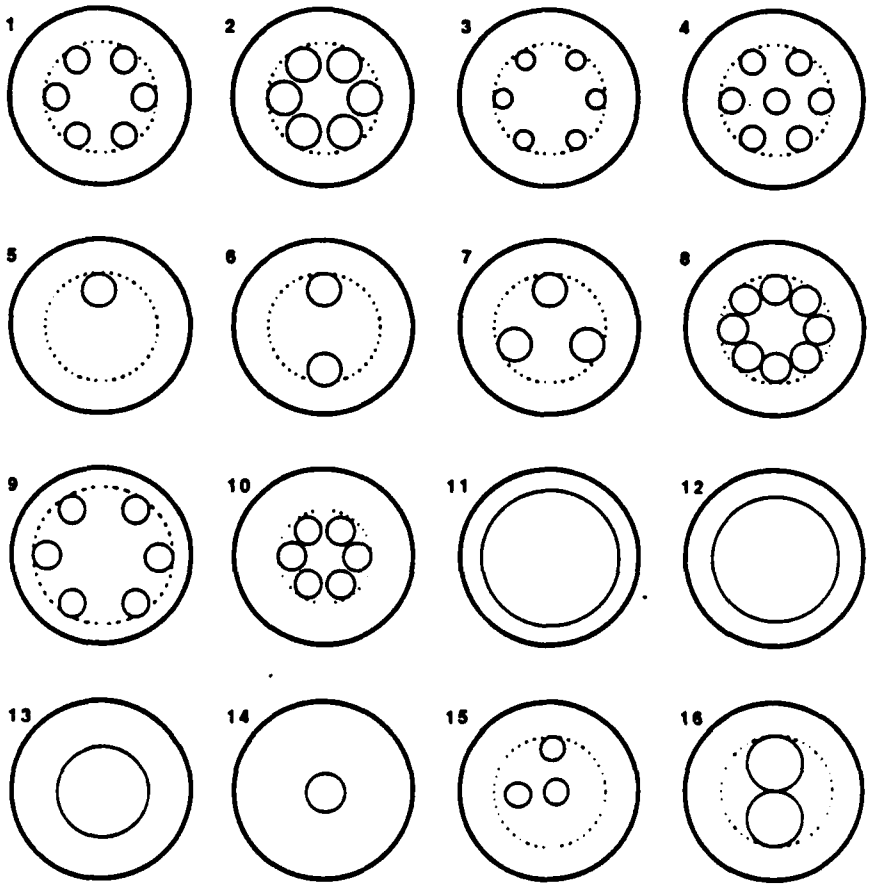

Figure A-1. The Geometries used for Specifications

The multiple apertures used in this thesis were designed and built with the following specifications.

1. the diameter of the individual sub-apertures

For a given multiple aperture, all sub-apertures had the same diameter.

2. the diameter of the aperture to be synthesized

The diameter of the aperture to be synthesized is the

diameter of the smallest circle that could be drawn that just encloses all of the sub-apertures.

3. the number of sub-apertures

All of the sub-apertures were equally spaced just touching the inside of the circle described above.

Figure A-1 illustrates these specifications. The dotted circles represent the apertures to be synthesized. Table A-1 provides the actual sizes used in this paper.

TABLE A-1

Aperture number	diameter of sub-apertures	diameter of aperture to be synthesized	number of sub-apertures
1	1/8 inch	1/2 inch	6
2	5/8 inch	1/2 inch	6
3	3/8 inch	1/2 inch	6
4	1/8 inch	1/2 inch	6 plus central
5	1/8 inch	1/2 inch	1
6	1/8 inch	1/2 inch	2
7	1/8 inch	1/2 inch	3
8	1/8 inch	1/2 inch	8
9	1/8 inch	5/32 inch	6
10	1/8 inch	3/32 inch	6
11	5/8 inch	5/8 inch	1
12	1/2 inch	1/2 inch	1
13	3/8 inch	3/8 inch	1
14	1/8 inch	1/8 inch	1
15	1/8 inch	1/2 inch	3*
16	1/4 inch	1/2 inch	2

* The three sub-apertures in Aperture-15 were arranged such that when the aperture was spun, the sub-apertures would rotate through the entire area of the aperture to be synthesized.

APPENDIX B

This appendix contains photographs of the impulse responses of each of the multiple apertures discussed in this thesis. The apertures and their corresponding impulse responses are shown side by side.

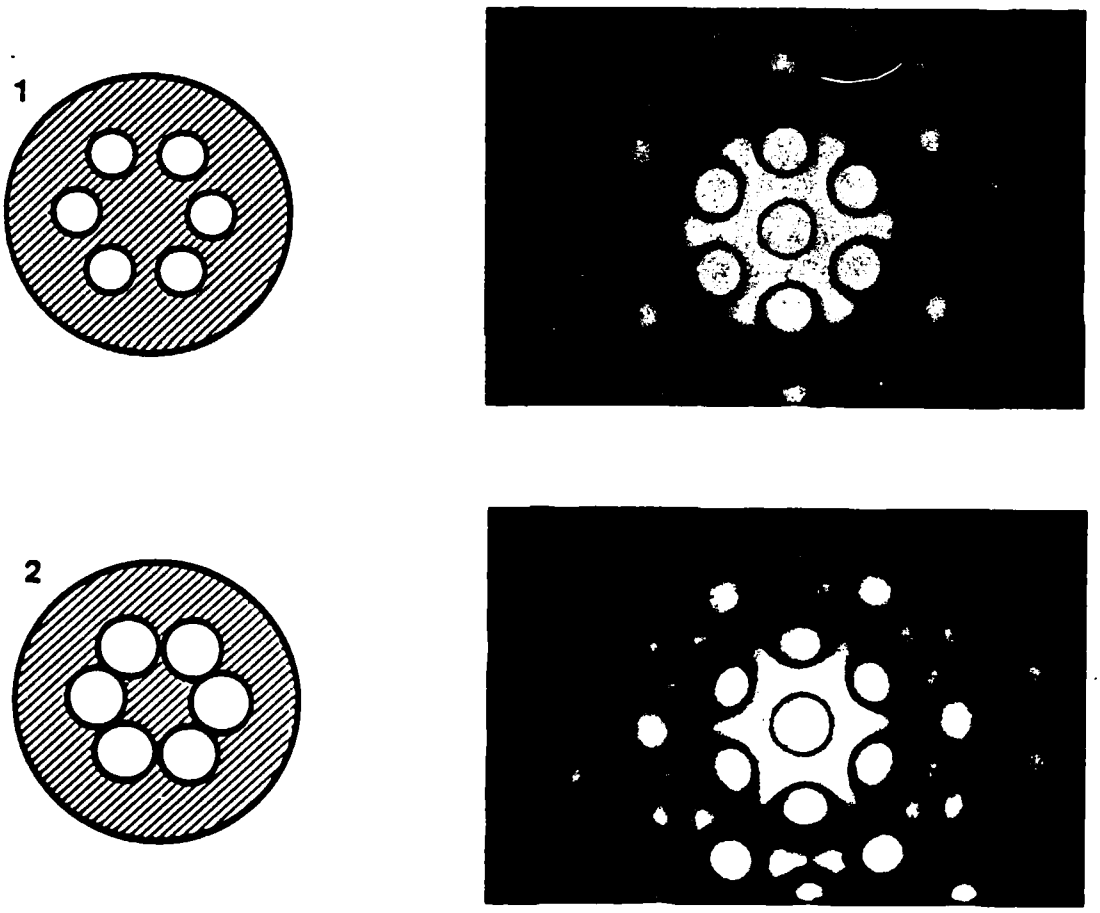

Figure B-1. Impulse Responses of Apertures 1 and 2

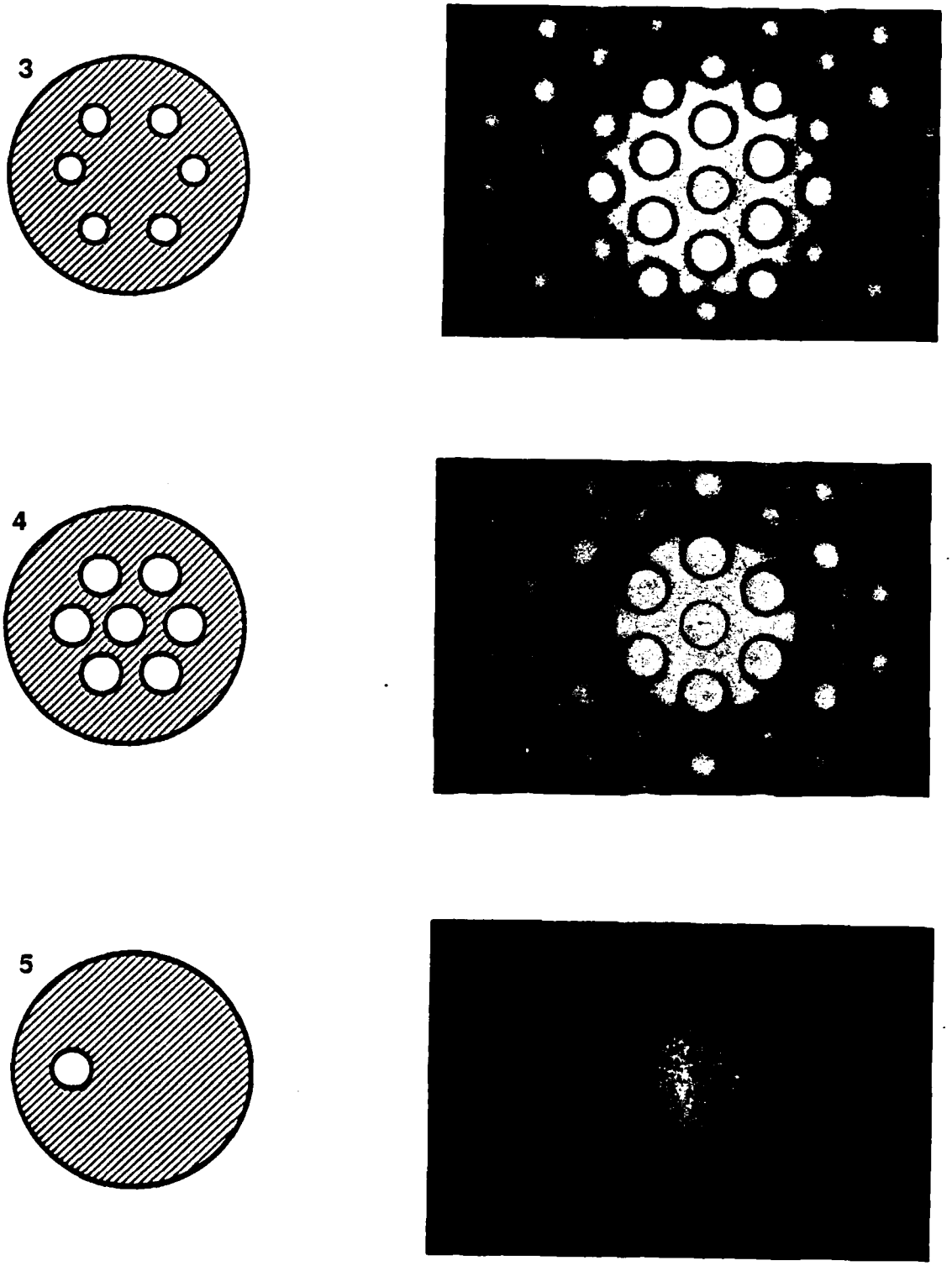

Figure B-2. Impulse Responses of Apertures 3, 4, and 5

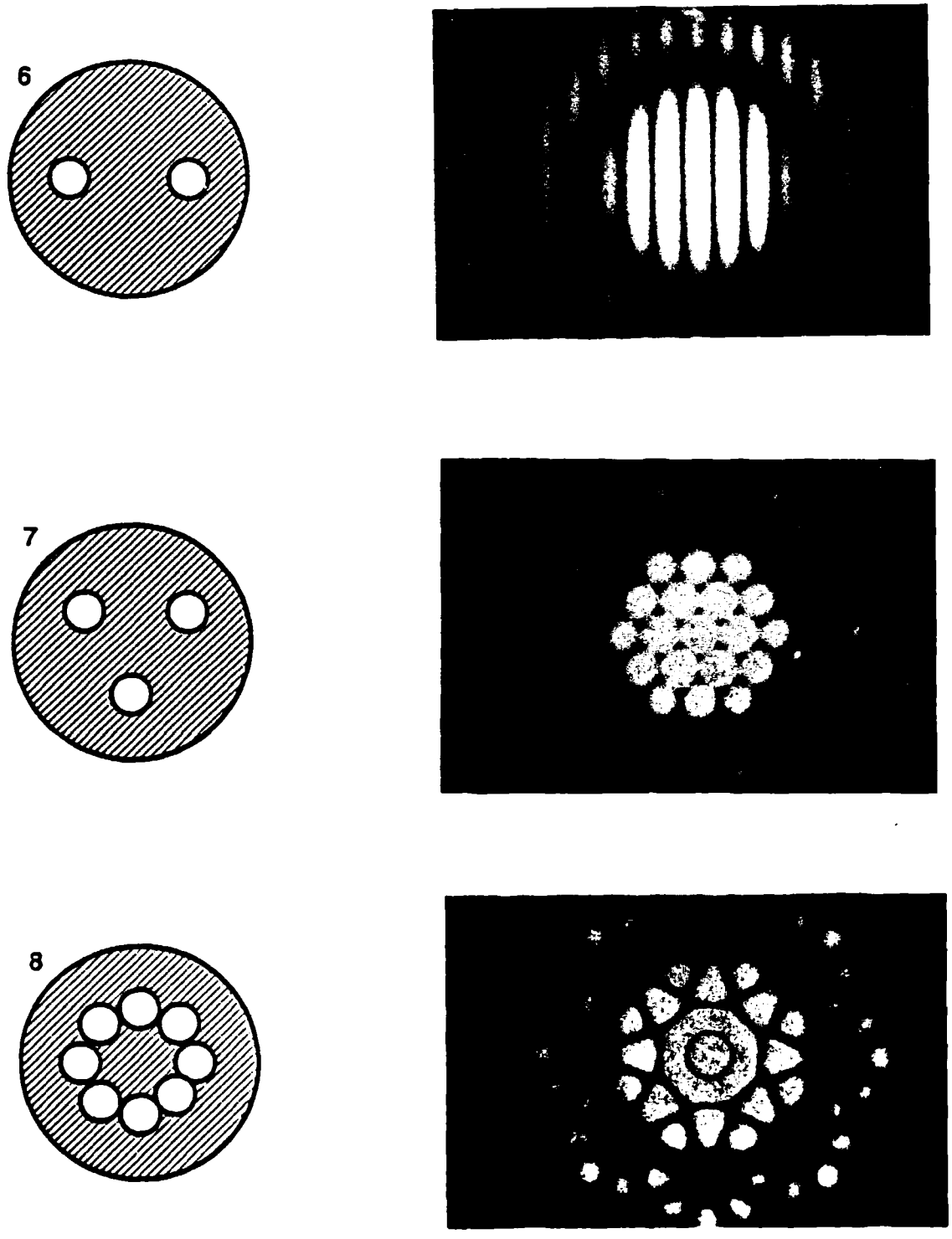

Figure B-3. Impulse Responses of Apertures 6, 7, and 8

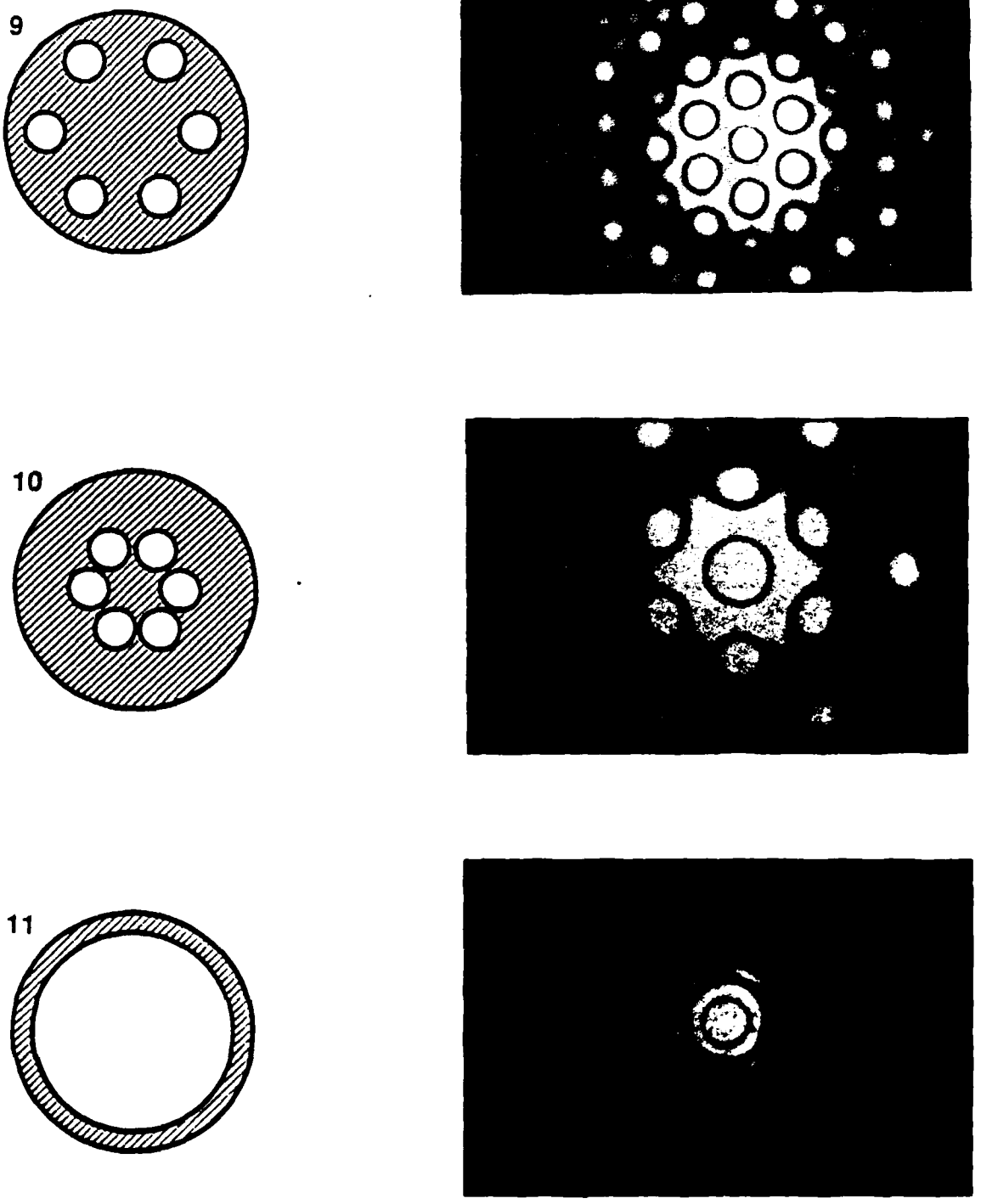

Figure B-4. Impulse Responses of Apertures 9, 10, and 11

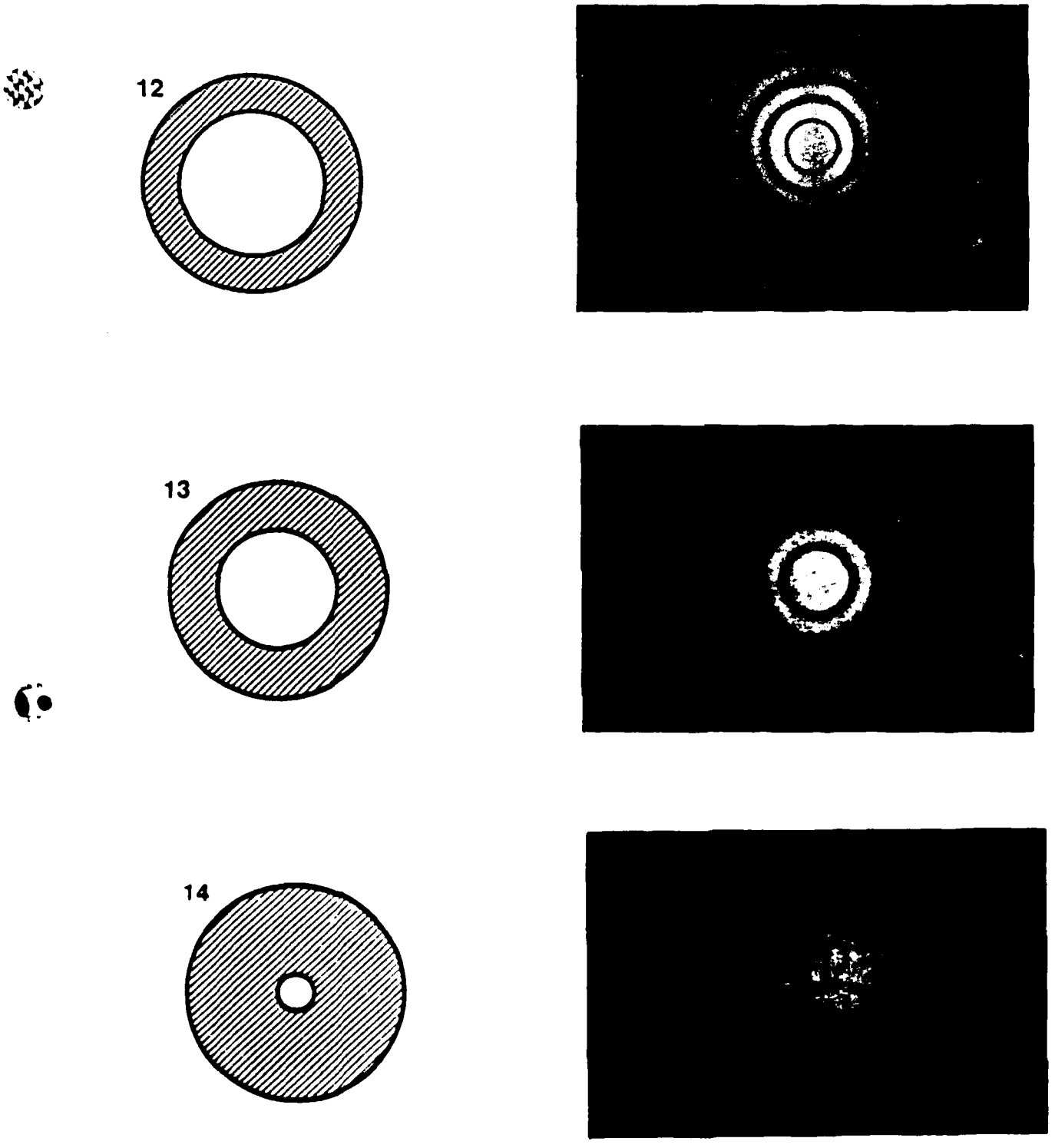

Figure B-5. Impulse Responses of Apertures 12, 13, and 14

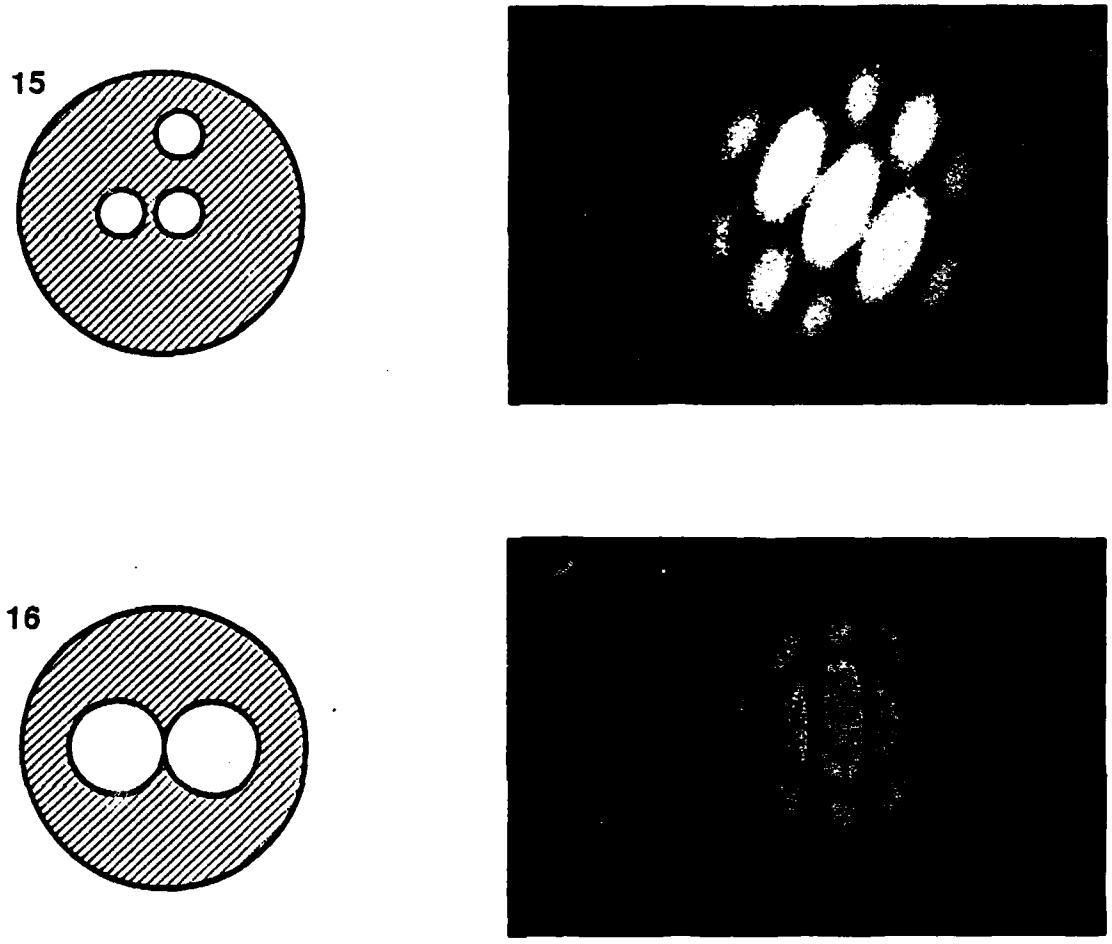

Figure B-6. Impulse Responses of Apertures 15 and 16

AD-A179 476 COHERENT MULTIPLE APERTURE OPTICAL IMAGING SYSTEMS: 2/2
ANALYSIS AND DESIGN(U) AIR FORCE INST OF TECH
WRIGHT-PATTERSON AFB OH SCHOOL OF ENGINEERING
UNCLASSIFIED D J BERGEY MAR 87 AFIT/GE/ENG/87M-1 F/G 20/6 NL

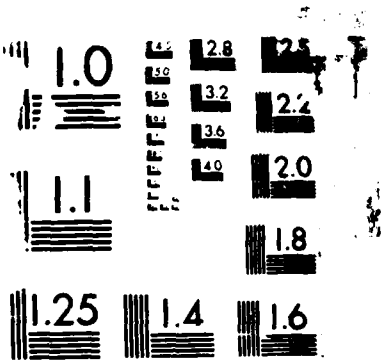
1.0
1.1
1.25
1.4
1.6
1.8
2.0
2.2
2.8
3.2
3.6
4.0

APPENDIX C

This appendix contains the code of program DELTA. This program calculates the edge shift that will be observed when viewing a slit through a coherent multiple aperture optical imaging system. The aperture to be analyzed is described by specifying the sub-aperture diameter and spacing (τ and α). These parameters, as well as other dimensions determined by the computer, are in the units of pixels. The program then calculates the field that would be produced if a single edge was imaged through the specified aperture. The program takes this edge field and adds to it an equivalent edge field that has been inverted about the edge and shifted by a number of pixels. The number of pixels the second edge field has been shifted is the slit width. The program takes the resulting field and determines its corresponding intensity pattern. From this array, the program finds the central zero in the pattern near the left edge and determines how many pixels it has shifted from the geometric position of the edge. The program repeats this process for slit half-widths of zero to three hundred pixels. The result is a file containing the half-widths and their corresponding edge shifts.

```
C
C       PROGRAM DELTA
C
C
      INTEGER IWK(1300000),TAU,ALPHA,BETA,W1,W2,DELTA(300)
      REAL WK(1300000),H(16384),INT(16384)
        COMPLEX G(16384),F(16384),Z(16384),REC(16384)
        OPEN(UNIT=25,STATUS='NEW',FILE='DEL.GRL')
C
C
C  READ PARAMETER VALUES FROM MIC FILE
C
C
      READ(5,20)N
      READ(5,20)TAU
      READ(5,20)ALPHA
20     FORMAT(I4)
40     FORMAT(I4,4X,I4)
C
C     N=NUMBER OF SAMPLE POINTS IN ONE DIMENSION
C   TAU=WIDTH OF SUB-APERTURE
C  ALPHA=SPACING OF SUB-APERTURES
C        {EXPRESSED AS MULTIPLE OF SUB-APERTURE WIDTH}
C
      PI=3.1415927
      N2=N/2
      NM1=N-1
C
C
C  INPUT FUNCTION - AN EDGE
C
C
      DO 60 I=1,N2
      G(I)=CMPLX(1.,0.)
60     CONTINUE
      DO 70 I=N2,NM1
      G(I+1)=CMPLX(0.,0.)
70     CONTINUE
C
C
C  PERFORM FIRST FOURIER TRANSFORM
C
C
      CALL FFTCC(G,N,IWK,WK)
C
C
C  MOVE ZERO SPATIAL FREQ TO CENTER OF APERTURE
C
C
      DO 100 I=1,N
      Z(I)=G(I)
100    CONTINUE
      DO 101 I=1,N2
      G(N2+I)=Z(I)
      G(I)=Z(N2+I)
101    CONTINUE
```

```
C
C
C  CIRCULAR APERTURES
C
C
      DO 200 I=1,N
         F(I)=CMPLX(0.,0.)
200   CONTINUE
      I1S=N2-ALPHA-TAU/2
      I1F=N2-ALPHA+TAU/2
      I2S=N2+ALPHA-TAU/2
      I2F=N2+ALPHA+TAU/2
      DO 210 I=I1S,I1F
      F(I)=G(I)
210   CONTINUE
      DO 220 I=I2S,I2F
      F(I)=G(I)
220   CONTINUE
C
C
C  PERFORM SECOND FAST FOURIER TRANSFORM
C
C
      CALL FFTCC (F,N,IWK,WK)
C
C
C  MOVE ZERO SPATIAL FREQ TO CENTER OF APERTURE
C
C
      DO 300 I=1,N
      Z(I)=F(I)
300   CONTINUE
      DO 301 I=1,N2
      F(N2+I)=Z(I)
      F(I)=Z(N2+I)
301   CONTINUE
C
C
C  FOR EACH BETA, DETERMINE DELTA (THE EDGE SHIFT)
C       {BETA IS THE HALF-WIDTH OF THE SLIT}
C
C
      DO 700 BETA=1,300
C
C
C  ADD THE TWO EDGES
C
C
      W1=N2-350
      W2=N2+350
      DO 320 I=W1,W2
         REC(I)=F(I+BETA)+F(N-I+BETA)
320   CONTINUE
```

```
C
C
C  CALCULATE INTENSITY
C
C
        VAL=0.
        DO 350 I=W1,W2
           FF=CABS(REC(I))
           IF (VAL.LT.FF) VAL=FF
350     CONTINUE
        DO 500 J=W1,W2
         X=J-N2
         I=J
        H(I)=(CABS(REC(I))/VAL)**2.
500     CONTINUE

C
C
C  FIND THE EDGE
C
C
        IF (H(N2-BETA-1).GT.H(N2-BETA)) THEN
           DIREC=1
        ELSE
           DIREC=-1
        END IF
        DO 600 I=1,100
           IF (H(N2-BETA+I*DIREC).GT.H(N2-BETA+(I-1)*DIREC)) THEN
              DELTA(BETA)=(I-1)*DIREC-1
              I=100
              GOTO 600
           ELSE IF (H(N2-BETA+I*DIREC).EQ.H(N2-BETA+(I-1)*DIREC)) THEN
              DELTA(BETA)=(I-1)*DIREC-1
              I=100
              GOTO 600
           END IF
600     CONTINUE
700     CONTINUE
        DO 800 I=1,300
        WRITE(25,40)I,DELTA(I)
800     CONTINUE
C
C
        CLOSE(UNIT=25)
1100      STOP
          END
```

APPENDIX D

This appendix contains the code of program CIRCLE. This program calculates the intensity of the two-dimensional image of an arbitrary circle through an arbitrary multiple aperture optical imaging system. The program requires the user to input the sub-aperture radius, the radius of the synthesized aperture, the number of sub-apertures, the rotation of the aperture, whether or not a central sub-aperture exists, and the radius of the circle to be imaged. The program takes the information about the circle to be imaged and calculates the field distribution of its Fourier Transform. After multiplying this field by the pupil function of the aperture, the program takes another Fourier Transform to determine the field in the image plane. From this field, the program calculates the two-dimensional intensity pattern which can be output to a file or imaged on an Evans and Sutherland PS-300 graphics terminal.

The images of rectangles were produced in the same manner. Instead of describing the transform of a circle, a different program described the transform of a rectangle and multiplied that by the pupil function. The remainder of the program was identical to program CIRCLE. To produce the impulse responses, the pupil function was multiplied by an array of ones.

```
C
C
C       PROGRAM CIRCLE
C
C
C    THIS PROGRAM CALCULATES THE INTENSITY
C    OF THE TWO-DIMENSIONAL IMAGE OF AN
C    ARBITRARY CIRCLE THROUGH AN ARBITRARY
C    MULTIAPERUTRE OPTICAL SYSTEM.
C
C
      INTEGER N,APE,PS,IER
      INTEGER IWK(4000),IA1,IA2,N1,N2,N3,IJOB,CNTR
      INTEGER*4 Out_Pictr(4,147456),Color_Pictr(3,384,384)
      REAL RWK(4000),ROT,NV,MMBSJ1,ARG,XB,CIRCR
      REAL M(96,96),INT(96,96)
      COMPLEX A(512,512),CWK(512),B(512,512)
C
        OPEN(UNIT=24,STATUS='NEW',FILE='INT.DAT')
C
C
C  READ PARAMETER VALUES FROM COM FILE
C
C
      READ(5,20)N
      READ(5,40)SRADIUS
      READ(5,40)RADIUS
      READ(5,40)APER
      READ(5,40)ROT
      READ(5,20)CNTR
      READ(5,40)CIRCR
      READ(5,20)PS
20      FORMAT(I4)
40      FORMAT(F15.4)
45      FORMAT(' Z = [')
46      FORMAT(F15.4,' ...')
47      FORMAT(F15.4)
48      FORMAT(' ];')
C
C       N=NUMBER OF SAMPLE POINTS IN ONE DIMENSION
C SRADIUS=RADIUS OF INDIVIDUAL SUB-APERTURES
C  RADIUS=OUTER RADIUS OF SYNTHESIZED APERTURE
C         (EXPRESSED AS MULTIPLE OF SUB-APERTURE RADIUS)
C    APER=NUMBER OF SUB-APERTURES IN THE ARRAY
C     ROT=ROTATION OF ARRAY (DEGREES)
C    CNTR=CENTER APERTURE (1=YES, 0=NO)
C   CIRCR=RADIUS OF CIRCLE BEING IMAGED
C      PS=DISPLAY ON EVANS AND SUTHERLAND (1=YES, 0=NO)
C
        APE=APER-1.
        IRAD=RADIUS*SRADIUS
        ORAD=IRAD
        IDIAM=2*IRAD
        SDIAM=2*SRADIUS
        PI=3.1415927
        Q1=3.*PI/4.
        DL=3.*PI/2.
```

```
          N2=N/2
          ROT=2.*PI/360.*ROT
C
C
C    BESSEL FUNCTION
C
C
       DO 102 I=1,N
       DO 100 J=1,N
          ARG=SQRT((N2-I)**2.+(N2-J)**2.)*2.*PI*CIRCR
          DEN=ARG/2/PI
          XB=MMBSJ1(ARG,IER)
       IF (DEN.EQ.0) THEN
          XB=1
       ELSE
          XB=XB/DEN
       END IF
          B(I,J)=CMPLX(XB,0.)
100    CONTINUE
102    CONTINUE
C
C
C  CIRCULAR APERTURE WITH VARIABLE TRANSMITTANCE
C
C
       IARG=256-SRADIUS+(ORAD-SRADIUS)*COS(ROT)
       JARG=256-SRADIUS+(ORAD-SRADIUS)*SIN(ROT)
C
       DO 107 I=1,N
       DO 105  J=1,N
          A(I,J)=CMPLX(0.,0.)
105     CONTINUE
107    CONTINUE
       DO 220 I=1,SDIAM
       DO 200 J=1,SDIAM
       RAD=SQRT((I-(SRADIUS+1.5))**2+(J-(SRADIUS+1.5))**2)
         IF(RAD.LT.SRADIUS-.5)GO TO 110
         IF(RAD.GT.SRADIUS+.5)GO TO 115
         SC=-RAD+SRADIUS+.5
         GO TO 112
110     A(I+IARG,J+JARG)=CMPLX(1.,0.)
       GO TO 120
112     A(I+IARG,J+JARG)=CMPLX(SC,0.)
       GO TO 120
115    A(I+IARG,J+JARG)=CMPLX(0.,0.)
120    CONTINUE
200    CONTINUE
220    CONTINUE
C
C
C  CREATE REMAINING SUB-APERTURES
C
C
```

```
      DO 227 I=1,APE
         L=(ORAD-SRADIUS)*COS(I*2.*PI/APER+ROT)
         U=L
         L=(ORAD-SRADIUS)*SIN(I*2.*PI/APER+ROT)
         V=L
         XP=255-SRADIUS+U
         YP=255-SRADIUS+V
         DO 225 J=1,SDIAM
         DO 223 K=1,SDIAM
            A(XP+J,YP+K)=A(XP+J,YP+K)+A(J+IARG,K+JARG)
            CZ=CABS(A(XP+J,YP+K))
            IF(CZ.GT.1.) THEN
               A(XP+J,YP+K)=CMPLX(1.,0.)
            END IF
223      CONTINUE
225      CONTINUE
227   CONTINUE
C
C
C     CREATE CENTER APERTURE IF DESIRED
C
C
      IF (CNTR.EQ.1) THEN
         XP=255-SRADIUS
         YP=255-SRADIUS
         DO 232 J=1,SDIAM
         DO 230 K=1,SDIAM
            A(XP+J,YP+K)=A(XP+J,YP+K)+A(J+IARG,K+JARG)
            CZ=CABS(A(XP+J,YP+K))
            IF(CZ.GT.1.) THEN
               A(XP+J,YP+K)=CMPLX(1.,0.)
            END IF
230      CONTINUE
232      CONTINUE
      END IF
C
C
C  MULTIPLY TRANSFORM OF RECTANGLE BY PUPIL FUNCTION (MULTIAPERTURE)
C
C
      DO 235 I=1,IDIAM
      DO 234 J=1,IDIAM
         INEW=256-IRAD+I
         JNEW=256-IRAD+J
         A(INEW,JNEW)=A(INEW,JNEW)*B(INEW,JNEW)
234   CONTINUE
235   CONTINUE
C
C
C  PERFORM FAST FOURIER TRANSFORM USING IMSL
C
C
240   IA1=N
      IA2=N
```

```
      N1=N
      N2=N
      N3=1
      IJOB=-1
      CALL FFT3D (A,IA1,IA2,N1,N2,N3,IJOB,IWK,RWK,CWK)
C
C
C  REDUCE SIZE OF ARRAY
C
C
        DO 250 I=1,48
           IARG=I
        DO 245 J=1,48
           JARG=J
        B(I,J)=A(IARG,JARG)
        B(I,48+J)=A(IARG,N-48+JARG)
        B(48+I,J)=A(N-48+IARG,JARG)
        B(48+I,48+J)=A(N-48+IARG,N-48+JARG)
245     CONTINUE
250     CONTINUE
C
C
C  SHIFT ZERO FREQUENCY TO ARRAY CENTER
C
C
        DO 260 I=1,96
        DO 255 J=1,48
        A(I,J)=B(I,49-J)
        A(I,48+J)=B(I,97-J)
255     CONTINUE
260     CONTINUE
        DO 270 I=1,48
        DO 265 J=1,96
        B(I,J)=A(49-I,J)
        B(48+I,J)=A(97-I,J)
265     CONTINUE
270     CONTINUE
C
C
C  FIND INTENSITY OF ARRAY
C
C
      WRITE(24,45)
        NV=0.0
      DO 390 I=1,96
      DO 380 J=1,96
      M(I,J)=CABS(B(I,J))/.00003468
        INT(I,J)=(M(I,J)**2.)*100000
        IF (INT(I,J).GT.NV) THEN
           NV=INT(I,J)
        END IF
  380 CONTINUE
  390 CONTINUE
```

```
            DO 410 I=1,96
            DO 408 J=1,96
            IF (J .EQ. 96) THEN
               WRITE(24,47)INT(I,J)
            ELSE
               WRITE(24,46)INT(I,J)
            END IF
            IF (INT(I,J).EQ.0.) THEN
              VAL=0
            ELSE
              Z=INT(I,J)/NV*500
              VAL=LOG(Z+1.)/LOG(501.)*255
            END IF
            DO 404 K=1,4
            DO 402 L=1,4
              Color_Pictr(1,4*J-4+K,4*I-4+L)=VAL
  402       CONTINUE
  404       CONTINUE
  408       CONTINUE
  410       CONTINUE
            DO 500 I=1,384
            DO 490 J=1,384
              Color_Pictr(2,I,J)=0
              Color_Pictr(2,I,J)=0
  490       CONTINUE
  500       CONTINUE
            WRITE(24,48)
C
            CLOSE(UNIT=24)
C
C
C  DISPLAY ON EVANS AND SUTHERLAND IF REQUESTED
C
C
            IF(PS.EQ.1)THEN
               CALL PS_RASTER_COLOR(384,384,Color_Pictr,Out_Pictr)
            END IF
C
C
 1100        STOP
             END
```

Bibliography

1. Airy, G. B. "On the diffraction of an object-glass with circular aperture," Trans. Camb. Phil. Soc. 5,283 (1835).

2. Department of the Air Force. Synthetic Aperture Optics Volume 1. Defense Documentation Center, Cameron Station Alexandrea, Virginia, 1969 (AD680806).

3. Fender, Janet S. "Synthetic Apertures: An Overview," Proceedings of SPIE. Vol 440. SPIE - The International Society for Optical Engineering Press, Bellingham WA, 1984.

4. Gaskill, Jack D. Linear Systems, Fourier Transforms, and Optics. New York: John Wiley Sons, 1978.

5. Goodman, Joseph W. Introduction to Fourier Optics. San Francisco: McGraw-Hill Book Company, 1968.

6. Heath, T. L. The Works of Archimedes. New York: Dover Publications, Inc., 1953.

7. Hooker, R. Brian. The Effects of Aberrations in Synthetic Aperture Systems. PhD dissertation, The University of Arizona, Tucson Arizona, 1974.

8. Hugghins, Capt Arley J. The Apodisation of Aberrated Coherent Multiaperture Optical Imaging Systems. MS thesis, 85D-6. School of Engineering, Air Force Institute of Technology (AU), Wright-Patterson AFB OH, December 1985.

9. Mills, James Patrick. The Effect of Aberrations and Apodisation on the Performance of Coherent Imaging Systems. PhD dissertation, University of Rochester, Rochester NY, 1984.

10. Mills, James Patrick., Major USAF. Personal interview. Air Force Institute of Technology (AU), Wright-Patterson AFB OH, January 1987.

11. Optical Sciences Center. Synthetic Aperture Optics. Technical Report No 58. Optical Sciences Center, University of Arizona, Tucson Arizona, 1970.

12. Shannon, Robert R. and James C. Wyant. Applied Optics and Optical Engineering. vol 9. New York: Academic Press, 1983.

13. Watson, Steven M. Two-Point Resolution Criterion For Multi-Aperture Optical Systems. MS thesis, GEP-87M. School of Engineering, Air Force Institute of Technology (AU), Wright-Patterson AFB OH, March 1987.

VITA

Lieutenant Dana J. Bergey was born on 19 November 1963 in Telford, Pennsylvania. He graduated from Souderton Area High School in 1981 and attended the Pennsylvania State University on an ROTC scholarship. In 1985, he graduated with high honors and received the degree of Bachelor of Science in Physics. A distinguished graduate of the ROTC program, Lieutenant Bergey received a regular commission in the USAF and reported directly to the Air Force Institute of Technology.

UNCLASSIFIED
SECURITY CLASSIFICATION OF THIS PAGE

AD-A179 476

REPORT DOCUMENTATION PAGE

Form Approved
OMB No. 0704-0188

1a. REPORT SECURITY CLASSIFICATION: UNCLASSIFIED	1b. RESTRICTIVE MARKINGS
2a. SECURITY CLASSIFICATION AUTHORITY	3. DISTRIBUTION/AVAILABILITY OF REPORT: Approved for public release; distribution unlimited
2b. DECLASSIFICATION/DOWNGRADING SCHEDULE	
4. PERFORMING ORGANIZATION REPORT NUMBER(S): AFIT/GE/ENG/87M-1	5. MONITORING ORGANIZATION REPORT NUMBER(S)
6a. NAME OF PERFORMING ORGANIZATION: School of Engineering; 6b. OFFICE SYMBOL (If applicable): AFIT/ENG	7a. NAME OF MONITORING ORGANIZATION
6c. ADDRESS (City, State, and ZIP Code): Air Force Institute of Technology, Wright-Patterson AFB, Ohio 45433	7b. ADDRESS (City, State, and ZIP Code)
8a. NAME OF FUNDING/SPONSORING ORGANIZATION; 8b. OFFICE SYMBOL (If applicable)	9. PROCUREMENT INSTRUMENT IDENTIFICATION NUMBER
8c. ADDRESS (City, State, and ZIP Code)	10. SOURCE OF FUNDING NUMBERS: PROGRAM ELEMENT NO. / PROJECT NO. / TASK NO / WORK UNIT ACCESSION NO.

11. TITLE (Include Security Classification): see box 19

12. PERSONAL AUTHOR(S): Dana I. Bergey, B.S., 2d Lt USAF

13a. TYPE OF REPORT	13b. TIME COVERED	14. DATE OF REPORT (Year, Month, Day)	15. PAGE COUNT
MS Thesis	FROM _____ TO _____	1987 March	107

16. SUPPLEMENTARY NOTATION

17. COSATI CODES			18. SUBJECT TERMS (Continue on reverse if necessary and identify by block number)
FIELD	GROUP	SUB-GROUP	multiaperture, synthetic aperture coherent imaging
20	06		

19. ABSTRACT (Continue on reverse if necessary and identify by block number)

Title: COHERENT MULTIPLE APERTURE OPTICAL IMAGING SYSTEMS: ANALYSIS AND DESIGN

Thesis Advisor: James P. Mills, Major, USAF

Approved for public release: IAW AFR 190-1.
LYNN E. WOLAVER 7 April 87
Dean for Research and Professional Development
Air Force Institute of Technology (AFC)
Wright-Patterson AFB OH 45433

20. DISTRIBUTION/AVAILABILITY OF ABSTRACT	21. ABSTRACT SECURITY CLASSIFICATION
☒ UNCLASSIFIED/UNLIMITED ☐ SAME AS RPT. ☐ DTIC USERS	UNCLASSIFIED

22a. NAME OF RESPONSIBLE INDIVIDUAL	22b. TELEPHONE (Include Area Code)	22c. OFFICE SYMBOL
James P. Mills, Major, USAF	513-255-2012	AFIT/ENP

DD Form 1473, JUN 86 — Previous editions are obsolete.

SECURITY CLASSIFICATION OF THIS PAGE

UNCLASSIFIED

The imaging of simple objects through coherent multiple aperture optical imaging systems was investigated. Multiple aperture telescopes are a candidate technology for the Strategic Defense Initiative missions of surveillance, tracking, and kill assessment. In this thesis, the multiaperture images of edges, slits, rectangles, and circles were theoretically predicted and experimentally produced. The images of the one-dimensional objects were predicted analytically, while a computer program was developed to predict the images of the two-dimensional objects. Photographs of the actual images produced in the lab were compared to the theoretical images, and the analytical and computer prediction techniques were found to be accurate.

All of the results were analyzed to determine how different multiaperture geometries affected the images. It was found that multiaperture imaging produces edge enhancement. The position of a single edge could be found exactly, while multiple edges sometimes produced slight edge shifts. A computer program was developed that predicts the edge shifts that will be observed when imaging through a given multiple aperture. Larger subaperture spacings were found to exhibit better resolution but produced more ringing about the edges. The possibility of rotating the multiple aperture system to gather more information was discussed, as well as designs that include a central subaperture. All of the important results were discussed as they apply to the design of systems that support the Strategic Defense Initiative.

END

5-87

DTIC